Dissertation

Study on Residual Stress for Hot Strip Rolling Bimetallic Rolls during the Heat Treatment Process

Hu Kejun/14595103

Kyushu Institute of Technology

2017

Dissertation

Study on Residual Stress for Hot Strip Rolling Bimetallic Rolls during the Heat Treatment Process

By

Hu Kejun

（Student Number: 14595103）

Supervisor: Pro. Nao-Aki Noda

Kyushu Institute of Technology

Graduate School of Engineering

Department of Mechanical Engineering

2017

Abstract

Bimetallic rolls are widely used in hot rolling mills because of excellent hardness, wear resistance and high temperature properties. During hot rolling process, thermal tensile-compressive stresses are caused by a cyclic sequence of heating – cooling over the roll surface due to hot strip contact and water cooling, resulting in thermal crack at the roll surface. Therefore, suitable compressive stresses at the roll surface are necessary for preventing the thermal crack extension. However, the tensile residual stress always appears at the roll center to balance the surface compressive residual stress. Under the combined action of tensile thermal stress and tensile residual stress at the roll center, another form of roll fracture known as thermal barrel breakage is originating near to the roll center and breaking out to the barrel surface. Therefore, keeping optimum surface compressive residual stress and minimizing the center tensile residual stress are desirable to reduce the risk of roll fracture and improve bimetallic roll using life. Since the residual stress can be controlled by the heat treatment, thus this thesis concentrated on the residual stress analysis of bimetallic roll during the heat treatment.

Chapter 1 gives the introduction of the high speed steel (HSS) bimetallic rolls used for hot strip rolling. In this chapter, the characteristics of the HSS rolls were introduced compared with the conventional single material rolls. An in addition, the development, applications and the different manufacturing methods of the HSS rolls were briefly introduced. Then the issues of the research on residual stress in the rolling rolls were reviewed.

Chapter 2 analyzes the residual stress of bimetallic roll during uniform heating quenching process. A thermo-elastic-plastic finite element simulation was performed by using large amount of shell and core material properties depending on the temperature. The residual stress generation mechanism and stress distribution during the uniform heating quenching process was investigated. Then, the effects of the shell-core ratio, roll diameter, phase transformation and material heat treatment process on the residual stress are discussed.

Chapter 3 analyzes the residual stress of bimetallic roll during non-uniform heating quenching process. In this chapter, the residual stress simulation was preformed including rapid heating and quenching process. The residual stresses were compared between uniform heating quenching process and non-uniform heating quenching process. The reason of the center tensile residual stress reduction in non-uniform heating quenching was investigated. Then, the usefulness of non-uniform heating quenching decreasing the roll center tensile residual stress is discussed considering the thermal stress during hot rolling process.

Chapter 4 briefly describes and explains the effect of creep analysis and tempering process on residual stress reduction of bimetallic roll during uniform heating quenching and non-uniform heating quenching processes. In this chapter, creep analysis was applied to the core material during the keeping process. Firstly, the creep equations were calculated based on the creep test using the time hardening law. Then the accuracy of creep equations is verified by the comparison of stress relaxation between FEM result and experimental result. At the last, the comparison of residual stress reduction considering tempering process after uniform heating quenching process and non-uniform heating quenching process was also discussed.

Chapter 5 analyzes the accuracy of disk method to predict roll residual stress. The disk method has been widely used in predicting the roll residual stress by measuring the stress of the thin sliced disk from the roll. The relation of stress between the original roll and the sliced disk stress should be discussed. In this chapter, therefore, the accuracy of disk method was investigated on the basis of thermo-elastic-plastic FEM analysis. Firstly, the stress simulations of single material rolls were performed using thermo-elastic analysis and thermo-elastic-plastic analysis considering the different quenching time, and in addition, the effect of disk thickness on the residual stress was also discussed. Then, the stress simulations of real bimetallic rolls were performed using thermos-elastic-plastic analysis under the different quenching time.

Chapter 6 gives the conclusions summary of this study.

Table of contents

List of Figures

List of Tables

Nomenclature

In this paper the following notations are used.

D	Bimetallic roll outer diameter
d	Bimetallic roll inner diameter
As	Area of shell
Ac	Area of core
T_{Start}	Quenching start temperature
T_{Keep1}	Keeping temperature during non-uniform heating quenching process
T_{Keep2}	Keeping temperature during uniform heating quenching process
T_{Fnish}	Quenching finish temperature
T_{EP}	Temperature of the roll surface changes into elastic-plastic state
$T_{Pearlite}$	Temperature of pearlite transformation
$T_{Bainite}$	Temperature of bainite transformation
$T_{Ambient}$	Ambient temperature obtained by experimentally measuring
$T_{Surface}$	Roll surface temperature obtained by experimentally measuring
$T_{Simulation}$	Roll surface temperature obtained by simulation
$T_{Tempering}$	Keeping temperature during tempering process
T_{tFnish}	Tempering finish temperature
t_1	Time of pearlite transformation starts at shell/core boundary
t_2	Time of pearlite transformation starts at roll center
t_3	Time of pearlite transformation ends at roll center
t_4	Time of keeping starting
E	Young's modulus
E_0	Young's modulus of the shell material at T_{Start}

$\boldsymbol{\nu}$	Poisson's ratio
$\boldsymbol{\nu_0}$	Poisson's ratio of the shell material at T_{Start}
$\boldsymbol{\sigma}$	Stress
$\boldsymbol{\sigma_0}$	Stress of the shell material at T_{Start}
$\boldsymbol{\sigma_z}$	Stress in z-axis direction
$\boldsymbol{\sigma_\theta}$	Stress in θ-axis direction
$\boldsymbol{\sigma_r}$	Stress in r-axis direction
$\boldsymbol{\sigma_{eq}}$	Equivalent stress
$\boldsymbol{\sigma_z^{Cylinder}}$	Stress of the cylinder in z-axis direction
$\boldsymbol{\sigma_\theta^{Cylinder}}$	Stress of the cylinder in θ-axis direction
$\boldsymbol{\sigma_r^{Cylinder}}$	Stress of the cylinder in r-axis direction
$\boldsymbol{\sigma_z^{Disk}}$	Stress of the sliced disk in z-axis direction
$\boldsymbol{\sigma_\theta^{Disk}}$	Stress of the sliced disk in θ-axis direction
$\boldsymbol{\sigma_r^{Disk}}$	Stress of the sliced disk in r-axis direction
$\boldsymbol{\sigma_z^{Roll}}$	Stress of the bimetallic roll in z-axis direction
$\boldsymbol{\alpha}$	Thermal expansion coefficient
$\boldsymbol{\alpha_0}$	Thermal expansion coefficient of the shell material at T_{Start}
$\boldsymbol{\lambda}$	Thermal conductivity coefficient
$\boldsymbol{\lambda_0}$	Thermal conductivity coefficient of the shell material at T_{Start}
$\mathbf{C}$	Specific heat
$\boldsymbol{C_0}$	Specific heat of the shell material at T_{Start}
$\mathbf{h}$	Heat transfer coefficient
$\boldsymbol{h_0}$	Heat transfer coefficient at T_{Start}

Chapter 1

Introduction

1.1 Characteristics of high speed steel rolling roll

Hot rolling process is one of the most important industrial processes used for metalworking [1]. Work rolls are the most important tool for the hot and cold forming to reduce the thickness of the metal stock [2, 3]. The production quality and the productivity are two of the most important concerns, which are depending strongly on the shape profile and surface quality of the work roll [4-6]. Generally, high wear resistance and good surface roughening resistance are required for the work rolls used for hot strip rolling mills [7-11]. Moreover, the demands for not only high quality of product shape and product surface condition but also high productivity and energy saving in rolling are increasing more and more in recent years. In order to adapt to severe hot rolling demands of a hot strip mill, the high speed steel roll (HSS roll) was developed and introduced to hot strip rolling roll [12-16]. Compared with conventional rolls, HSS rolls compound by a shell layer formed by high speed steel with high wear resistance and surface roughening resistance, and a core layer consisted of cast iron or forged steel with a high hard toughness [17-20]. Brief explanation on the properties of HSS roll is provided as follows.

1. Mechanical properties

Table 1-1 shows the comparison of material properties between HSS rolls and conventional rolls [21]. Table 1-2 shows the comparison of physical properties between HSS rolls and conventional rolls [21].

The hardness of 80-85Hsc of high speed steel material is mainly used for the work rolls, which is higher than the conventional high chrome cast iron of 70-80Hsc and high alloy grain cast iron of 75-85Hsc. The high speed steel tensile strength and compressive strength are also

increased compared with the conventional roll materials. A steel-base core material with high toughness and Young's modulus is used for the high speed steel rolls, which provides bending strength and flexural rigidity about 2 and 1.2 times higher than those of the conventional rolls. In terms of physical properties, the high speed steel rolls feature high thermal expansion in the shell and have good thermal conductivity in the core.

2. Microstructures properties

Table 1-3 shows the comparison of chemical compositions and metallurgical properties between HSS rolls and conventional rolls for hot strip mill [21].

The high speed steel material is cast alloys of Fe-C-Cr-W-Mo-V system which results in improved wear resistance. The carbides are M7C3 (HV2500) for conventional high chromium roll and Fe3C (HV1300) for indefinite chilled roll. This new compound roll contains mainly MC (HV3000), M7C3 (HV2500) and M6C (HV2000) [13]. The microstructure consists of the fine proeutectic MC carbide mainly formed by V, fine eutectic M6C carbide mainly formed by iron, Cr, Mo, and a quenched and tempered matrix. The matrix is usually tempered martensite to optimize hardness. Both Cr and Mo exhibit a precipitation hardness effect, which ensures high matrix hardness at high temperature. Co improves the red hardness for the high speed steel material.

The HSS rolls exhibit a beautiful metallic luster and have minimal surface roughness. The roughness depth of HSS rolls are almost l/2-1/3 compared with conventional rolls, which will effectively increase the rolling life and the smooth surface of sheet product [21, 22].

Table 1-1 Comparison of mechanical properties between HSS rolls and conventional rolls [21].

Division	Item	Unit	Roll material (shell)		
			High speed steel	High chrome cast iron	High alloy grain cast iron
Shell	Hardness	Hsc	70-90	70-80	75-85
	Tensile strength	MPa	700-1,000	700-900	400-600
	Compressive strength	MPa	2,500-3,200	1,700-2,200	1,900-2,500
	Fracture strength	MPa	25-28	21-34	18-35
Core	Tensile strength	MPa	700-1,000	400-500	300-500

Table 1-2 Comparison of physical properties between HSS rolls and conventional rolls [21].

Roll making process	Material ($\frac{\text{Shell}}{\text{Core}}$)	Thermal conductivity (W/m•K)	Specific heat (kJ/kg•K)	Specific weight (kg/m^3)	Linear expansion coefficient (10^{-5}/K)	Young's modulus (GPa)	Poisson ratio
Centrifugal pouring casting	High speed steel / Alloy forged steel	25.5	0.50	7700	13.0	235	0.27
		42.0	0.50	7850	14.0	206	0.29
Centrifugal casting	High chrome steel / Ductile cast iron	20.0	0.59	7600	13.0	220	0.30
		27.0	0.59	7200	12.0	205	0.30
	High alloy grain cast iron / Ductile cast iron	23.5	0.54	7500	8.0	175	0.27
		27.0	0.59	7200	12.0	205	0.30

Table 1-3 Comparison of chemical compositions and metallurgical properties between HSS rolls and conventional rolls for hot strip mill [21].

Roll material	Chemical composition (wt%)	Top: Graphite Middle: Carbide Bottom: Maxtrix	Hardness (Hsc)
High speed steel	C: 1.5-2.4 Ni: - Cr: 2-10 Mo: 2-10 V: 2-10 W: 2-10 Co:≤10	None MC+M_6C Tempered martensite	80-90
High chrome cast iron	C: 1.0-3.0 Ni:1-2 Cr: 10-25 Mo: 1-3 V: ≤3	None M_7C_3 Tempered martensite	70-90
High alloy grain cast iron	C: 3.0-3.4 Ni:4-5 Cr:≤ 2 Mo:≤1	≤5% Fe_3C Bainite	70-85

3. High temperature hardness and hardenability

Figure 1-2 shows the hardness depending on the temperature and the hardenability the for high speed steel and conventional material rolls for hot strip mill [13, 21]. The high speed steel rolls can still maintain higher hardness at high temperature than that of conventional roll material rolls. Moreover, the hardness can be improved by adding the Co element. The hardness range HsC80-90 of outer layer is suited to prevent the hardness softening and keep wear-resistance at rolling. The hardness range HsC30-45 of core is suited to prevent wear at rolling. The hardness decreasing from roll surface to core at room temperature is less than HsC3at 50mm inside of the outer shell, which is less than that of indefinite chilled iron roll.

4. Wear resistance and surface roughness resistance

Figure 1-2 shows the wear depth of HSS rolls at the finishing rolling process compared with the conventional rolls [21]. When the high speed steel was used in an actual mill for the finishing stands of a hot strip mill, they also have a better performance than the conventional rolls. The wear depth of the HSS rolls is much smaller than that of conventional rolls, and the wear resistance is significantly increased [21, 23].

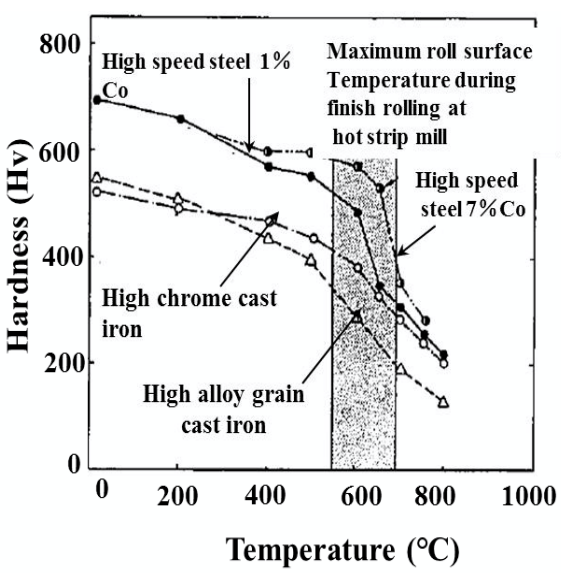

(a) Hardness at the high temperature

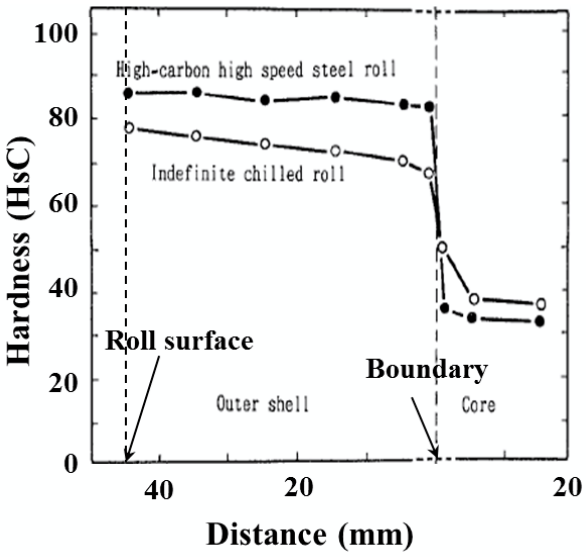

(b) Hardness distribution

Figure 1-1 Hardness depending on the temperature and hardenability for high speed steel compared with the conventional rolls for hot strip mill [13, 21]

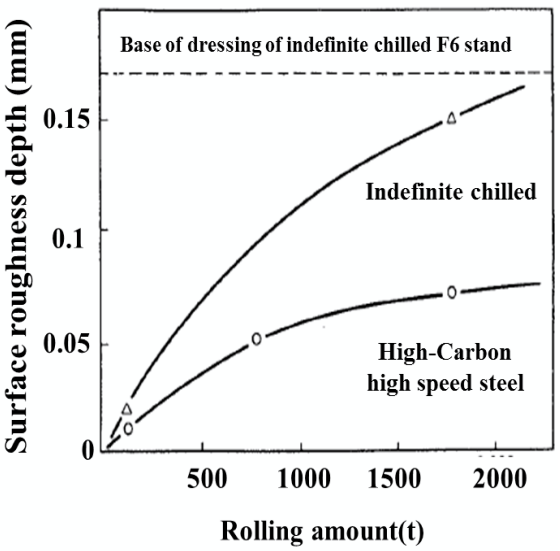

(a) Wear resistance

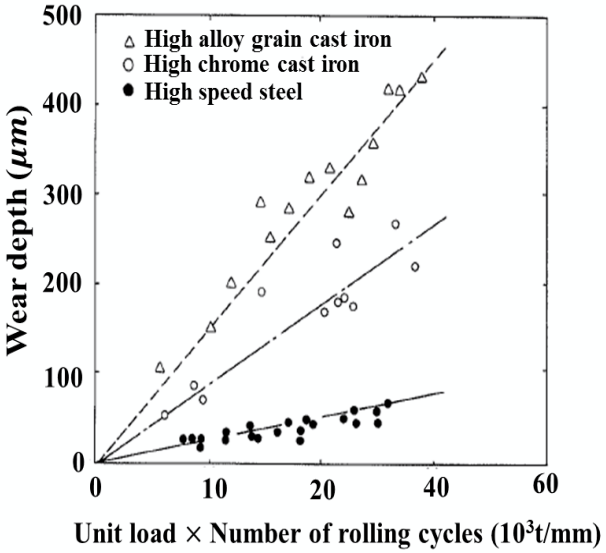

(b) Surface toughness resistance

Figure 1-2 Wear resistance and surface toughness resistance of high speed steel rolls compared with conventional rolls for hot strip mill [21, 23]

1.2 Manufacturing methods of high speed steel rolling roll

Recently, many methods such as centrifugal casting (CC)[24-26], continuous pouring for cladding (CPC) [13, 27] and electric slag re-melting (ESR) [28, 29], etc., have been used to fabricate the HSS work rolls. The manufacture processes can be listed as following.

1. Centrifugal casting (CC) process

The molten metal (shell layer) is firstly poured in a rotating mold, when the shell layer just solidified, and then the core metal is poured in the concentric cavity, so that the performance of two different materials to achieve complete metallurgical bond. Centrifugal casting is one of the main methods for HSS rolls in the early stage because of simple operation, less equipment investment and stable roll quality. However, since larger amounts of the alloy elements (Cr, Mo, V, W) contained in the shell layer and these elements density are different, the severe segregation occurs at the shell layer of the HSS rolls for the centrifugal casting method.

2. Centrifugal pouring casting (CPC) process

This is the most popular method of HSS rolls manufacturing. Bimetallic HSS rolls are produced by pouring the molten metal, which formed the shell layer, in the gap between the vertically placed core the water cooled mould. Heat is supplied to the core and the molten metal to ensure complete adherence. This process produces good bonding between the shell and the core. Another advantage of this process is that the core can be a forged alloy, thus ensuring higher toughness.

3. Electroslag re-melting (ESR) process

A water-cooled mold placed concentrically around the cylindrical core material, which will become the roll core and journal. The pipe shaped electrode which will form the outer layer of the roll is inserted in the space between the core material and the mold. This electrode is melted by ESR method and the core and the mold are rotated synchronously during melting by ESR method. The space between the core and the mold is continuously filled with the molten

electrode. The HSS roll manufactured by ESR has the clean outer layer with sound and fine microstructure and high boundary strength.

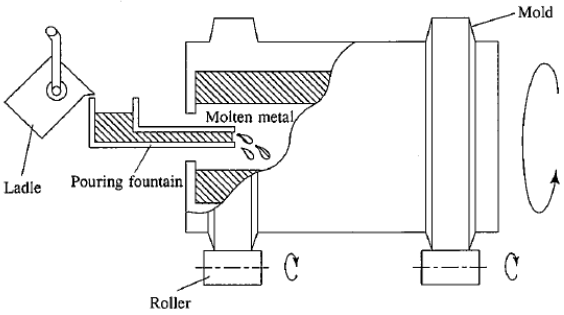

(a) Centrifugal casting process

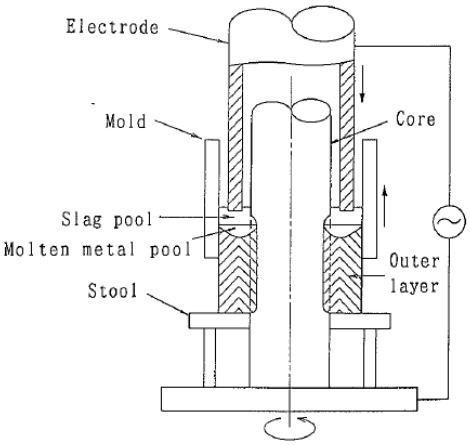

(c) Electroslag re-melting process

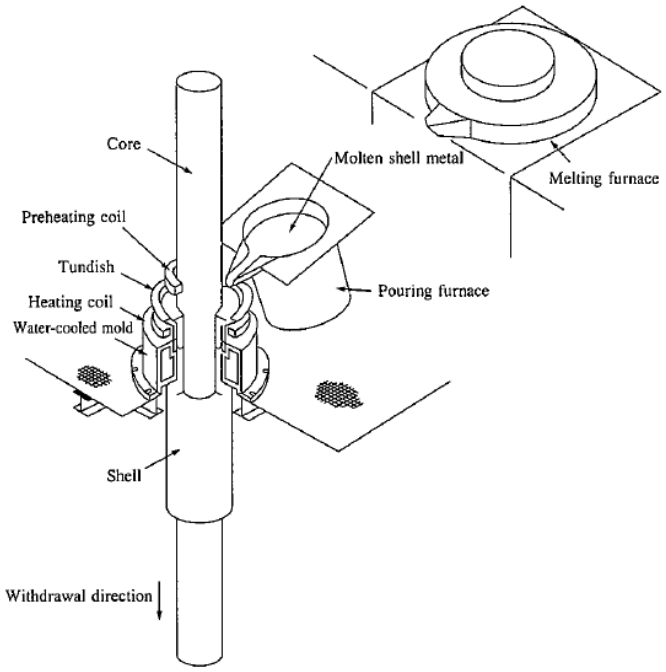

(b) Continuous pouring casting process

Figure 1-3 Manufacturing methods for high speed steel bimetallic rolls

1.3 Historical development and applications of high speed steel rolling roll

1.3.1 Historical development of high speed steel rolling roll [30]

In the 19th century, unalloyed grey iron was mainly modified only by different carbon content and cooling rates using grey iron chill moulds or sand moulds, and the forged steel was used for rolls. In this period, the roll consisted of white iron shell layer and grey iron core and necks due to reduced cooling rate. This type roll was used for flat rolling without any roll cooling in sheet mills. Later on cast steel rolls were developed with carbon content up to 2.4% with and without graphite, and are still produced today.

Around 1930, indefinite chill double poured (ICDP) rolls were invented for hot rolling, especially for work rolls in finishing mills of hot strip mills, which were also used for many other applications such as roughing stands of hot strip mills and work rolls in plate mills. This grade was to become the world standard for many years with very limited variations. Until today no other material could replace this grade for some applications. In the late 1990's finally ICDP enhanced with carbide improved roll performance and started a new phase for this old grade, still successfully in use today in work rolls for early finishing stands of finishing hot strip mills and for plate mills.

Around 1950 nodular iron was invented and introduced into roll manufacturing, unalloyed as well as frequently (Cr) Ni, Mo-alloyed, giving good wear resistance and strength at the same time. The use of high chromium iron (2-3% C, 15-20% Cr) and later on high chromium steel (1-2% C, 10-15% Cr) brought new materials with high wear resistance. But this was only one major step towards greater productivity of rolls.

In 1985 by starting high speed tool steel (HSS) materials were introduced into rolls and evolved the so-called semi tool steel grades. After initial problems all changes brought new opportunities for better roll performance. After the introduction of new grades to the mills it was

often necessary to change or improve rolling conditions. However, after some time rolls also improved and there were no further problems with new grades, only a better performance.

1.3.2 Applications of high speed steel rolling roll

Casting high speed steel roll for hot rolling was developed in Japan in 1988, and applied to hot strip rolling mills. In the 1990s, high speed steel began to be introduced to the United States, and in Europe [31]. At present, dozens of enterprises worldwide have used high speed steel bimetallic rolls, had achieved some results, including the Nippon Steel Corporation of Japan (NSSC), the Inland Steel Company of the United States and Dofasco of Canada.

1. Application in Japan

Based on the report, the bimetallic roll of high speed steel produced by the NSSC in the way of CPC had relatively high wear resistance [32-34]. After applying high speed rolls, the cost of rolls declined significantly, with significant decrease of time in changing rolls, reduce of stock removal, improvement in roll capacities, decline of fuel and energy, which are helpful to reduce the cost of rolls and improve the quality of strip.

Since 1992, the Hitachi Limited of Japan has produced and applied over 150 semi-high speed steel bimetallic rolls with the roll diameter of 250 to 630 mm, and achieved good results in rolling [35]. Compared with common forged steel rolls with 5% of Cr and 10% of Cr, the abrasion of semi-high speed steel is less, with shallower surface toughness. Hence, the cost of rolls reduces significantly. When producing the same amount of cold strip steel, the cost of rolls is only 21% of that by 5% of Cr steel.

The Hawasaki Iron Company in Japan has tried high speed steel rolls on continuous rolling mills, and the compositions are as following: 2%-3% C, 5%-8% Cr, 5%-7% V, 1%-3% Nb [36]. Results have shown that when using nodular casting iron rolls, the average roughness (Ra) of pass roughness increased as the quantity of rolling increased, and should be changed after rolling

2000 steel pipes. When using high chromium steel rolls, Ra increased with the quantity of rolling at the beginning, but without significant changes afterwards. Meanwhile, when using high speed steel rolls, since the beginning of rolling, Ra stayed in a relatively low number, and can roll 12,000 steel pipes. Hence, using high speed rolls can prolong the life of rolls and reduce the cost of rolls significantly.

2. Application in Canada

Since 1993, when Canada Dofasco Company tried casting high speed steel rolls, the percentage of use has increased continuously [37]. At present, casting high speed steel rolls have all adopted on F2, F3 and F4. After using high speed steel rolls, the cost of rolls have reduced significantly, and the efficiency of rolls improved significantly. The average rolling amount of Machine F4 has increased from 360t/h in June, 1992 to 490t/h in November, 1994, with a 20% increase of strip surface quality.

3. Application in China

In recent years, China has launched the research of high speed steel rolls [38-40]. It is reported that China Iron and Steel Research Institution has cooperated with Tangshan Lianqiang Metallurgical and Rolls Ltd., to develop high speed steel bimetallic rolls. Adopting the method of centrifugal casting, the rolls are used on the machine of mill coils products to produce the plain carbon steel with the thickness of 2.1 mm and the width between 120 to 183 mm. When producing the plain carbon steel, the amount of steel rises 2.5 to 3 times compared with that using high ni-cr infinite cold hardness cast iron roll, but with only one fourth of grinding quantity of the original, and the comprehensive efficiency is more than 10 times than original. Baosteel has also introduced several high speed steel rolls from overseas, whose lifespan double to triple of high chromium casting rolls. When being used on hot strip mill, it has achieved success.

1.4 Residual stress in rolling roll

Residual stresses are inevitable introduced into the rolls during the manufacturing process of casting, heat treatment process of quenching and tempering and the subsequent machining process of grinding and turning, which have a significant impact on the roll performance and roll life [30, 41, 42]. Generally, it is known that compressive residual stresses at roll surface are beneficial for increasing fatigue strength, reducing crack propagation and reducing shear stress at the roll barrel surface and work-hardening [13, 30, 42]. On the other hand, the tensile residual stresses at the roll center may cause roll breakage. In principle, the surface compressive stresses and the center tensile residual stresses are balance each other over the cross section of the roll. Therefore, the large enough surface compressive stress and low center tensile stress has to be controlled. Table 1-4 gives statistical results on the roll damages and the damage sources for hot strip mill at the finishing stand [41].

Over the years, the investigation of residual stress for mill rolls was mainly measured experimentally [43-50]. Many different methods have been developed to measure residual stress for the mill rolls in order to determine the roll residual stress distribution. The methods may be classified into destructive or non-destructive one. Destructive mechanical methods including deep hole-drilling method, ring core method, disk-cutting method and Sachs boring method and non-destructive methods including X-ray diffraction method and Barkhausen magnetic method have been applied to the measuring of roll residual stress. However, the non-destructive methods are only the surface near regions can be investigated and not suitable for measuring the interior stress of large rolls, as well as the main destructive methods such as hole-drilling method and ring-core method. Although the deep hole-drilling method, disk cutting method and Sachs boring method have been used for measuring the residual stress from center to surface of large rolls, these methods are extreme time consuming and damaging the testing rolls.

Recently, it is highly fashionable to investigate residual stresses by computer simulation on

the basis of finite element method (FEM). The FEM simulation is an effective way to help to understand the generation mechanism of residual stress [51-52]. However, for the residual stress simulation of the rolls which treated on casting process or heat treatment process, a large amount of material properties are necessary regarding two different materials in the bimetallic roll [53-54]. Those data have to be obtained under the wide range of temperature including high temperature region which are difficult to be obtained. Therefore, despite a number of studies focused on residual stress in the past decades, most studies dealt with small size components [55-61]. Recently, Torres et al. analyzed bimetallic work rolls during post casting cooling stage [62-63]. Although they have studied the prediction of the residual stress on the high chrome steel roll, the most critical quenching process has not been covered yet.

1.5 Motivation and Objectives

As have been introduced in above, considerable residual stress is inevitably introduced in to bimetallic rolls due to temperature gradient and phase transformation during heat treatment process. In addition, for the hot strip roliing rolls, thermal stresses are caused by a cyclic sequence of heating – cooling over the roll surface due to hot strip contact and water cooling during hot rolling process, resulting in thermal crack initiation named firecrack at the roll surface. If severe thermal tensile stress has been added under the rolling trouble, the thermal crack starts to propagate. Therefore, suitable compressive stresses are necessary for preventing the thermal crack extension. However, the tensile residual stress always appears at the roll center to balance the surface compressive residual stress. Under the combined action of thermal stress and residual stress, another form of roll fracture is known as thermal barrel breakage. This thermal breakage was originating near to the roll center and breaking out to the barrel surface. The residual tensile stress affects the thermal breakage because if the total tensile stress exceeds the strength of core material, a sudden thermal breakage happens. Thus, to improve roll using life, minimizing the

center tensile residual stress and keeping optimum surface compressive residual stress are required for bimetallic rolls used in hot rolling mills. Heat treatment of rolls is most critical for residual stresses but if well controlled, residual stresses are controlled as well. Therefore, it is desirable to investigate the residual stress distribution and generation mechanism for bimetallic roll during the heat treatment.

Table 1-4 Statistical results on the roll damages and the damage sources for hot strip mill at the finishing rear stand [41].

Rolling condition	Breakage	Source of breakage				
		Roll material			Rolling condition	
		Defect	Strength	Residual stress	Thermal stress	Rolling stress
Normal	Body breakage	○	○	○	○	---
	Large spalling at center	○	○	○	Δ	○
	Large spalling at boundary	○	○	○	Δ	○
	Large spalling from surface	○	---	---	---	Δ
	Small spalling from surface	○	---	---	---	Δ
Abnormal	Large spalling※	---	---	---	○	○
	Small spalling	---	---	---	○	○
	Crack by cobble	---	---	---	○	○
	Crack by mill stopage	---	---	---	○	---

Remarks: ○ Strong effect; Δ Small effect;

--- Little or no effect; ※ Accompanied with body breakage, sometimes

1.6 Outline of the dissertation

The objectives of the study in this thesis aims to minimize the center tensile residual stress and keep optimum surface compressive residual stress for bimetallic rolls used in hot rolling mills. In this study, a thermo-elastic-plastic finite element simulation will be performed by using MSC.Marc2012 to investigate the residual stress during heat treatment. The thesis outline is composed of 6 chapters as following:

Chapter 1 gives the introduction of the high speed steel (HSS) bimetallic rolls used for hot strip rolling. In this chapter, the characteristics of the HSS rolls were introduced compared with the conventional single material rolls. An in addition, the development, applications and the different manufacture methods of the HSS rolls were briefly introduced. Then the issues of the research on residual stress in the rolling rolls were reviewed.

Chapter 2 analyzes the residual stress of bimetallic roll during uniform heating quenching process. A thermo-elastic-plastic finite element simulation was performed by using large amount of shell and core material properties depending on the temperature. The residual stress generation mechanism and stress distribution during the uniform heating quenching process was investigated. Then, the effects of the shell-core ratio, roll diameter, phase transformation and material heat treatment process on the residual stress are discussed.

Chapter 3 analyzes the residual stress of bimetallic roll during non-uniform heating quenching process. The residual stresses were compared between uniform heating quenching process and non-uniform heating quenching process. Then, the usefulness of non-uniform heating quenching decreasing the roll center tensile residual stress is discussed considering the thermal stress during hot rolling process.

Chapter 4 briefly describes and explains the effect of creep analysis and tempering process on residual stress reduction of bimetallic roll during uniform heating quenching and non-uniform heating quenching processes. In this chapter, creep analysis was applied to the core material

during the keeping process. Firstly, the creep equations were calculated based on the creep test using the time hardening law. Then the accuracy of creep equations is verified by the comparison of stress relaxation between FEM result and experimental result. At the last, the comparison of residual stress reduction considering tempering process between uniform heating quenching process and non-uniform heating quenching process was also discussed.

Chapter 5 analyzes the accuracy of disk method to predict roll residual stress. The disk method has been widely used in predicting the roll residual stress by measuring the stress of the thin sliced disk from the roll. The relation of stress between the original roll and the sliced disk stress should be discussed. In this chapter, therefore, the accuracy of disk method was investigated on the basis of thermo-elastic-plastic FEM analysis. Firstly, the stress simulations of single material rolls were performed using thermo-elastic analysis and thermo-elastic-plastic analysis considering the different quenching time, and in addition, the effect of disk thickness on the residual stress was also discussed. Then, the stress simulations of real bimetallic rolls were performed using thermos-elastic-plastic analysis under the different quenching time.

Chapter 6 gives the main conclusions of this study for the residual stress analysis of bimetallic rolls during the uniform heating quenching and non-uniform heating quenching processes, and the other influence factors on residual stress.

Reference

1. Spuzic S., Strafford K. N., Subramanian C. and Savage, G., Wear of hot rolling mill rolls: an overview. Wear, 176(2), pp. 261-271, 1994.
2. Tseng, A. A., Finite-difference solutions for heat transfer in a roll rotating at high speed. Numerical Heat Transfer, 7(1), pp.113-125, 1984.
3. Eibe, W. W., History of the Development of Rolling Mills and Their Rolls., Rolls for the Metalworking Industries, R.B. Corbell, Ed., Iron and Steel Society, Inc., pp.1-22, 1990.

4. Boccalini, J. M, Sinatora A., Microstructure and wear resistance of high speed steels for rolling mill rolls. Proceedings of the 6th International Tooling Conference, Sweden, pp.425-437, 2002.
5. Tanaka, T., Hashimoto, M., Koie, T., Otomo, S., Ayagaki, M., Inoue, T. and Yamashita, M., High speed steel type cold rolling mill roll by continuous pouring process for cladding. Nippon Steel Technical Report, 86, pp.80-85, 2002.
6. Li, C. S., Yu, H. L., Deng, G. Y., Liu, X. H. and Wang, G. D., Numerical simulation of temperature field and thermal stress field of work roll during hot strip rolling. Journal of Iron and Steel Research, 14(5), pp. 18-21, 2007.
7. 佐野義一, 最近の熱間薄板圧延機用作業ロ-ル(圧延設備< 特集>). 日立評論, 67(4), pp.303-308, 1985.
8. 野口紘, 渡辺靖夫, 熱間圧延用ロール材の高温における摩擦と摩耗. 川崎製鉄技報, 19 (3), pp.195-201, 1987.
9. Noguchi, H., Hiraoka, H., Watanabe, Y., and Sayama, Y., Hardness and wear resistance of adamite for work rolls in hot rolling mill. Transactions of the Iron and Steel Institute of Japan, 28(6), pp.478-484, 1988.
10. J.R. Davis, ASM Speciality Handbook, Tool Materials, ASM International, Materials Park, OH, pp.187-194, 1995.
11. Choi, J. W. and Kim, D., Mechanisms of surface deterioration of high-Ni grain roll for hot strip rolling. ISIJ international, 39(8), pp.823-828, 1999.
12. 佐野義一，村上文男，大島昌彦，服部敏幸，大畑拓巳, 特殊複合ロールの開発, 日立金属技報, 4, pp.91, 1988.
13. Sano, Y., Hattori, T. and Haga, M., Characteristics of High-carbon High Speed Steel Rolls for Hot Strip Mill. ISIJ international, 32(11), pp. 1194-1201, 1992.
14. Hashimoto, M., Otomo, S., Yoshida, K., Kimura, K., Kurahashi, R., Kawakami, T. and

Kouga, T., Development of High-performance Roll by Continuous Pouring Process for Cladding. ISIJ international, 32(11), pp. 1202-1210, 1992.

15. Takigawa, H., Tanaka, T., Ohtomo, S.and Hashimoto, M., Development of High-Speed Tool Steel Rolls and Their Application to Rolling Mills. Nippon Steel Technical Report, 74, pp.77-83, 1997.
16. Fu, H., Zhao, A. and Xing, J., Development of centrifugal casting high speed steel rolls. Journal of University of Science and Technology Beijing, 10(6), p. 61-66, 2003.
17. Ooshima, M., Sugimura, Y. and Sano, Y., The development of the new type high performance compound rolls for hot rolling. 32nd Mechanical Working and Steel Processing, 28, pp.31-34, 1990.
18. Kamata, T., Shitamura, O., Kodama, H., Sano, Y. and Ohata, T., Newly developed high performance composite type rolls, Hitati Giho, 72(5), pp.69-76, 1990.
19. Xavier, R. R., Carvalho, M. A., Cannizza, E., Kerr, E. J. and Silva, C. S., Successful Strategy for HSS Rolls Implementation. Materials Science and Technology, 4, pp.55-64, 2005.
20. Lecomte-Beckers, J., Tchoufang Tchuindjang, J., Pirard, E. and Breyer, J. P., Physical metallurgy of a HSS material for hot rolling mill rolls. In Proceedings of the 14th Rolling Conference-1st Conference on Uses of Steel, San Nicolas, pp. 507-516, 2002.
21. Hashimoto, M., Oda, T., Hokimoto, K., Kawakami, T. and Kurahashi, R., Development and application of high-speed tool steel rolls in hot strip rolling. Nippon Steel Technical Report, 66, pp.82-90, 1995.
22. 王蕊, 侯红娟, 王磊磊. 高速钢轧辊在热轧板带中的生产应用探讨. 太原科技大学学报, 27, pp.94-96, 2006.
23. 山本徹夫, 中村丈人, 小島誠治. 熱延仕上スタンドへのハイスロールの導入, 材料とプロセス, 6, pp.516, 1993.
24. Fu H, Qu Y, Xing J, et al. Investigations on heat treatment of a high-speed steel roll. Journal

of Materials Engineering and Performance, 17(4), pp. 535-542, 2008.

25. K. Ichino, Y. Kataoka, and T. Koseki, Development of Centrifugal Cast Roll with High Wear Resistance for Finishing Stands of Hot Strip Mill, Kawasaki Steel Tech. Rep., 37, pp. 13-18, 1997.
26. K. Gong, Y. Dong, and C. Gao, Research and Manufacture of Compound High Speed Steel Rolls, Iron Steel (Peking), 33(3), pp.67-71, 1998.
27. M. Hashimoto, S. Otomo, and K. Yoshida, Development of High-Performance Roll by Continuous Pouring Process for Cladding, ISIJ Int., 32(11), pp. 1202-1210, 1992.
28. M. Shimizu, O. Shitamura, S. Matsuo, T. Kamata, and Y. Kondo, Development of High Performance New Composite Roll, ISIJ Int., 32(11), pp. 1244-1249, 1992.
29. Medovar, B., Medovar, L., Chernets, A., Electroslag Surfacing by Liquid Metal - a New Way for HSS-rolls Manufacturing, 38th MWSR Conference Proceedings, Vol. XXXIV, Cleveland, Ohio, pp. 83-87, 1996.
30. K. H. Schroder, A basic understanding of the mechanics of rolling mill rolls, Eisenwerk Sulzau-Werfen, ESW-Handbook, pp.71, 2003.
31. Odin G, Terrasse R. Steel Used for Cluster Mill Work Rolls-Interest of Grades with High Vanadium Content.30th Mechanical Working and Steel Processing Conference. Michigan, USA, pp.379-389, 1988.
32. 井崎正義, 梅田孝, HIP 複合熱間圧延ロール, 神戸製鋼技報, 43(2), pp.145-145, 1993.
33. 早漱直树, 手柴东光, 中西敏修, 冷間タンデムミルにおけるセミハイス鍛鋼ワークロールの適用, CAMRISIL, 6(2), pp.503, 1993.
34. 王世栋译, 新日铁公司开发的 CPC 高速钢轧辊具有极高耐磨性, 世界金属导报,1998.
35. 符寒光，邢建东，赵爱民，高速钢复合辊环离心铸造技术研究. 钢铁，37, pp.67-71, 2002.
36. 张朝生, 日本热带钢连轧机组用高速钢轧辊的开发和应用. 辽宁冶金, 4, pp.56-58, 1997.
37. 王世栋，加拿大多法斯科公司热轧带钢用高速钢轧辊的经验. 世界金属导报, 1998.

38. 周宏，大成桂作，王全国, 轧辊用高碳高速钢系合金的 KIC 及力学性能. 钢铁, 32(8)，pp.59-62, 1997.

39. 邵素云，王刚，宋威，谈高速钢轧辊．轧钢, 2, pp.37, 1996.

40. 刘海峰，刘耀辉. 高速钢复合轧辊的研究现状及进展．钢铁研究学报，11，p.67-71, 1999.

41. 佐野義一, 木村和夫, ホットストリップミル仕上後段作業ロールに生じるスポーリングの統計的解, 鐵と鋼:日本鐵鋼協會々誌, 73(9), pp.1154-1161, 1987.

42. Roll failures manual: Hot mill cast work rolls, The European Foundry Association, Roll Section, pp. 19, 2002.

43. E. Kingston and D. J. Smith, Residual stress measurements in rolling mill rolls using deep hole drilling technique, Ironmaking & Steelmaking, 32, pp.379-380, 2005.

44. F. Hosseinzadeh, D. J. Smith and C. E. Truman, Through thickness residual stresses in large rolls and sleeves for metal working industry. Materials Science and Technology, 25(7), pp.862-873, 2009.

45. X. Zhang, X. Song, L. Zhu and M. V. Li, Measurement and Prediction of Residual Stresses in Heat Treated Large Forgings, 5th International Conference on Thermal Process Modeling and Computer Simulation, USA, pp. 9-13, 2014.

46. Q. He and J. J. Xu, Residual stress assessment of the larger forged steel bearing roller, 6th Baosteel Biennial Academic Conference, Shanghai, 2015.

47. E. Kingston and D. J. Smith, Residual stress measurements in rolling mill rolls using deep hole drilling technique, Ironmaking & Steelmaking, 32, pp.379-380, 2005.

48. M. Hinnemann, P. J. Mauk, V. Goryany, C. Zybill, and R. Braun, Measurement of residual stress in work roll and backup rolls for strip and plate mills and its effect on the finial load situation, Key Engineering Materials, 622, pp.949-955, 2014.

49. J. H. Zheng. Analysis of residual stress and residual austenite detection in roller, Henan Metallurgy, 15, pp.53-56, 2007.

50. J. Pacyna, A. Kokosza and A. S Wojtas, Residual Stress Measurement in Steel Mill Rolls Using Magnetic Barkhausen Noise Analysis, NDT.net, 4(8), 1994.

51. C. C. Liu, X. J. Xu Z. Liu, A FEM modeling of quenching and tempering and its application in industrial engineering. Finite elements in analysis and design, 39(11), pp.1053-1070, 2003.

52. J. Pan, Y. Li and D. Li, The application of computer simulation in the heat-treatment process of a large-scale bearing roller, Journal of materials processing technology, 122(2), pp. 241-248, 2002.

53. 岡村一男，熱処理シミュレーションに必要な材料特性とデータベース. 熱処理, 42(5), pp.319-325, 2002.

54. 井上達雄，熱処理シミュレーションの歴史と現状．熱処理，42, pp.304−311, 2002.

55. G. Totten. M. Howes and T. Inoue, Handbook of residual stress and deformation of steel. ASM international, 2002.

56. C. Şimşir and C. H. Gür, 3D FEM simulation of steel quenching and investigation of the effect of asymmetric geometry on residual stress distribution. Journal of materials processing technology, 207(1), pp.211-221, 2008.

57. 寺崎俊夫，長谷川弘毅，福谷理明, 円柱の焼入れにより生じる残留応力について: 第 1 報 焼入れ過程で生じる温度分布の数値解析方法について．日本造船学会論文集，196, pp.17-23, 2004.

58. 寺崎俊夫，福谷理明，川上博己, 円柱の焼入れにより生じる残留応力について: 第 2 報 相変態で生じる応力の数値解析方法について．日本船舶海洋工学会論文集, 2, pp.169-177, 2005.

59. 井上達雄，田中喜久昭，変態を考慮した焼入れの解析. 材料, 22(234), pp.218-223, 1973.

60. 門河昌宏，長岐滋，井上達雄，鋼の焼入れと低温焼戻しにおける組織変化と応力解析. 材料，29(327), pp.1173-1179, 1980.

61. 王志剛，井上達雄，相変態の応力依存性を考慮した鋼の焼入れにおける温度組織および応力の解折，材料，32(360), pp.991-996, 1983.

62. I. Neira Torres, G. Gilles, J. Tchoufang Tchuindjang, J. Lecomte-Beckers, M. Sinnaeve and A. M. Habraken, Study of residual stresses in bimetallic work rolls, Advanced Materials Research. Trans Tech Publications, 996, pp. 580-585, 2014.

63. I. Neira Torres, G. Gilles, J. Tchoufang Tchuindjang, J. Lecomte-Beckers, M. Sinnaeve and A. M. Habraken, FE modeling of the cooling and tempering steps of bimetallic rolling mill rolls. International Journal of Material Forming, pp.1-19, 2015.

Chapter 2

Residual Stress Simulation during Uniform Heating Quenching

2.1 Introduction

Work rolls are used in the roughing stands of hot strip mill to reduce the steel thickness. They have to meet the requirements of hardness, wear resistance at the surface and toughness at the center [1-3]. Traditional single material roll cannot satisfy these conflicting properties at the same time. Many studies have been done to improve roll performance in the past decades. The bimetallic roll is one of the most important developments to resolve above problem [4, 5]. As shown in Figure 2-1, the bimetallic roll is manufactured by centrifugal casting method, using HSS as shell material and the ductile casting iron (DIC) as core material.

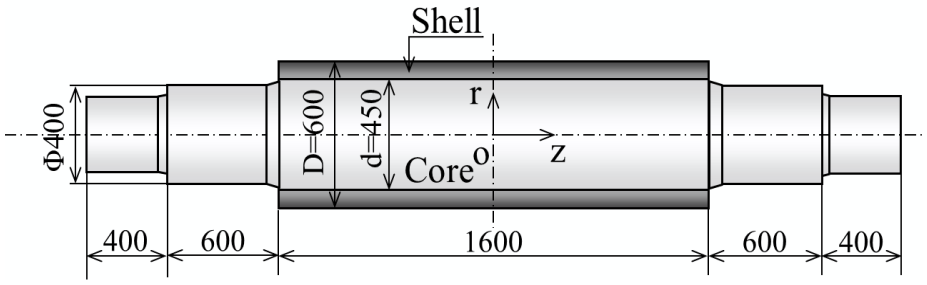

Figure 2-1 Schematic diagram of the HSS bimetallic roll (mm)

During heat treatment, residual stress is inevitably introduced due to temperature gradient and phase transformation [4, 10, 11]. The residual stress is self-equilibrating within the roll, independent of the any external loads. In addition, thermal stress is produced by heating-cooling thermal cycles during subsequent hot rolling process [12-15]. The existing residual stress will be added to thermal stress, leading to roll fracture. In order to prevent the thermal crack caused by

thermal behavior, suitable compressive stresses are necessary at the roll surface [16]. However, the tensile stress appearing at the center may cause the risk of fracture from the inside of the roll, whose distribution has not been investigated until now. The stable quality of the work roll is closely related to the quality of rolling product and manufacture cost [9, 12]. Therefore, the investigation of the residual stress is necessary and urgent in order to improve service life of the work roll. Despite a number of studies focused on residual stress caused by quenching in the past decades, most studies dealt with small size components [24-27]. Recently, Torres et al. analyzed bimetallic work rolls during post casting cooling stage [28]. Although they have studied the prediction of the residual stress on the high chrome steel roll, the most critical quenching process has not been covered yet.

In this chapter, a thermo-elastic-plastic finite element simulation will be performed by using MSC.Marc2012 to investigate the residual stress during quenching. In the first place, the simulation of bimetallic roll will be performed to investigate the generation mechanism and distribution of residual stress. Then, the effects of the shell-core ratio, diameter, phase transformation and material heat treatment process on the residual stress will be discussed.

2.2 Uniform heating quenching process for bimetallic roll

Figure 2-2 shows the schematic diagram of the heat treatment process including pre-heating, quenching and tempering. In pre-heating process, the whole roll is heated up to the uniform temperature of T_{Start} and kept for several hours. Then, the roll temperature drops rapidly through air cooling. After that, the roll is put into the furnace again and maintained at T_{Keep1} to prevent excessive thermal stresses caused by rapid cooling. After keeping period, the roll is cooled down slowly until to the temperature of T_{Finish}. After quenching process, the tempering process will be performed 2 to 4 times to release the residual stress and obtained the stable microstructure. The effect of tempering process will be studied in the Chapter 4.

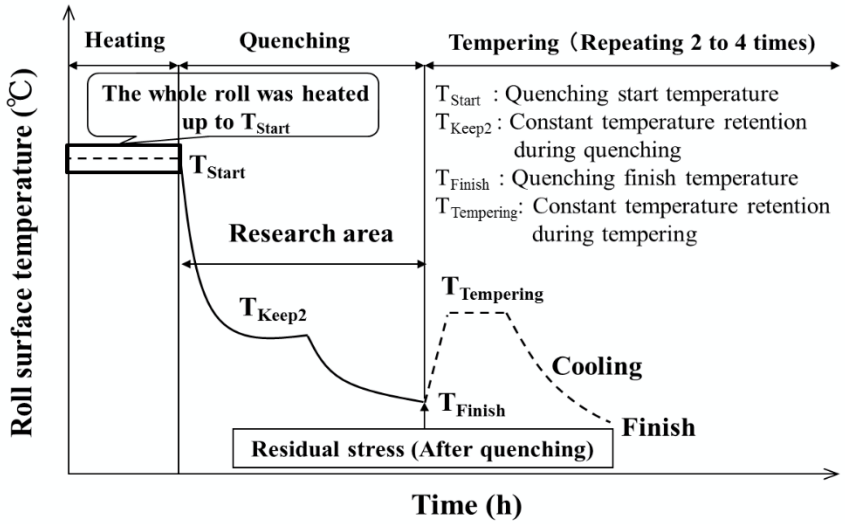

Figure 2-2 Uniform heating quenching process for bimetallic roll

2.3 Analysis method and FEM modeling

2.3.1 FEM model

As shown in Figure 2-1, the HSS bimetallic rolls with diameter of 600mm, body length of 1600mm and shell thickness of 75mm, consist of the high speed steel (HSS) as outer layer and the ductile casting iron (DCI) as inner layer and roll neck.

In this study, the MSC.Marc 2012 software is used to carry out FEM elastic-plastic analysis to simulate the quenching process for HSS bimetallic rolls. Figure 2-3 shows the axisymmetric FEM model of HSS bimetallic roll. The roll clutch with the length of 400mm is ignored because of the small effect on the residual stress at the central section. A 4-node linear axisymmetric quad element with the mesh size of 5×5mm is adopted for the transient-static simulation. The displacement boundary conditions and thermal isolation conditions are applied to z=0 due to the symmetry. In this study, roll surface temperature $T_{Surface}$ obtained by measuring experimentally is imposed to the roll surface.

At the beginning of this study, the heat transfer coefficient was obtained to confirm the FEM result. In this case, since the heat transfer coefficient depends on many factors, such as,

material, size, surface conditions of a part, the accurate heat transfer coefficient can be obtained in the following way. First, a value of heat transfer coefficient is assumed from the reference and applied to the roll surface. Second, $T_{Ambient}$ is applied to FEM model of the roll, then roll surface temperature $T_{Simulation}$ is obtained by the simulation and compared with $T_{Surface}$. Here, the ambient temperature $T_{Ambient}$ is obtained by measuring experimentally. Third, the reference heat transfer coefficient is changed repeatedly if $T_{Simulation} \neq T_{Surface}$. The real heat transfer coefficient is finally obtained when $T_{Simulation} = T_{Surface}$. The calculated heat transfer coefficients including effect of radiation are shown in Figure 2-4.

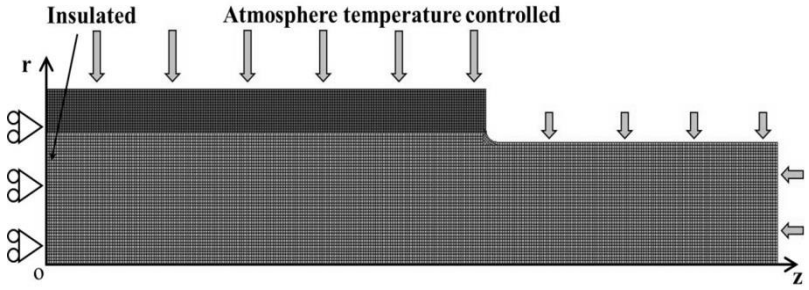

(mesh size: 5mm×5mm)

Figure 2-3 FEM model and boundary conditions for bimetallic roll

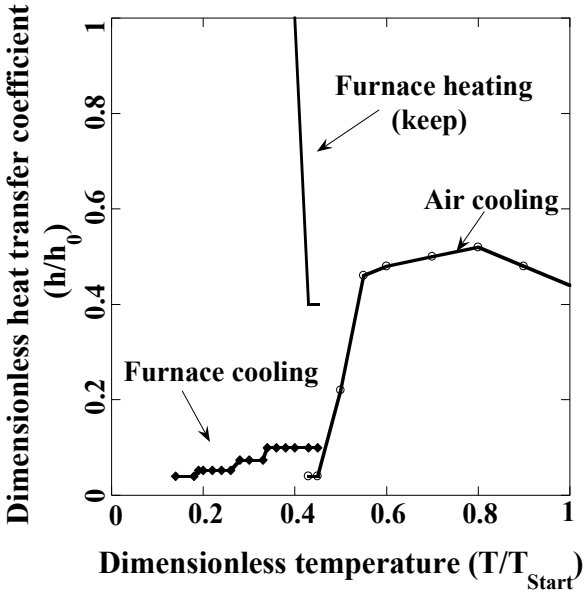

Figure 2-4 Heat transfer coefficients for bimetallic roll during uniform quenching process

2.3.2 Material properties used for FEM analysis

To analyze quenching process, a large amount of material properties are necessary regarding two different materials in the bimetallic roll. Those material properties include Young's modulus, thermal expansion coefficients, specific heat, density, yield stress, thermal conductivity and Poison's ratio. Table 2-1 shows the chemical compositions of high speed steel and ductile casting iron for the common high speed steel bimetallic rolls. Table 2-2 shows the summary of material properties required for FEM analysis at room temperature.

Table 2-1 Chemical compositions of high speed steel and ductile casting iron for high speed steel roll /mass%

Composition	C	Si	Mn	P	S	Ni	Cr	Mo	Co	V	W	Mg
HSS	1-3	<2	<1.5			<5	2-7	<10	<10	3-10	<20	<10
DCI	2.5-4	1.5-3.1		<0.1	<0.1	0.4-5	<1.5	0.1-1				0.02-0.08

Table 2-2 Mechanical properties of high speed steel and ductile casting iron at room temperature

Property	Shell	Core
0.2% proof stress [MPa]	(1282)[*1]	415
Young's modulus [GPa]	233	173
Poisson's ratio	0.3	0.3
Density [kg/m^3]	7.6	7.3
Thermal expansion coefficient [K^{-1}]	12.6×10^{-6}	13.0×10^{-6}
Thermal conductivity [W/(m・K)]	20.2	23.4
Specific heat [J/(kg・K)]	0.46	0.46

[1)] Tensile strength of the shell material is indicated as the 0.2% proof stress because the deformation at break is small

Since the required material properties are depending on the temperature, therefore, those data have to be obtained under the wide range of temperature including high temperature region which are difficult to be obtained. In this study, the material properties of shell and core material were measured from room temperature to T_{Start} at a certain temperature interval. In order to ensure the accuracy of simulation, the experimental data are obtained along the same temperature process of quenching.

2.3.2.1 Tensile test

The tensile test was conducted by using a standard testing machine INSTRON 5587 with the tensile speed 2.5%/min. The specimens shown in Figure 2-5 were prepared from HSS bimetallic roll. The temperature conditions of the specimen for the tensile test is shown in Figure 2-6. The specimens were heated up to T_{Start} with the speed of 500℃/h, then, cooled down to the testing temperature including room temperature, and T_{Start} -100℃ at the interval of 100℃. The cooling speeds of the specimens were the same as the speeds of roll quenching. The specimens were kept at the testing temperature for 20 minutes after cooling process. Young's modulus, yield stress and Poison's ratio are obtained from tensile test.

2.3.3.2 Dilatometer experiment

The tests are conducted by using thermal mechanical analysis method.[29] The specimens were prepared from HSS bimetallic roll, with 8mm thickness, 8mm width and 17mm length. The cooling speed is the same as the one of quenching without considering keeping temperature process of real roll in Figure 2-2. The test temperature was in the region from T_{Start} to room temperature. Thermal expansion coefficients are obtained from dilatometer experiment.

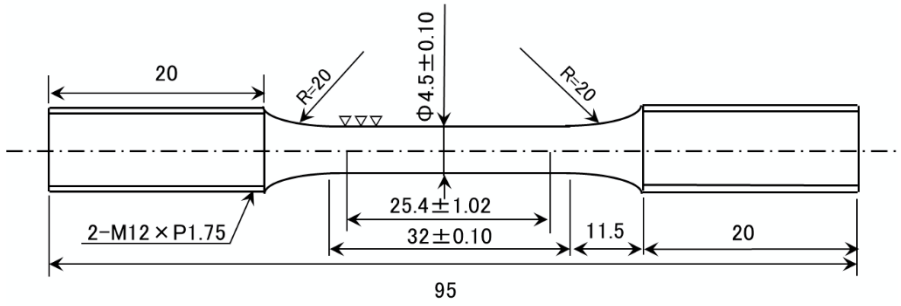

Figure 2-5 Specimen of the tensile test (mm)

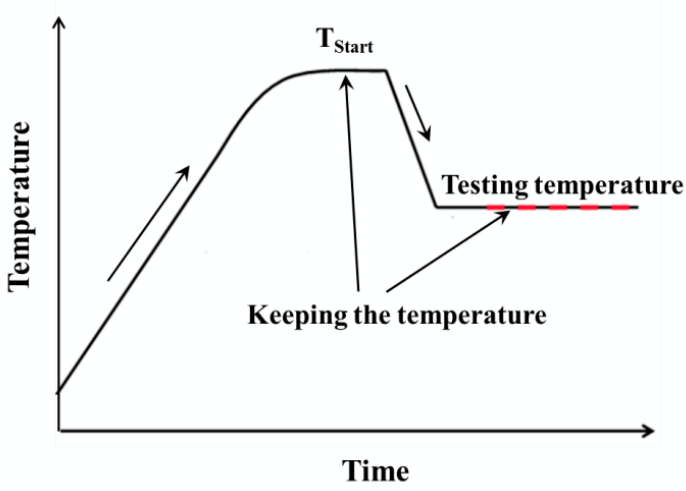

Figure 2- 6 Temperature conditions of the specimen for the tensile test

The input data of material properties of high speed steel and ductile casting iron depending on temperature are shown in Figure 2-7. In this study, those material data cannot be indicated in detail because they are confidential data of the roll manufacturing company. According to the custom of this industrial field, the chemical composition, dissolution method, casting conditions and heat treatment, especially the high temperature properties, are regarded as the trade secret belonged to the owner. In this paper, therefore，the dimensionless values have to be used to characterize the material properties heat treatment process. Since the purpose of this paper is to clarify the residual stress during quenching process, the simulation results are still useful enough

for the readers to understand the generation mechanism and the residual stress distribution.

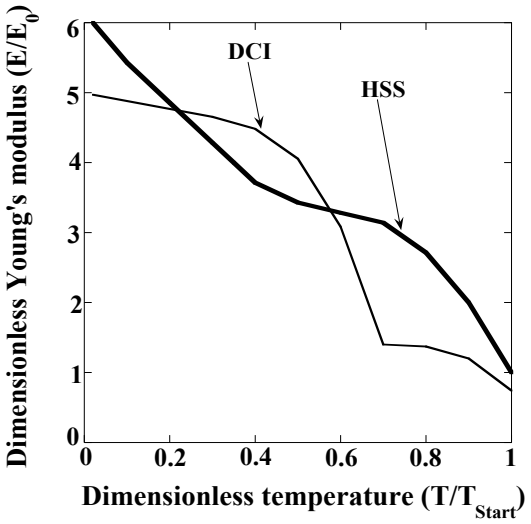

(a) Young's modulus

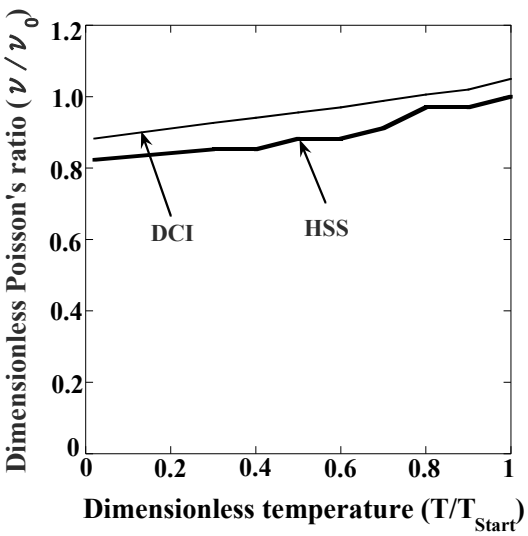

(b) Poisson's ratio

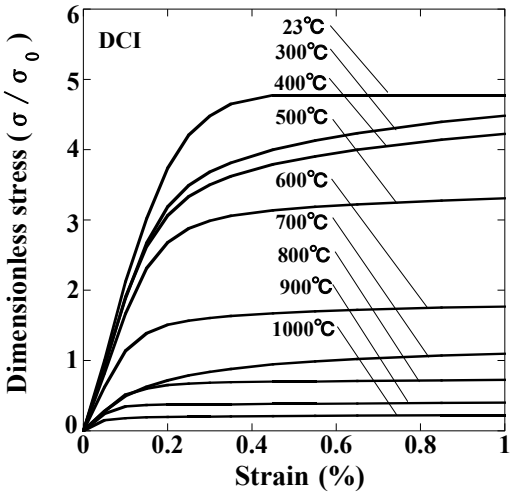

(c) Stress-strain curves of ductile casting iron

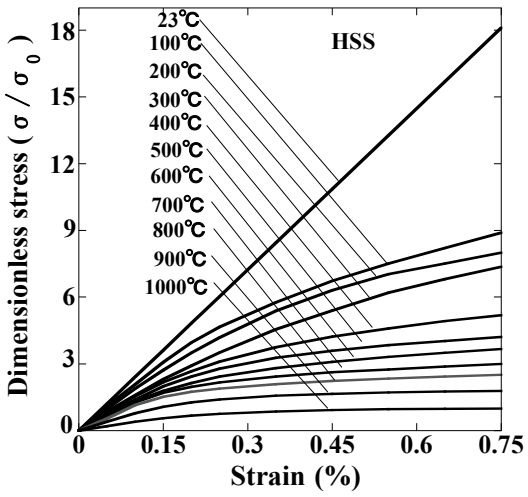

(d) Stress-strain curves of high speed steel

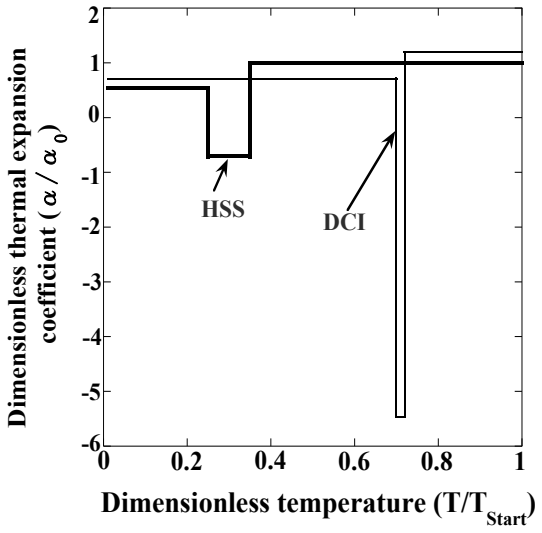

(e) Thermal expansion coefficient

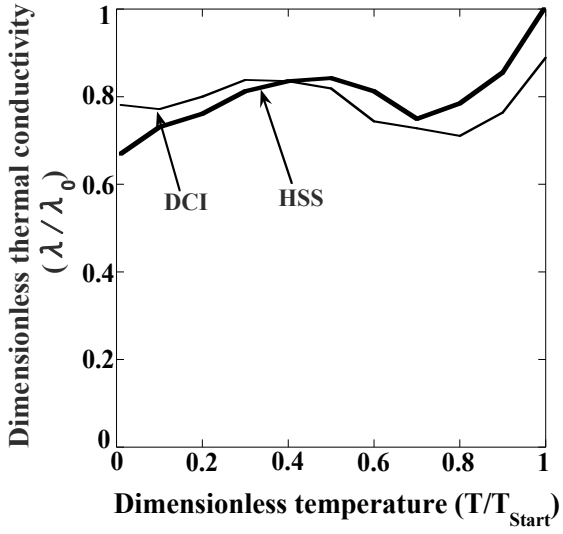

(f) Thermal conductivity

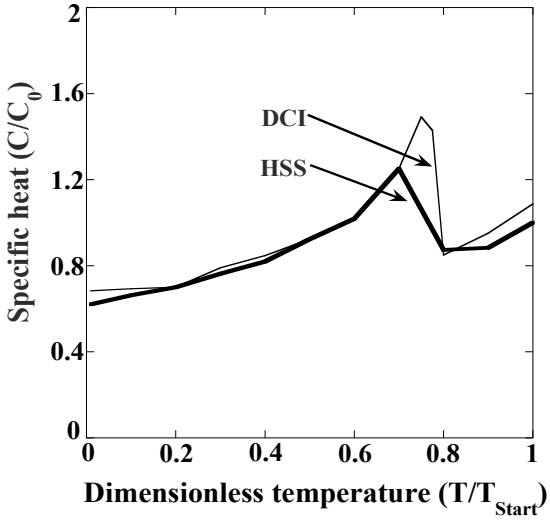

(g) Specific heat

Figure 2- 7 Material properties dependent on temperature for high speed steel and ductile casting iron

2.4 Residual stress generation mechanism for single material roll

In the first place, by taking an example of a single material roll of ductile casting iron, the generation mechanism of residual stress will be discussed during quenching process. To simplify the simulation, an axisymmetric FEM model is performed without considering the phase transformation and roll diameter change in the z-direction.

Figure 2-8 shows the histories of (a) temperature, (b) stress σ_z and (c) Young's modulus for the roll during quenching process. Since FEM elastic-plastic analysis needs Young's modulus even under high temperature, a specific stress point is focused when the strain reaches 0.05% on the stress-strain curve. Then, the Young's modulus is defined as the gradient of the line connecting the origin and the specific point. Figure 2-8(c) shows the Young's modulus during quenching process, which varies depending on temperature.

The quenching process is divided into Region Ⅰ, Region Ⅱ and RegionⅢ classified by the dominant elastic or plastic state at the surface and center. In the Region Ⅰ, the yield strength of shell and core is very low due to high temperature, the stress rapidly increases and exceeds the yield stress. Therefore, the large plastic deformation occurs at both roll surface and roll center. In the Region Ⅱ, since the surface becomes elastic due to surface cooling, the surface Young's modulus increases with decreasing temperature although the center still keeps high temperature and plastic state. In the RegionⅢ, since both surface and the center become elastic, both Young's modulus increases as the cooling continues.

In Region Ⅰ, at the beginning of the cooling, the surface temperature drops faster than the center temperature, leading to the temperature gradient in the r-direction (Fig.2-8(d)①). Afterwards, the roll surface shrinks relative to the center in the axial direction and results in tensile stress. In order to balance the stresses in the roll interior, the compressive stress appears in the roll center. With increasing the temperature gradient, the stress at the roll surface and center increase together continuously.

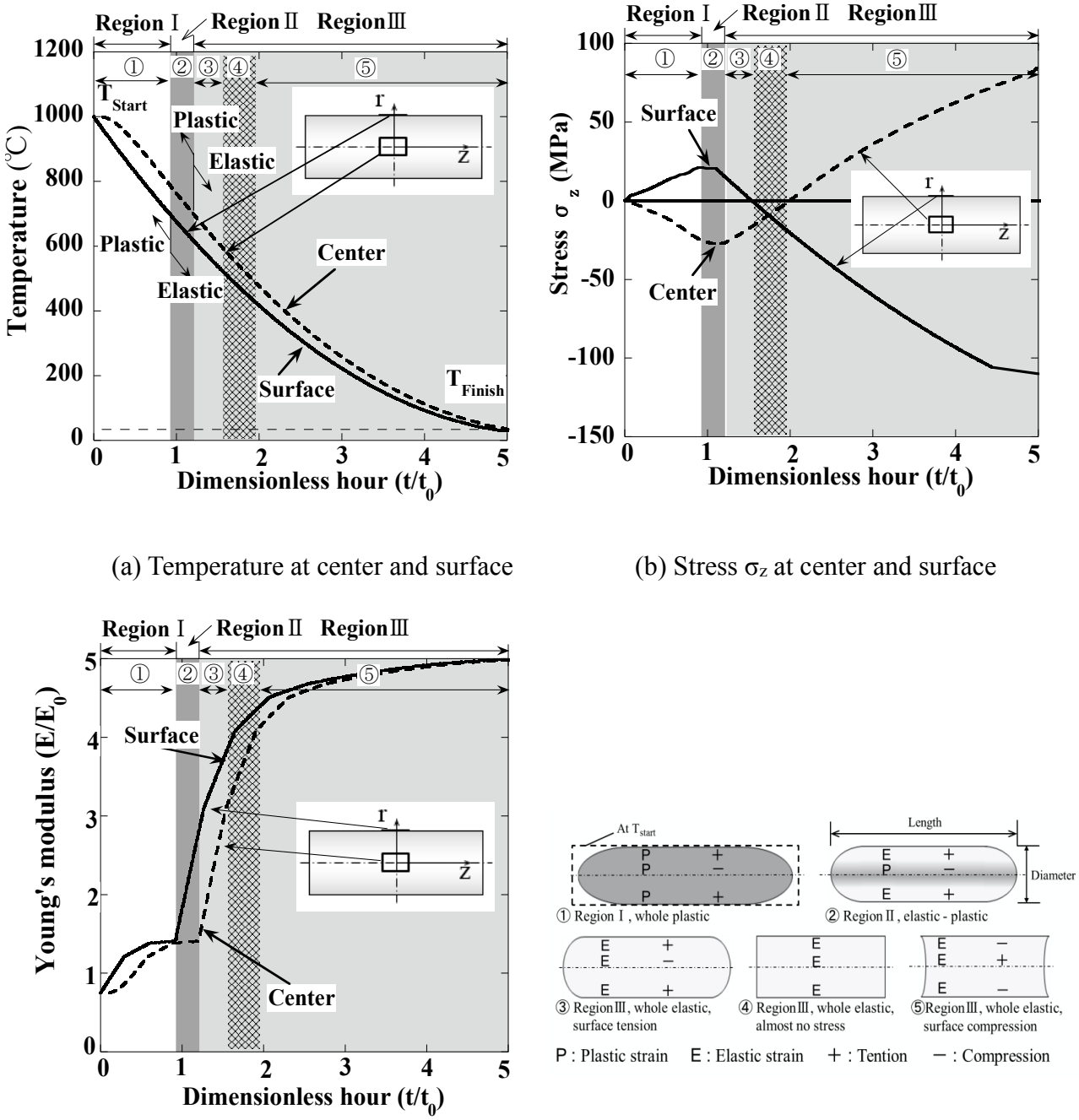

(a) Temperature at center and surface

(b) Stress σ_z at center and surface

(c) Young's modulus at center and surface

(d) Deformation and stress state

Figure 2-8 Residual stress generation mechanism for single material roll

In Region Ⅱ, due to continuous cooling, the roll surface turns to be elastic with increasing the Young's modulus. Meanwhile, the roll center is still plastic keeping high temperature (see

Figure 2-8(d)②). In this period, the thermal contraction at the surface is restricted due to the appearing of elastic state. However, the thermal contraction rate at the center is faster than that one at the surface, causing the thermal strain differences decreasing. Finally, both surface and center stresses reach peak values.

In Region Ⅲ, thermal strain differences decreasing due to the center's thermal contraction rate is larger than surface, both surface and center stresses start decreasing (Figure 2-8 (d)③). As the cooling continues, the surface thermal contraction is approximately equal to the center thermal contraction, then the stresses state are interchanged (Figure 2-8(d)④). Since the center contraction is larger than surface, the tensile stress increases at the roll center (Figure 2-8(d)⑤). Since Young's modulus increases in regionⅢ(Figure 2-8(c)), the compressive stresses at the roll surface increases as well as the tensile stress at the roll center. Finally, the compressive at the surface and tensile stress at the center are generated as shown in Figure 2-8(b).

2.5 Residual stress generation mechanism for HSS bimetallic roll

Figure 2-9 shows the histories of (a) temperature, (b) stress σ_z and (c) Young's modulus for the bimetallic roll during quenching process. The initial residual stress before quenching can be eliminated because of the pre-heating to high temperature of T_{Start}. In the Region Ⅰ, the roll is cooled down from T_{Start}, the surface temperature rapidly drops. As a result, tensile stress is produced at the surface and compressive stress is produced at the center.

In the Region Ⅱ, at the temperature of T_{EP}, the surface changes into elastic-plastic while the center still keeps plastic. In addition, the dropping speed of surface temperature decreases. As a result, the center thermal contraction becomes larger than surface thermal contraction, leading to the stresses at the center and the surface decrease. As center temperature dropping to the temperature of $T_{Pearlite}$, pearlite transformation happens near the boundary and expands toward the center. In this period, the center is shrunk relative to the other parts of the core which expand

gradually due to pearlite transformation. Hence, the compressive stress at the center decreases until becomes tensile stress. The tensile stress reverses to compressive stress rapidly when the pearlite transformation reaches to the center.

In the Region Ⅲ, the center is further contracted relative to the surface because of larger temperature change. Then, the surface stress state interchanges from tension to compression, and the center stress state interchanges from compression to tension. Until reaching T_{Keep1}, both surface and center stresses increase continuously. During keeping T_{Keep1}, the stresses at the surface and the center decrease because of the decreasing of temperature gradient. At the temperature of $T_{Bainite}$, bainite transformation occurs at the surface, causing a volume expansion and the surface compressive stress increases. To balance the increase of surface stress, the center tensile stress also increases. After the bainite phase transformation, the thermal contraction difference becomes larger and Young's modulus increases with decreasing temperature. Eventually, both surface and center residual stresses increase continuously.

Figure 2-10 shows the residual stress for HSS roll with D=600mm in Figure 2-1 in comparison with the previous experimental results σ_θ for HSS rolls with D=335mm [16], D=600~850mm [30]. Here, it should be noted that the casting method and core material between roll in Figure 2-2 and HSS rolls with D=335mm, D=600~850mm are different. Although usually the different casting process and core material cause different residual stress, the residual stresses are nearly the same because of the following reasons. First, the effect of different casting method can be eliminated because of the pre-heating to the high temperature of T_{Start} before quenching. Second, the effect of different core materials is smaller during the same quenching process because thermal expansion properties are similar and only the pearlite transformation occurs for both materials during this process [31]. Third, the effect of diameter on the residual stress was previously investigated by the roll industry and it was found that the surface residual stresses are similar when the rolls have the same diameter. The results in later chapter in this paper also show

that the surface residual stresses under the same roll diameter are almost independent of the shell-core ratio. Therefore, these three results can be compared, especially at the roll surface.

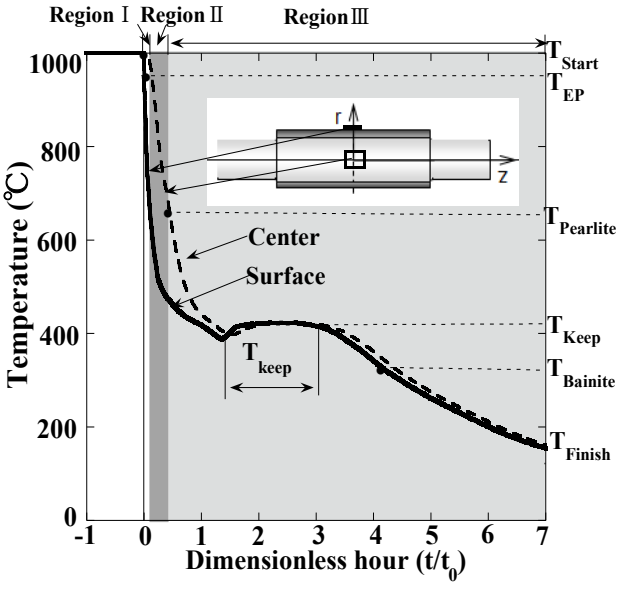

(a) Temperature histories

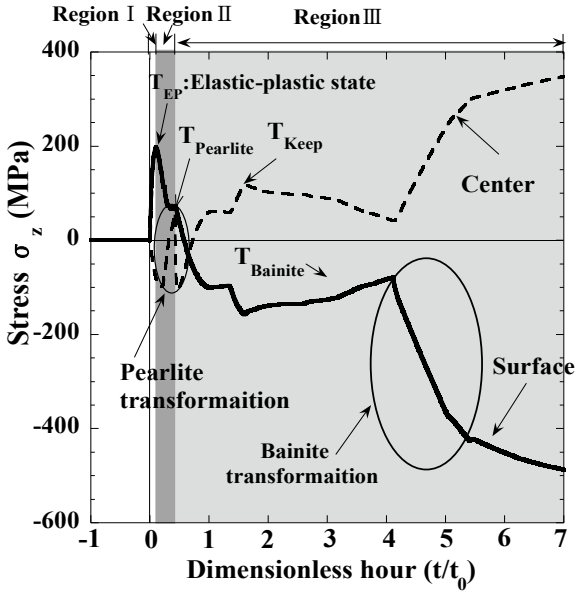

(b) Residual stress σ_z histories

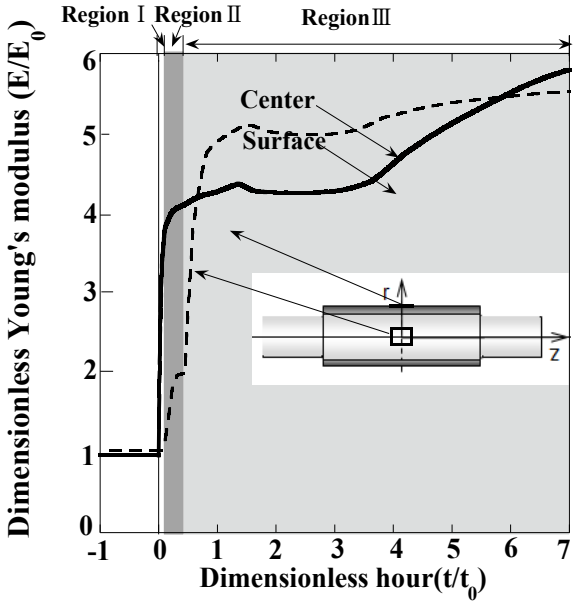

(c) Young's modulus histories

Figure 2-9 Residual stress generation mechanism of bimetallic roll during uniform heating quenching

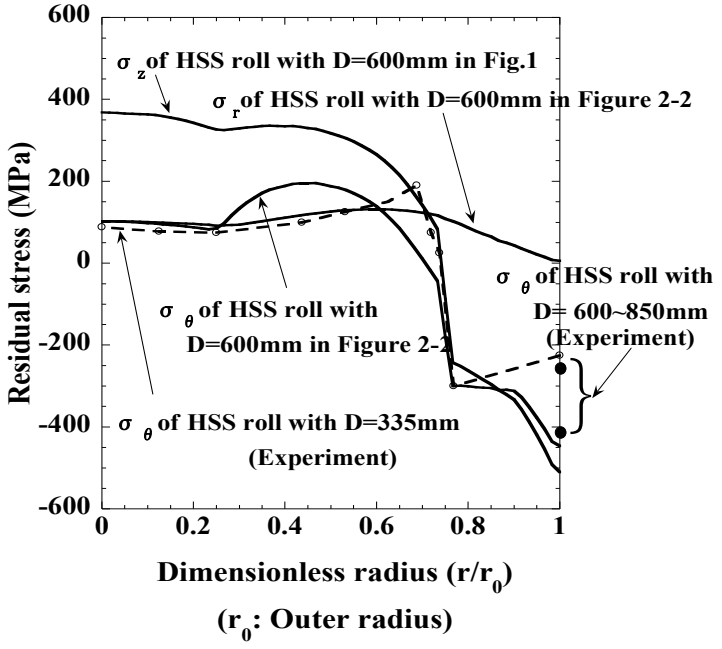

Figure 2-10 Simulation residual stress in comparison with the previous experimental results σ_θ of HSS roll with the steel shaft [16, 30]

2.6 Results and Discussion

2.6.1 Effect of shell-core ratio on residual stress

Because of the difference between the shell material and core material of the bimetallic roll, the component ratio of the shell and core influences roll performance. Hence, we should pay attention to the effect of shell-core ratio on residual stress. The equation of shell-core ratio is given as Equation 1:

$$\frac{A_S}{A_C} = \frac{D^2 - d^2}{d^2} \tag{1}$$

where As is the shell area, Ac is the core area, D is the shell diameter, d is the core diameter.

During the hot strip rolling process, since the work roll is subject to severe thermal stress, it

is necessary to grind the roll surface every time after a certain amount of wear appears. In addition, the oxidation, fire cracks and sticking might sometimes occurring on the roll surface must be removed by grinding if troubles happen [32]. After being repeatedly polished, the shell thickness is gradually thinned until to the limit, then the roll becomes useless.

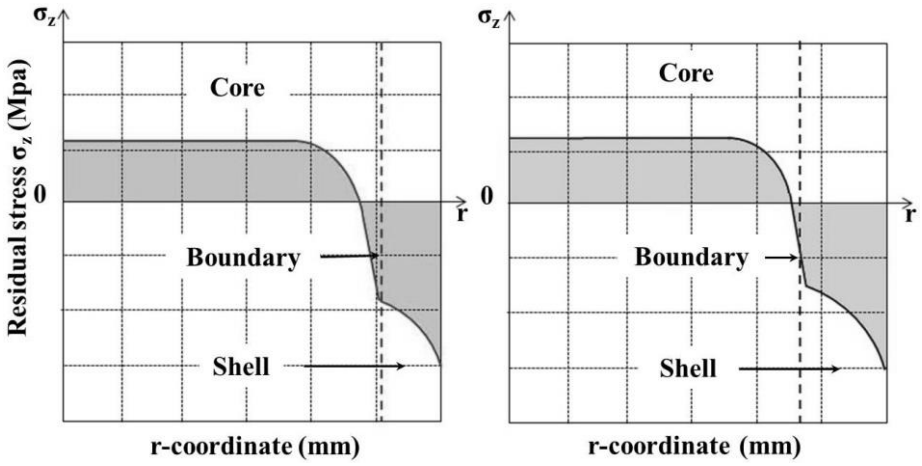

a) A_s/A_c=small b) A_s/A_c=large

Figure 2-11 Schematic diagram of residual stress distribution

Although the larger shell-core ratio enhances roll service life under the same roll diameter, the larger tensile stress at center will be produced and causes risk of fracture. Figure 2-11 shows a schematic illustration of the residual stress. It shows that under larger shell-core ratio, the larger tensile stress should appear at the core in order to balance the larger compressive region. Therefore, it has been thought that the larger shell-core ratio results in larger risk of fracture. To confirm the validity of this conventional conception, the effect of shell-core ratio on the residual stress will be discussed.

Figure 2-12 shows the residual stress distribution for different shell-core ratios when roll diameter D = 600mm. Here, the analysis method and roll surface temperature are the same as the one in Figure 2-3. Although the As/Ac of the real roll lies in the range of 0.4 to 0.6, a larger

range of 0.2 to 0.8 is chosen to clarify the effect. In Figure 2-12, the tensile residual stress at the center increases with increasing As/Ac. The tensile stress increases by 9％ in the range of 0.2 to 0.8, while only increases by 2％ in the range of 0.4 to 0.6. The compressive stresses at the surface are almost unchanged. The results show that the shell-core ratio has a little influence on the residual stress of the bimetallic roll.

As shown in Figure 2-11, the compressive residual stress rapidly decreases from the surface to the boundary, and the compressive stress region dose not increase with increasing As/Ac. As a result, the increasing of compressive stress region is smaller than the increase imaged conventionally. Therefore, the effect of shell-core ratio on the residual stress is less than expected result.

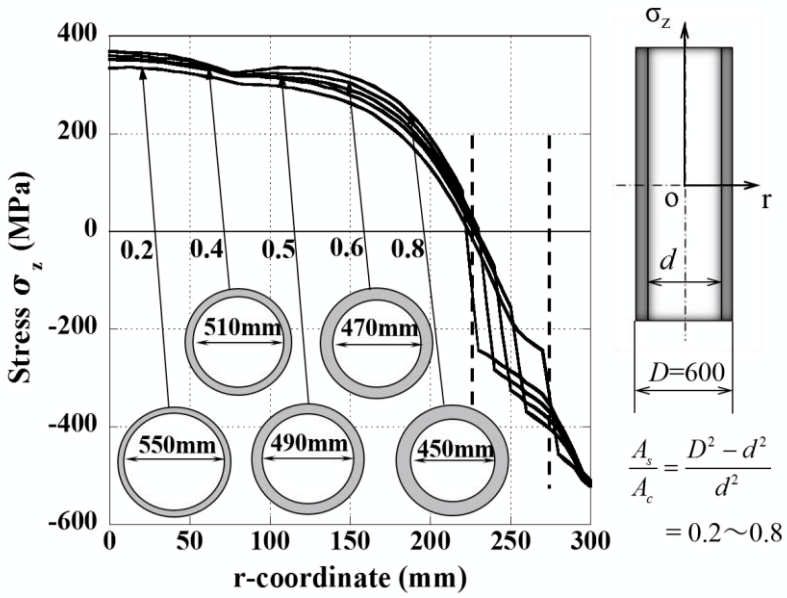

Figure 2-12 Distribution of residual stress σ_z for different As/Ac when D=600mm

2.6.2 Effect of roll diameter on residual stress

Figure 2-13 shows the residual stress distribution of bimetallic roll with diameter D = 500mm ~ 1000mm at As/Ac = 0.4. Here, the analysis method and roll surface temperature are the same as the one in Figure 3. The center stress increases by 51% and the surface stress increases by 55% with increasing roll diameter. By contrast, the center stress increases by 13% and the surface stress increases 19% in the range of 600mm to 800mm of real roll. The results show that the roll diameter has a significant effect on the residual stress. However, the center stress decreases when D = 900mm ~ 1000mm. However, it can be found that the most of the maximum residual stress in the core occur at r = d/2. The maximum residual stress is important for the evaluation of the roll strength. Therefore, we focus on this stress instead of the stress in the center. The stress at r = d/2 is shown in the solid circle ● in the Figure 2-13. It is seen that representative stress at r = d/2 increases with increasing roll diameter.

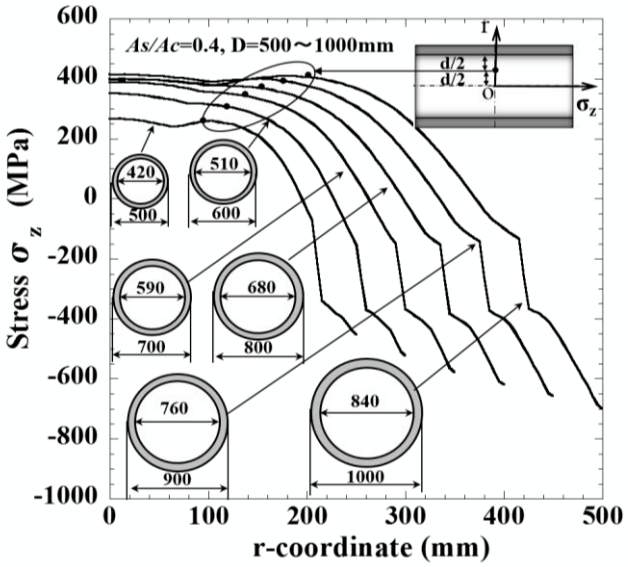

Figure 2-13 Distributions of residual stress σ_z of bimetallic roll for different roll diameter when As/Ac=0.4

2.6.3 Effect of phase transformation on residual stress

During quenching process, the pearlite transformation occurs in the core material and bainite transformation occurs in the shell material. Volume expansions of core and shell happen with the phase transformations. The amount of expansion in the phase transformation has a significant effect on the residual stress. Therefore, the effect of the expansion on the residual stress will be discussed.

The solid lines in Figure 2-14 show the dilatometer curves of shell and core material during quenching process, which is obtained from dilatometer experiment. In order to analyze the effect of the expansion on the residual stress quantitatively, the dilatometer curve with half amount of expansion is assumed. As shown by dotted lines in Figure 2-14(a), the starting point of the half expansion curve is assumed along the middle point of the beginning and ending point of the real phase transformation. The gradient of the half expansion curve is assumed as the middle value of the curves gradient before and after phase transformation. It should be noted that the changes of the others material properties caused by this half dilatometer curves are assumed to be ignored. In the simulation, the effect of expansion is expressed by thermal expansion coefficient. Figure 2-15 shows the thermal expansion coefficients used as the input data of FEM, which is calculated based on dilatometer curves. The thermal expansion coefficient with the half expansion of pearlite transformation is called half pearlite (Half P) as well as the half bainite (Half B). The real thermal expansion coefficients are called real pearlite (Real P) and real bainite (Real B). In FEM analysis, only the thermal expansion coefficient will be changed and the other parameters remain unchanged.

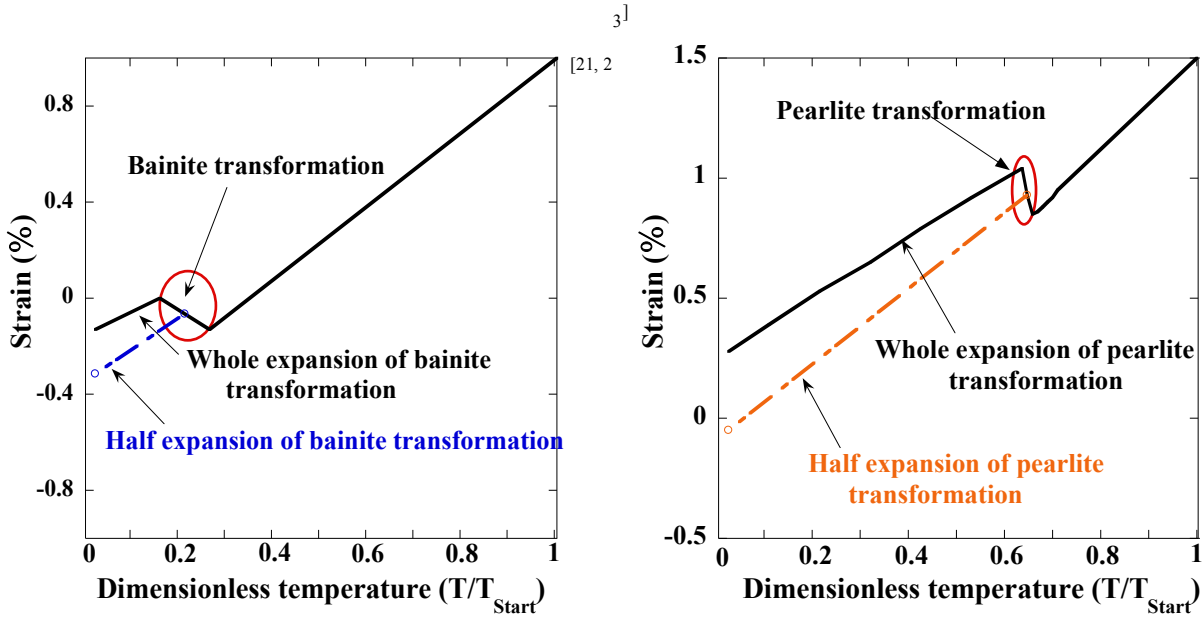

(a) Dilatometer curve of high speed steel (b) Dilatometer curve of ductile casting iron

Figure 2-14 Dilatometer curve of high speed steel and ductile casting iron during uniform heating quenching process

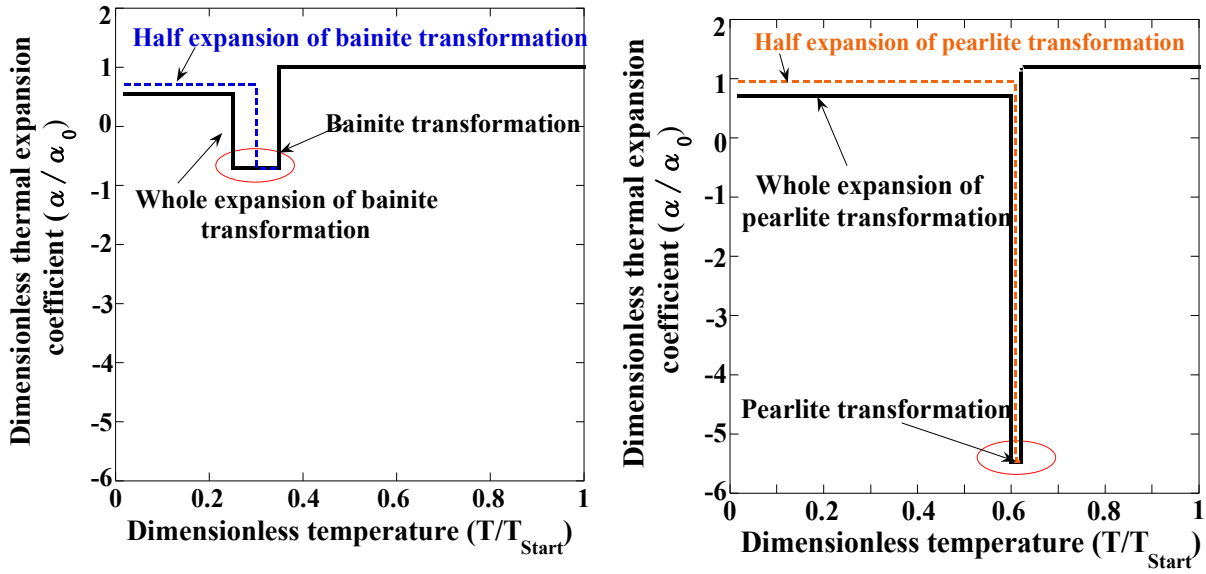

(a) High speed steel (b) Ductile casting iron

Figure 2-15 Thermal expansion coefficient of high speed steel and ductile casting iron during uniform heating quenching process

The simulation is initially performed when the thermal expansion coefficients of shell and core material are changed together. Figure 2-16 shows the comparison of residual stress between Half P + Half B and Real P + Real B. The center stress increases by 24% and the surface stress increases by 60%. The result shows that phase transformation has a significant effect on the residual stress.

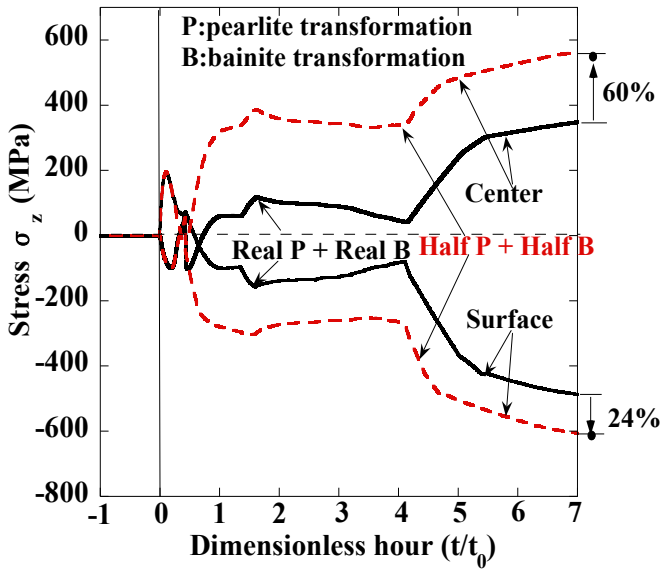

Figure 2-16 Effect of half P + Half B on residual stress

In order to clarify the distinct effect of pearlite transformation and bainite transformation, the half P and half B is performed independently. The two cases are performed: 1) Half P + Real B; 2) Real P + Half B.

In the case of Half P + Real B, the center stress increases by 76% and the surface stress increases by 41%. As shown in Figure 2-17, in the case of Half P, the center stress decreases by only half compared with the result of Real P. In addition, the tensile state of the surface is released because the expansion value of core material decreases. Therefore, the surface stress obviously decreases compared with the result of Real P at the ending of the pearlite transformation. As a result, the center tensile stress and the surface compressive stress obviously

increases in the case of Half P + Real B. The results show that the pearlite transformation contributes to decreasing the residual stress.

In the case of Real P + Half B, the center stress decreases by 40％ and the surface stress decreases by 33％. As shown in Figure 2-18, the stresses of center and surface are the same as the results of Real P + Real B before the bainite transformation. Since the surface stress is in tensile state when bainite transformation happens, the expansion will intensify this state and the surface stress will increase. Therefore, the tensile stress will decrease with decreasing expansion. In the case of Real P + Half B, the surface stress only increases by half compared with the result of Real P + Real B. As a result, the center tensile stress and the surface compressive stress obviously decreases in the case of Real P + Half B. The results show that bainite transformation results in increasing of residual stress.

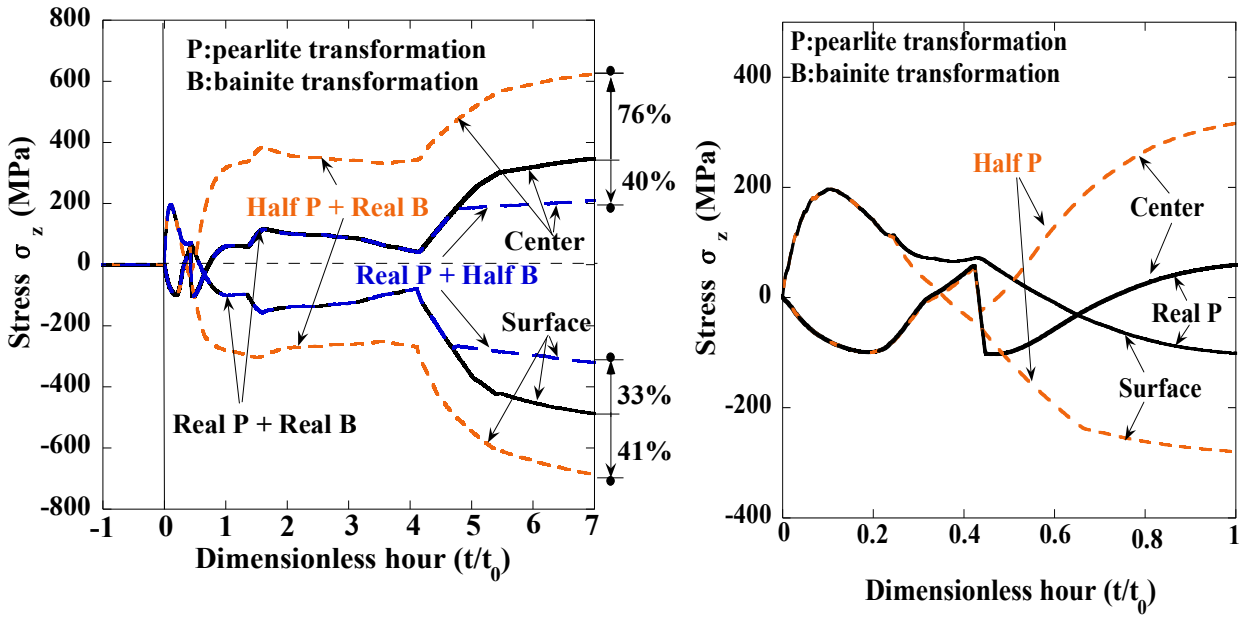

(a) Half P + Real B and Real P + Half B (b) Initial of quenching process

Figure 2-17 Difference effects of Half P + Real B and Real P + Half B

2.6.4 Effect of material's heat treatment on residual stress

Material property depends on heat treatment as well as the temperature. To ensure the simulation accuracy, the material properties should be distinguished in the heating process from room temperature and in the cooling process from T_{Start}. The tensile test of the cooling process from T_{Start} has been described in Chapter 2.3.2.1, and the heating process from room temperature is described as follows. The specimens were heated up to temperature testing temperature from room temperature with the speed of 500℃/h and kept at this temperature for 20 minutes. The testing temperature of heating process includes room temperature, and 100 ~ T_{Start} at the interval of 100℃.

In Figure 2-18, the stress-strain curves of the shell material at 600℃ are compared after heating from room temperature and cooling from T_{Start}. Here, σ_0 is the maximum stress corresponding to ε=0.65% of the shell material at 600℃ after heating process from room temperature. In Figure 2-18 the maximum stress difference reaches 67% between the two heat treatment processes. It is found that the heat treatment significantly affects material mechanical property. The specimens were prepared from the shell of the roll that was quenched and tempered. The stress-strain curve indicated as "After heating process" in Figure 2-18 was obtained from the tensile test specimens after heated up to 600℃ from room temperature. In this case, although the specimens are tempered, the strength is not very much smaller than the strength under room temperature. On the other hand, the stress-strain curve indicated as "After cooling process" in Figure 2-18 was obtained from the tensile test specimens after heated up and cooled down from T_{Start} (about 1000℃) to 600℃ by using the same cooling speed of roll quenching. In this case, since the specimens are quenched, the material strength is similar to the strength of austenite state and therefore much smaller than the strength of "After heating process" in Figure 2-18.

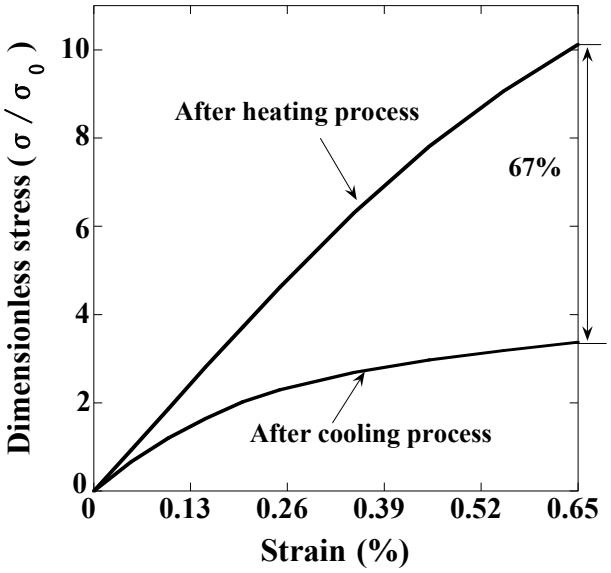

Figure 2-18 Stress - strain curves for the shell material at 600℃ after heating process from room temperature and cooling process from T_{Start}

Figure 2-19 shows the contours of residual stress σ_z after quenching. At the central cross section, the maximum compressive stress appears at the surface and the maximum tensile stress occurs at the center independent of the roll neck. Significant difference can be seen due to the data difference between cooling process form T_{Start} and heating process from room temperature.

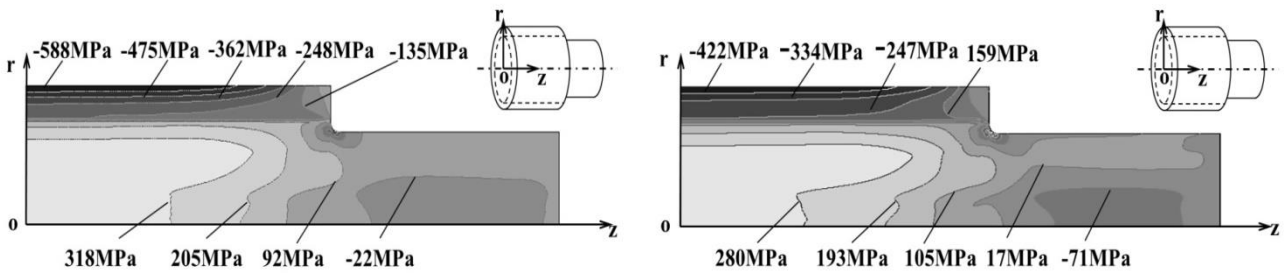

(a) Using the heating process data (b) Using the cooling process data

Figure 2-19 σ_z after quenching for using heating process data and cooling process data

Figure 2-20 shows the distribution of σ_z at z=0. By using the cooling process data, the center stress decreases by 15% and the surface stress decreases by 27%. The residual stresses obtained from the cooling process data are similar to the results of HSS roll with the alloyed steel shaft.[33] Therefore, the necessity of cooling process data to the simulation is verified. However, the tensile stress of 368MPa at the center and the compressive stress of 510MPa at the surface are still larger than the previous result. In Figure 2-20, σ_z at the roll center reaches 430MPa, which is larger than the yield stress 415MPa given in Table 2. However, Mises equivalent stress at the same point is only 289MPa, which is smaller than the yield stress.

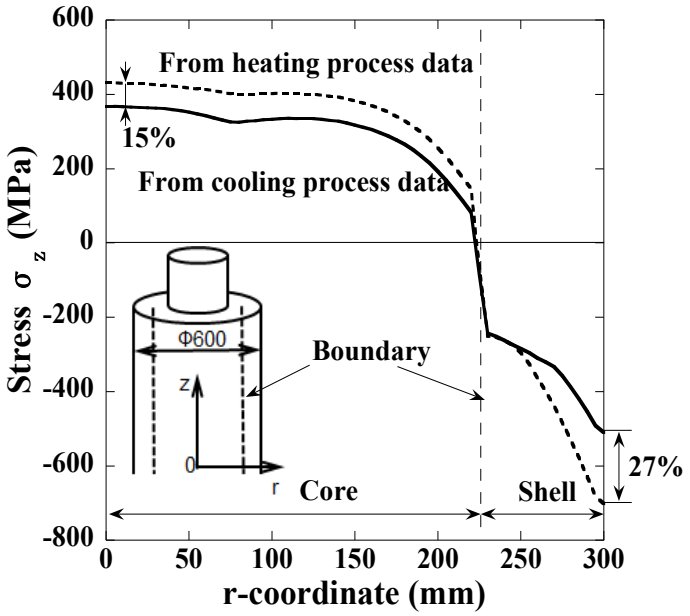

Figure 2-20 Distributions of residual stress σ_z obtained from heating process from room temperature and cooling process from T_{Start}

2.7 Conclusions

In this Chapter, FEM analysis is performed to predict the residual stress generated during uniform quenching for bimetallic work rolls using for hot strip rolling. The generation mechanisms of the residual stress have been discussed for single material roll and bimetallic roll.

The results of the current study can be summarized as follows.

(1) Predicting the residual stress of the bimetallic roll during quenching is realized by FEM simulation efficiently with lower cost and higher accuracy compared with experimental measurement. After quenching, the compressive stress appears at the shell while the tensile stress appears at the core.

(2) The effect of shell-core ratio on the residual stress is very small. The center stress increases only by 2% and the surface stress is almost unchanged with increasing As/Ac from 0.4 to 0.6.

(3) The roll diameter has a significant effect on the residual stress. The center stress increases by 13% and the surface stress increases by 19% with increasing the diameter from D=600mm to D=800mm. However, the center stress decreases with increasing from D=900 to D=1000mm.

(4) Phase transformation has a significant effect on the residual stress. Pearlite transformation contributes to decreasing the stress, while bainite transformation leads to increasing of stress.

(5) Material properties depend on the heat treatment as well as the temperature. Therefore, by using the cooling process data, the center residual stress decreases by 15% and the surface residual stress decreases by 27% compared with the results by using the heating process data.

Reference

1. J. W. Choi and D. Kim, Mechanisms of surface deterioration of high-Ni grain roll for hot strip rolling, ISIJ Int. 39(8), pp. 823-828, 1999.
2. 野口紘, 渡辺靖夫, 熱間圧延用ロ-ル材の高温における摩擦と摩耗, 川崎製鉄技報, 19(3), pp. 195-201, 1987.
3. M. Nilsson and M. Olsson, Microstructural, mechanical and tribological characterisation of

roll materials for the finishing stands of the hot strip mill for steel rolling, Wear. 307(1), pp. 209-217, 2013.

4. K. Ichino, Y. Kataoka and T. Koseki, Development of centrifugal cast roll with high wear resistance for finishing stands of hot strip mill, Kawasaki Steel Technical Report. 37, pp. 13-18, 1997.
5. M. Shimizu, O. Shitamura, S. Matsuo, T. Kamata and Y. Kondo, Development of high performance new composite roll, ISIJ Int. 32(11), pp. 1244-1249, 1992.
6. H. G. Fu, A. M. Zhao and J. D. Xing, Development of centrifugal casting high speed steel rolls, J. Univ. Sci. Technol. Beijing. 10(6), pp.61-66, 2003.
7. H. Takigawa, T. Tanaka, S. Ohtomo, Development of high-speed tool steel rolls and their application to rolling mills, Nippon Steel Tech. Rep. 74, pp. 77-83, 1997.
8. H. G. Fu, H. J. Zhao, Z. Z. Du, Z. J. Feng, Y. P. Lei, Y. Zhang, M. W. Li, Y. H. Jiang, R. Zhou and H. X. Guo, Heat treatment of centrifugally cast high carbon high vanadium high speed steel mill roll, Ironmaking & Steelmaking. 38(5), pp. 338-345, 2011.
9. Jr. M. Boccalini and A. Sinatora, Microstructure and wear resistance of high speed steels for rolling mill rolls, Proc. of 6th Int. Tooling Conference. Karlstads University, Karlstad, 2002, 425.
10. L. D. V. Z. VRO and E. Valjanje, A modified heat treatment to improve the properties of double-layer cast rolls, Mater. Tehnol., 48(6), pp. 983-990, 2014.
11. B. Podgornik, S. Milanović, and J. Vižintin, Effect of different production phases on residual stress field in double-layer cast rolls, J. Mater. Proc. Technol., 210(8), pp. 1083-1088, 2010.
12. C. F. Onisa and D. C. J. Farrugia, Investigations into roll thermal fatigue in hot rolling, Int. J. Mater. Form. 1(1), pp. 363-366, 2008.
13. A. Pérez, R. L. Corral, R. Fuentes and R. Colás, Computer simulation of the thermal behavior of a work roll during hot rolling of steel strip, J. Mater. Process. Technol., 153, pp.

894-899, 2004.

14. D. Benasciutti, On thermal stress and fatigue life evaluation in work rolls of hot rolling mill, J. Strain Analysis. 47(5), pp.297-312, 2012.
15. D. F. Chang, Thermal stresses in work rolls during the rolling of metal strip, J. Mater. Proc. Technol., 94, pp.45-51, 1999.
16. Y. Sano, T. Hattori and M. Haga, Characteristics of high-carbon high speed steel rolls for hot strip mill, ISIJ Int. 32(11), pp. 1194-1201, 1992.
17. G. S. Schajer, Practical residual stress measurement methods, John Wiley & Sons, Hoboken, 2013, 7.
18. E. Kingston and D. J. Smith, Residual stress measurements in rolling mill rolls using deep hole drilling technique, Ironmaking & Steelmaking. 32, pp.379-380, 2005.
19. G.Sachs, The determination of residual stresses in rods and tubes, Zeit Metallkunde.,19, 352, 1927.
20. Y. Higashida and T. Kikuma, Measurement method of residual stress of rolls and countermeasure to thermal stress breaking, Tetsu-to-Hagane. 72, pp. 308, 1986.
21. C. Neto, 34th Mechanical Working and Steel Processing Conference Proceedings. Iron and Steel Society, Warrendale, 1993, 199.
22. J. Pacyna, A. Kokosza and A. S. Wojtas, Residual stress measurement in steel mill rolls using magnetic Barkhausen noise analysis, Journal of Nondestructive Testing & Ultrasonics, 4(8), 1994.
23. J. Yasuhiro, 33th Mechanical Working and Steel Processing Conference. Iron and Steel Society, Warrendale, 1992, 187.
24. S. H. Kang and Y. T. Im, Thermo-elasto-plastic finite element analysis of quenching process of carbon steel, J. Mater. Proc. Technol. 192, pp. 381-390, 2007.
25. S. Kamamoto, T. Nishimori and S. Kinoshita, Analysis of residual stress and distortion

resulting from quenching in large low-alloy steel shafts, Mater. Sci. Technol., 1(10), pp. 798-804, 1985.

26. A. Majorek, B. Scholtes, H. Muller and E. Machrauch, Influence of heat transfer on the development of residual stresses in quanched steel cylinders, Steel Res., 65(4), pp. 146-151 1994.
27. H. M. Cheng, X. Q. Huang and H. G. Wang, Calculation of the residual stress of a 45 steel cylinder with a non-linear surface heat-transfer coefficient including phase transformation during quenching, J. Mater. Process. Technol., 89, pp. 339-343 1999.
28. I. Neira Torres, G. Gilles, J. Tchoufang Tchuindjang, J. Lecomte-Beckers, M. Sinnaeve and A. M. Habraken, Study of residual stresses in bimetallic work rolls, Adv. Mater. Res., 996, pp. 580-585, 2014.
29. ASTM E831-14, Standard Test Method for Linear Thermal Expansion of Solid Materials by Thermomechanical Analysis, ASTM International, West Conshohocken, PA, 2014
30. 関本靖裕, 杉村幸彦, 平田一雄, 熱間圧延用ワークロールのかみどめ熱き裂 (ロール特集), 日立評論, 50(6), pp. 549-552, 1968.
31. Z. J. Chen, J. Zhang, L. Yu and G. J. Huang, imental research on the effect of induction reheating on the microstructure and mechanical properties of hot-rolled low-alloy steel plate, Mater.Res., 17(6), pp. 1601-1609, 2014.
32. O. Shitamura, H. Kodama and Y. Sano, Newly developed high performance composite type rolls, Hitachi Review. 69, pp. 461-467, 1990.
33. A. Noda, E. Matsunaga, T. Hattori and Y. Sano, New HINEX roll for highly-improved cobble crack resistance, Hitachi Giho, 13, pp. 89-92, 1997.

Chapter 3

Usefulness of Non-Uniform Heating and Quenching Method for Residual Stress of Bimetallic Roll

3.1 Introduction

During hot rolling process, thermal stresses are caused by a cyclic sequence of heating – cooling over the roll surface due to hot strip contact and water cooling [1-4], resulting in thermal crack initiation named firecrack at the roll surface. If severe thermal tensile stress has been added under the rolling trouble, the thermal crack starts to propagate. Therefore, suitable compressive stresses are necessary for preventing the thermal crack extension [5]. However, the tensile residual stress always appears at the roll center to balance the surface compressive residual stress. Under the combined action of thermal stress and residual stress, another form of roll fracture is known as thermal barrel breakage. This thermal breakage was originating near to the roll center and breaking out to the barrel surface [6-8]. The residual tensile stress affects the thermal breakage because if the total tensile stress exceeds the strength of core material, a sudden thermal breakage happens. Decreasing the center tensile stress is therefore desirable to reduce the risk of fracture from the roll center. Since the residual stress can be controlled by the heat treatment, an appropriate quenching process has been required to improve bimetallic roll quality.

Although previous studies treated the quenching process for HSS bimetallic roll, they mainly focused on the quenching temperature affecting the microstructure and mechanical properties of material [9-11]. For example, the previous experimental results shows that the hardness of HSS roll increases with increasing the quenching temperature and the hardness decreases when the temperature exceeds 1040℃. However, no detail studies are available for the

effect of quenching process on the residual stress. Therefore, in our previous study, the residual stress simulation was performed for quenching of bimetallic rolls after the roll was heated up uniformly [12]. Then, the generation mechanism and distribution of residual stress were investigated. Also, the effects of the shell-core ratio, diameter, phase transformation and material heat treatment process on the residual stress were discussed. However, the effects of creep behavior and thermal stress on residual stress of bimetallic rolls have not yet been considered in the previous study.

In this chapter, the simulation will be performed for quenching after non-uniform heating, which is a different quenching method recently developed and widely used for bimetallic rolls [13-15]. Although the previous studies referred the residual stress due to this quenching after non-uniform heating, the detail effect on the residual stress generation has not been discussed yet. Therefore, in this study, the usefulness of this method for the residual stress will be investigated for bimetallic rolls. The stress relaxation caused by creep behavior will be also considered. Then, the results will be compared with the results of quenching after uniform heating. The effect of non-uniform heating on the residual stress of HSS bimetallic roll will be clarified through the comparison. The results will be useful for determining an appropriate quenching process of HSS bimetallic rolls.

3.2. Quenching after non-uniform heating

Figure 3-1 illustrates the non-uniform heating quenching process in comparison with Figure 3-2, which illustrates the uniform heating quenching process. In the uniform heating process, the whole roll is heated up to the higher temperature equaling to T_{Start} before the quenching process. In the non-uniform heating process, the whole roll is heated up to the uniform lower temperature of T_{Heat} and kept at T_{Heat} for some hours, then rapidly heated up to T_{Start} as the non-uniform heating before quenching. This rapid heating provides temperature difference

between the roll surface and roll center. The quenching processes after non-uniform heating and uniform heating are similar, but the keeping temperature $T_{Keep1} > T_{Keep2}$. The quenching process after non-uniform heating quenching can be described in the following way.

The roll is put out from the heating furnace and cooled down rapidly from T_{Start} by using the spray cooling. After rapid cooling, the roll is maintained for several hours when the surface temperature drops to T_{Keep1}. Here, keeping T_{Keep1} is beneficial to relaxing the excessive thermal stresses caused by rapid surface cooling. After keeping T_{Keep1}, the roll is put out from the furnace and slowly cooled down in air until to T_{Finish}. Since the tempering process has not been performed, these residual stresses just after quenching process are called middle residual stresses. After quenching process, usually the tempering process will be performed 2 to 4 times to release the residual stress and obtained the stable microstructure.

Compared with the uniform heating quenching, the advantages of non-uniform heating quenching can be summarized in the following way.

① The quenching temperature of the core material is lower than 900℃， which contributes to prevent material deterioration induced by excessive heating.

② The experience shows that the center residual stress can be reduced when center temperature is lower than surface temperature during pre-heating process.

③ The material microstructure can be fined and a few martensitic structures can be produced due to the rapid cooling rate of quenching. As a result, a hard shell is obtained to improve the impact strength and strength of roll during the hot rolling.

④ The pre-heating time is shortened by using non-uniform heating method, which contributes to energy saving.

⑤ The quenching time is also shortened as well as pre-heating time by using the non-uniform heating quenching, which contributes to shorten the operation time of high temperature.

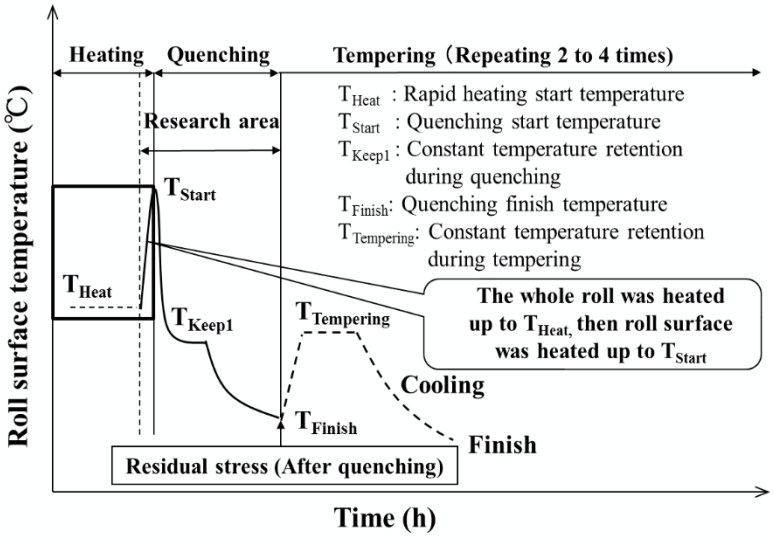

Figure 3-1 Non-uniform heating and quenching process

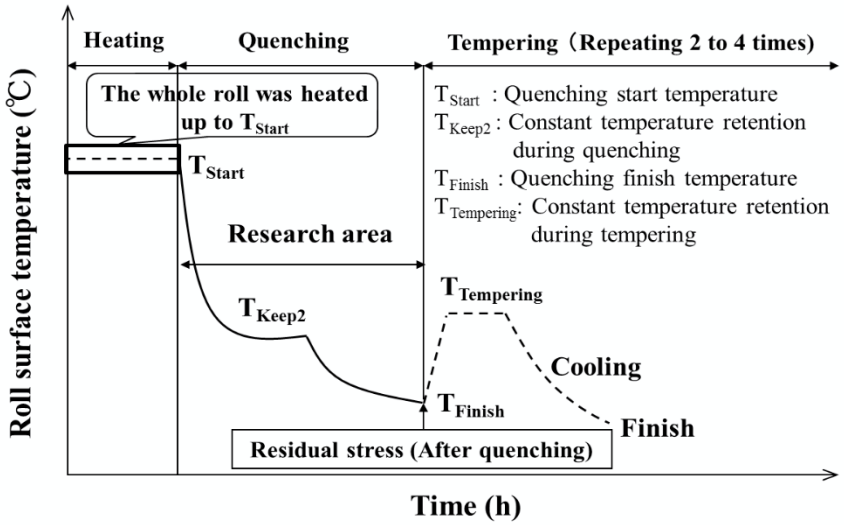

Figure 3-2 Uniform heating and quenching process

3.3 Analysis method and FEM modeling

3.3.1 FEM model

As shown in Figure 3-3, the roll diameter is 660mm, body length is 1600mm and shell thickness is 60mm, consisting of the high speed steel as shell and the ductile casting iron as core

and roll neck. As shown in the Figure 3-4, the analysis method and FEM model during non-uniform heating quenching process are similar to the one during uniform heating quenching process.

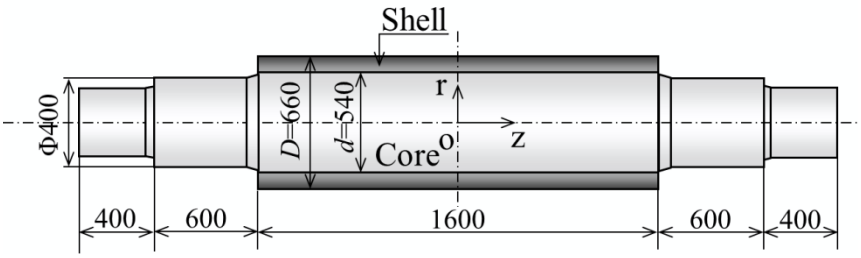

Figure 3-3 Dimension of the HSS bimetallic roll (mm)

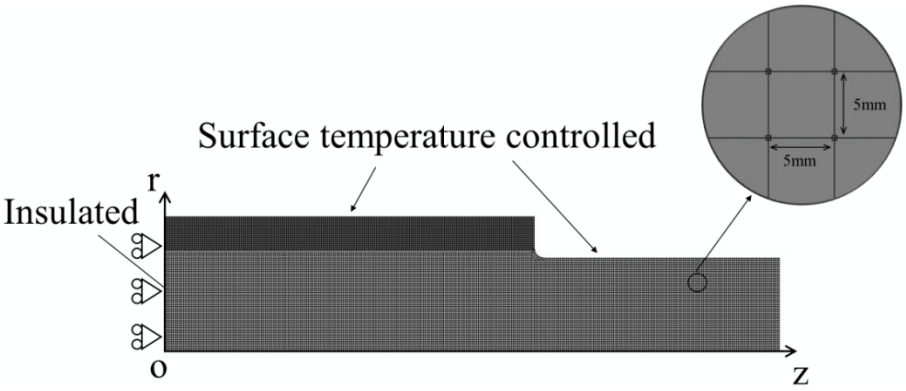

Figure 3-4 FEM analysis of bimetallic roll during non-uniform heating quenching process

3.3.2 Material properties of the bimetallic roll during non-uniform heating quenching

Similarly to the analysis of residual stress during uniform heating quenching process, a large amount of material properties of the bimetallic roll are also necessary for the analysis of residual stress during non-uniform heating quenching process. Since the rapid heating process is considered during non-uniform heating process, the material properties of Young's modulus, thermal expansion coefficients and shell stress-strain curves during rapid heating process are measured to ensure the analysis accuracy as shown in Figure 3-5. The others material properties during rapid heating process are the same as that during uniform heating quenching process as shown in Figure 2-7. The material properties during the quenching after rapid non-uniform

heating are the same as that during quenching after uniform heating process.

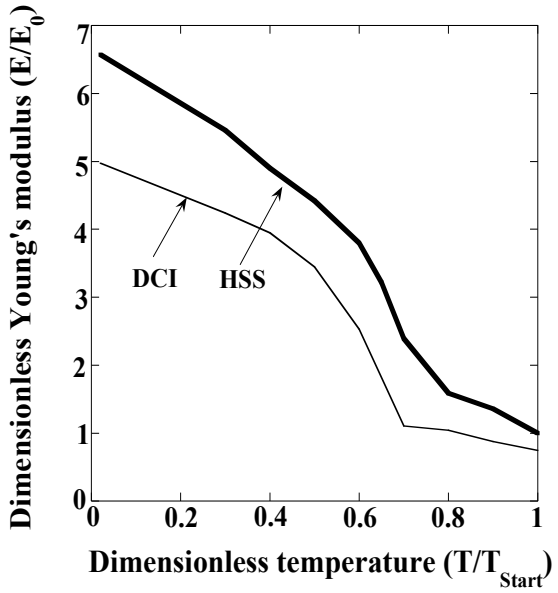

(a) Young's modulus

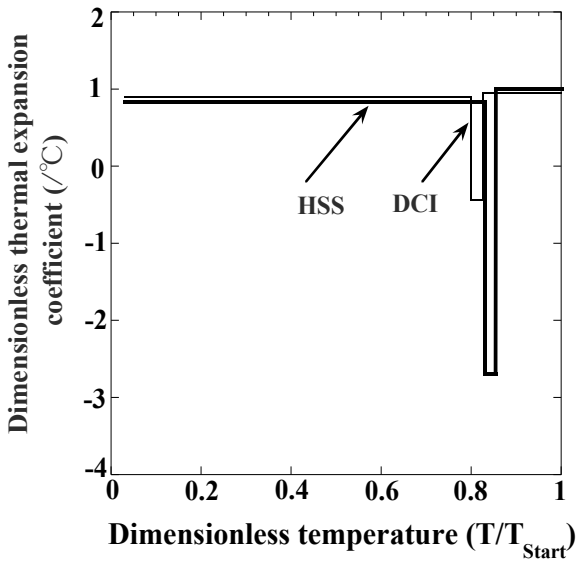

(b) Thermal expansion coefficient

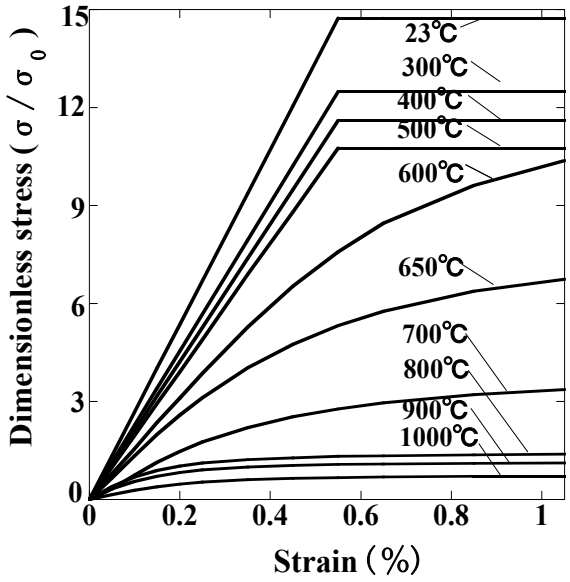

(c) Stress-strain curves of high speed steel

Figure 3-5 Material properties dependent on temperature for high speed steel and ductile casting iron during the rapid heating process

3.4 Summary of residual stress due to uniform heating quenching

In the Chapter 3, the residual stress of bimetallic roll with diameter 600mm was discussed for the quenching process after conventional uniform heating. However, for the non-uniform heating quenching, the roll diameter changes into 660mm according to the requirement of the company. Therefore, the results of bimetallic roll with diameter 660mm for the uniform heating quenching is firstly summarized to easily compared with results of non-uniform heating quenching. Figure 3-6 shows (a) temperature histories and (b) stress σ_z histories at the surface and center under uniform heating quenching process. The residual stresses for the uniform heating quenching process can be summarized in the following way for heating process Ⓐ and quenching process ⒷⒸⒹⒺ.

In the heating processⒶ, the whole roll is slowly heated up to uniform temperature of T_{Start} in Figure 3-6. The stress does not appear since the temperature gradient is small enough between the surface and center during the heating process.

In the processⒷ at the beginning of the cooling, the tensile stress appears at the surface due to rapid surface cooling. Then, the center thermal contraction becomes larger than that at the surface, leading to the center stress changes from compression to tension. As a result, tensile stress at the surface reaches peak values then turn to opposite direction. As center temperature dropping to the temperature $T_{Pearlite}$ in Figure 3-6, pearlite transformation (expansion) happens near the shell/core boundary at time $t_1$and expands toward the center (see Ⓟ from t_1 to t_3 in Figure 3-6(b)). In this period, the center is shrunk relative to the other parts of the core which expanded gradually due to pearlite transformation. Hence, the compressive stress at the center decreases until becomes tensile stress.

In the processⒸ, the tensile stress reverses to compressive stress rapidly when the pearlite transformation reaches to the center. After the pearlite transformation, the compressive stress at the center decreases until becomes tensile stress due to the larger temperature change at the

center(see ⓣ from t_3 to t_4 in Figure 3-6(b)). Then, the surface stress state interchanges from tension to compression, and the center stress state interchanges from compression to tension. These stress states are kept until the end of keeping process.

In the process Ⓓ, at the beginning of T_{Keep2}, both stresses at the center and surface increase due to the roll is transferred into holding furnace and the surface temperature slightly increases. After surface temperature reaching the stable temperature of T_{keep2} in Figure 3-6, the stresses at the surface and the center decrease gradually because of the decreasing of temperature gradient.

In the process Ⓔ, bainite transformation occurs at the surface, causing a volume expansion and the surface compressive stress increasing. To balance the increase of surface stress, the center tensile stress also increases. After the bainite phase transformation, the thermal contraction difference becomes larger and Young's modulus increases with decreasing temperature. Eventually, both surface and center residual stresses increase continuously.

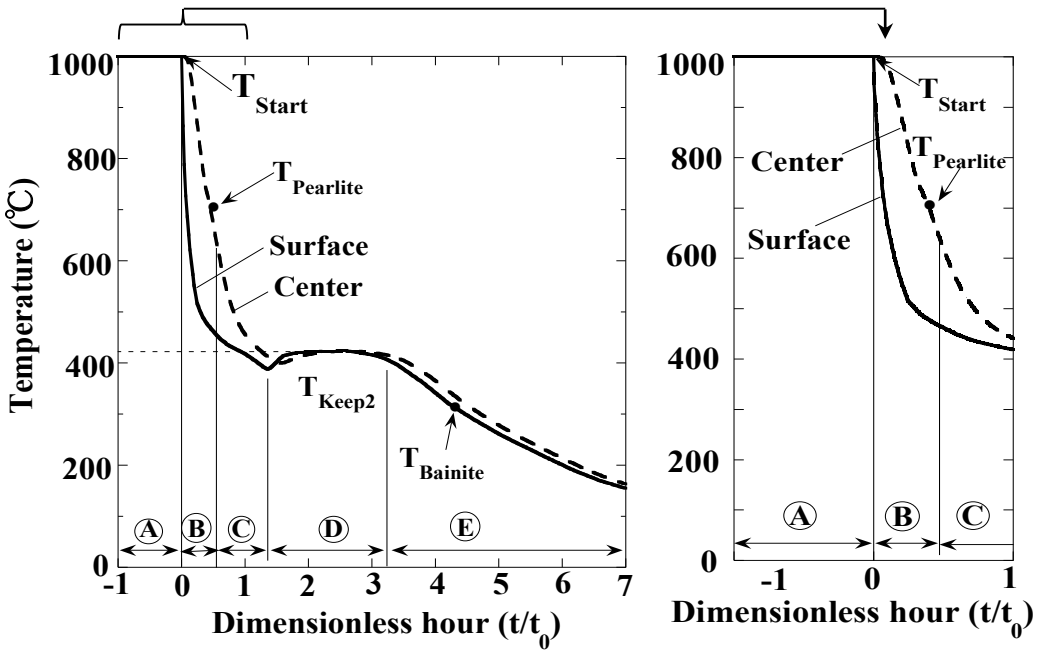

(a) Temperature histories at the center and surface

Ⓐ High-uniform temperature period； Ⓑ Rapid surface cooling period

Ⓒ Core material phase transformation period； Ⓓ Keeping temperature period

Ⓔ Furnace cooling and shell material phase transformation period

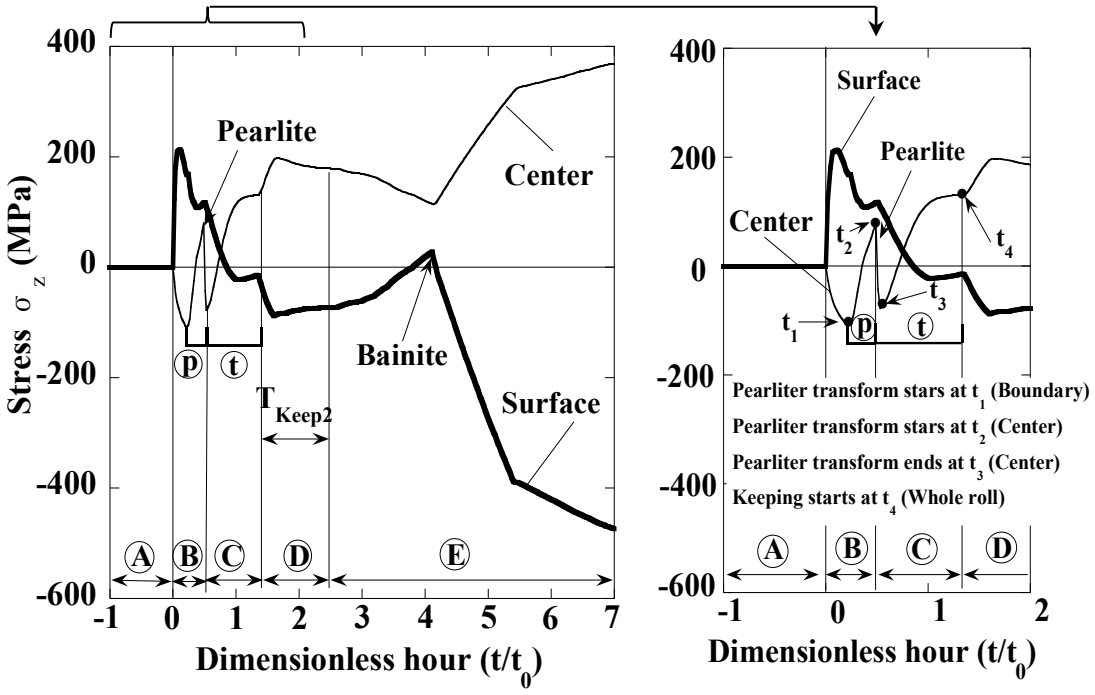

(b) Stress σ_z histories at center and surface

ⓟ Effect of pearlite transformation; ⓣ Effect of temperature decreasing

Figure 3-6 Histories of temperature and stress during non-uniform heating quenching process

Figure 3-7 shows the residual stress distributions of the component σ_z, σ_r, σ_θ and Mises stress σ_{eq} after uniform heating quenching. Similarly to the results of bimetallic roll with diameter of 600mm shown in Figure 2-10, it is seen that the tensile stress σ_z=388MPa is much larger than the stress σ_{eq}=269MPa at the roll center, and other stresses σ_θ, σ_r are much smaller around the center. The maximum stress σ_z = 388MPa is close to the tensile strength 415MPa indicated in Table 2-2 and risky for roll thermal barrel breakage if thermal tensile stress is added during hot rolling process.

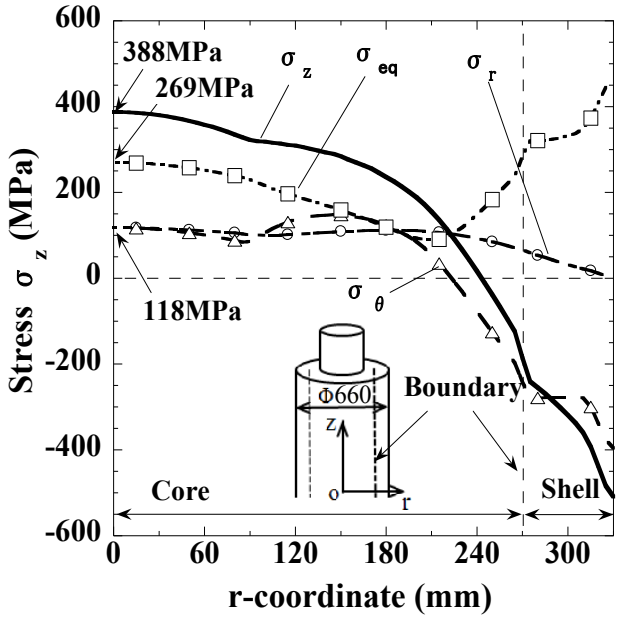

Figure 3-7 Residual stress distribution after uniform heating quenching process

3.5 Residual stress during non-uniform heating quenching

Figure 3-8 shows (a) temperature histories and (b) stress σ_z histories at the surface and center under non-uniform heating quenching process. The residual stress during non-uniform heating quenching process can be explained in the following way.

In the process Ⓐ of non-uniform heating, the whole roll is heated up to T_{Heat} and kept at T_{Heat} for several hours. After that, as shown in Figure 3-8(a), the roll is rapidly heated up before the roll surface temperature reaches T_{Start}. During this rapid heating process, the surface temperature rises faster than the center temperature, causing the compressive stress at the surface and causing the tensile stress at the center. When surface temperature is heated up to the temperature $T_{Austenite}$ in Figure 3-8(a), the austenite transformation occurs at the surface. The volume shrinkage due to the austenite transformation leads to the compressive stress decreases until becomes tensile stress at the surface as shown in ⓐ in Figure 3-8(b). However, since the austenite transformation extends toward the shell-core boundary, the tensile stress at the surface

becomes compressive stress immediately. After austenite transformation, since the temperature difference between the surface and core becomes smaller, the compressive stress at the surface decreases and the tensile stress at the center also decrease.

In the processes Ⓑ Ⓒ, due to the rapid cooling of surface temperature, the larger peak tensile stress appears at the roll surface (see ⓑ in Figure 3-8(b)). Similarly to the pearlite transformation during uniform heating quenching (see ⓟ in Figure 3-7(b)), the compressive stress at the center firstly decreases and then increases (see ⓟ from t_1 to t_3 in Figure 3-8(b)). However, the center stress is always in compression during pearlite transformation. After the pearlite transformation, the compressive stress at the center decreases slightly (see ⓣ from t_3 to t_4 in Figure 3-8(b)).

In the process Ⓓ the roll is transferred into holding furnace resulting in surface temperature rising. As a result, surface stress moves from tension to compression. To balance the surface stress, the center compressive stress decreases. The temperature gradient decreases gradually during the keeping process at T_{Keep1}, and both of tensile stress and compressive stress are slightly changed.

In the process Ⓔ, after the keeping period at T_{Keep1}, the roll is transferred out holding furnace and cooled in air. The surface temperature is dropped fast, causing temperature gradient increasing. As a result, compressive stress at the center decreases until becomes to tensile stress, and compressive stress at the surface increases. Similar to the bainite transformation during uniform heating quenching, volume expansion occurs at roll surface and the stress reverses from tension to compression. Meanwhile, the center compressive stress decreases to balance the surface stress.

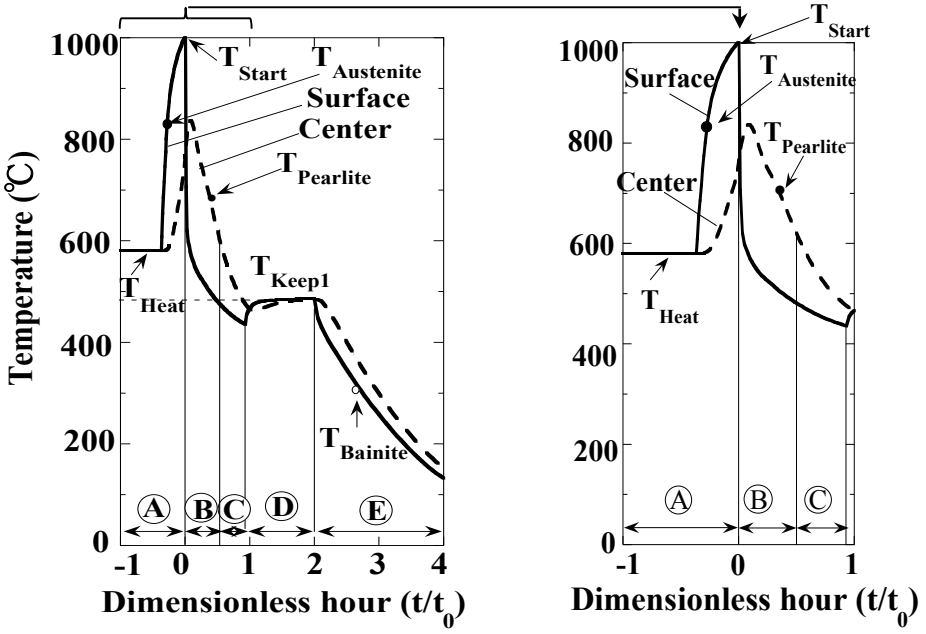

(a) Temperature histories at the center and surface

Ⓐ Rapid surface heating period; ⒷRapid surface cooling period;

Ⓒ Core material phase transformation period; Ⓓ Keeping temperature period

Ⓔ Air cooling and shell material phase transformation period

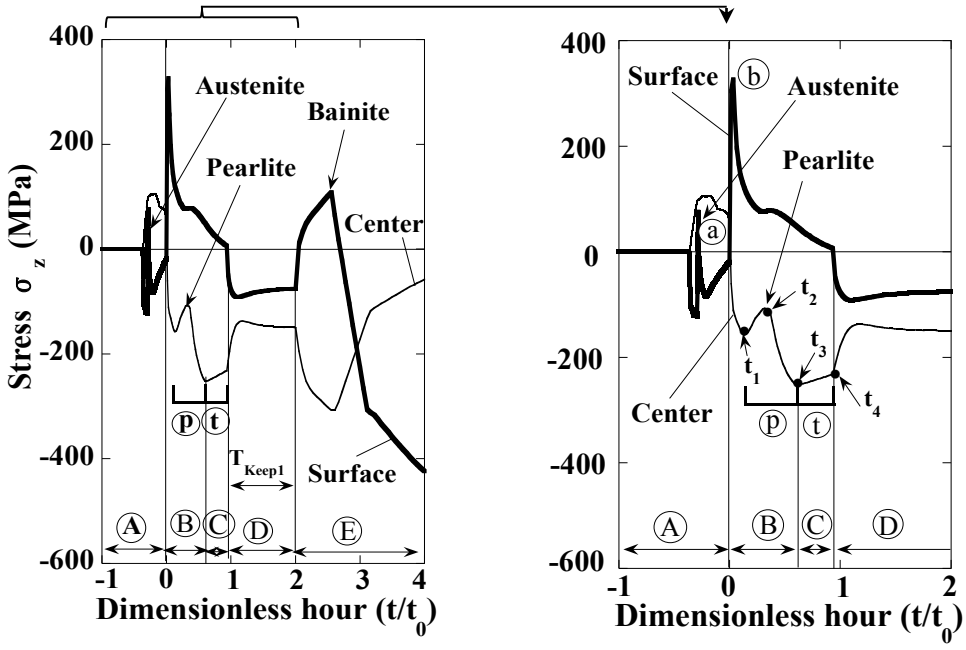

(b) Stress σz histories at the center and surface

ⓐ Austenite transformation; ⓑ Peak tensile residual stress at the surface

Figure 3-8 Histories of temperature and stress during non-uniform heating quenching process

Figure 3-9 shows the residual stress distributions of the components σ_z, σ_r, σ_θ, σ_{eq} after non-uniform heating quenching. All stress components σ_z, σ_r, σ_θ are compressive at the center. The maximum tensile stress σ_z=216MPa at r=200mm in Figure 3-9 is much smaller than the maximum σ_z =388MPa at the roll center in Figure 3-7. Those residual stress distributions are useful for reducing the risk of fracture. Since σ_z is larger than other stress components, σ_z will be mainly discussed in the following sections.

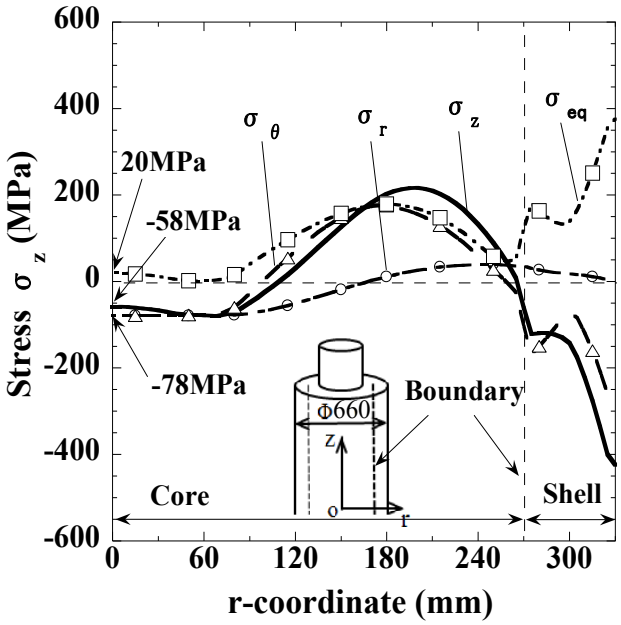

Figure 3-9 Residual stress distribution after uniform heating quenching process

3.6 Comparison of residual stress between non-uniform heating quenching and uniform heating quenching process

Figure 3-10 shows stress distributions σ_z along the central cross section where z=0. It is seen that the residual stress distributions are quite different depending on the non-uniform and uniform heating methods. The maximum tensile stress of the non-uniform heating appears near the shell/core boundary since the center stress decreases by (388) - (-58) = 446MPa compared

with the one of uniform heating. Although the surface compressive stress is smaller for the non-uniform heating quenching, the value looks large enough to prevent the thermal crack. The results show that the non-uniform heating quenching is useful for reducing the risk of roll fracture by providing sufficient compressive stresses at the roll surface as well as smaller tensile stresses at the roll center.

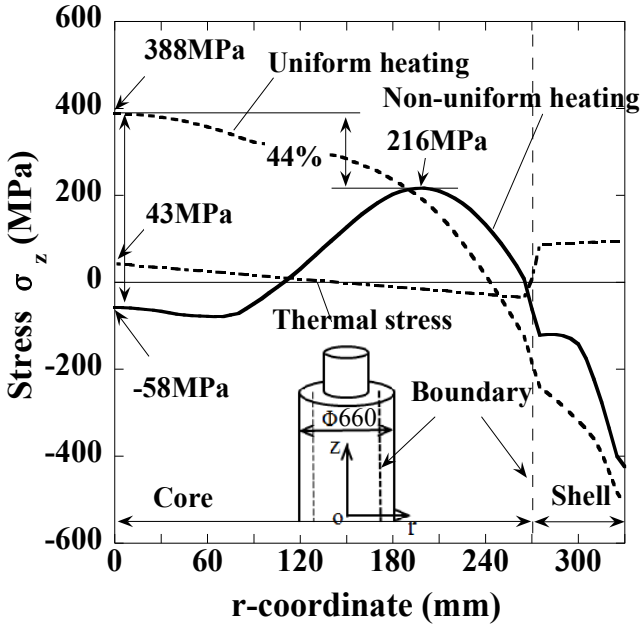

Figure 3-10 Comparison of residual stress distributions σ_z due to quenching after non-uniform and uniform heating

In this paper, as shown in Figure 3-11 and Figure 3-12, two aspects will be focused in order to explain why the center stress can be reduced in non-uniform heating quenching. One is the pearlite transformation effect in ⓟ and temperature effect in ⓣ before keeping T_{Keep1} and T_{Keep2}(see Figure 3-11), and the other is the cooling effect after keeping T_{Keep1} and T_{Keep2} (see Figure 3-12).

Figure 3-11 shows the residual stress distributions σ_z during the period Ⓑ and Ⓒ at $t_1 \sim t_4$ indicated in Figure 3-6 and Figure 3-8. Here , t_1 is the beginning time of pearlite transformation at shell/core boundary, t_2 is the beginning time of pearlite transformation at roll center, t_3 is the

ending time of pearlite transformation at the roll center, t_4 is the beginning time of keeping process.

At t_1, the tensile stress appears at shell and compressive stress appears at core after the rapid cooling for two kinds of quenching. Since the higher surface cooling speed in non-uniform heating quenching, the tensile stress and compressive stress is larger than that in uniform heating quenching.

At t_2, the pearlite transformation occurs at shell/core boundary, therefore, the compressive stresses near to the boundary increase and the compressive stresses near to the center decrease. From t_1 to t_2, the center stress change is (-106) - (-157) = 51MPa in non-uniform heating quenching and it change is (80) - (-108) = 188MPa in uniform heating quenching. The center compressive stress change is much smaller in non-uniform heating quenching compared with the stress in uniform heating quenching. This is because the center cooling speed in non-uniform heating quenching is lower than that in uniform heating quenching.

At t_3, the pearlite transformation occurs at center, therefore, the center compressive stresses increase. From t_2 to t_3, the center stress change is (-253) - (-106) = -147MPa in non-uniform heating quenching and it changes (-78) - (80) = -158MPa in uniform heating quenching. The center compressive stress changes are very close from t_2 to t_3.

From t_3 to t_4, the center stress change is (-232) - (-253) = 21MPa in non-uniform heating quenching and the change is (130) - (-78) = 208MPa in uniform heating quenching. The center compressive stress change is much smaller in non-uniform heating quenching compared with the change in uniform heating quenching. This is also because the center cooling speed in non-uniform heating quenching is lower than that in uniform heating quenching. It may be concluded that the center stress for non-uniform heating quenching increases slightly before and after pearlite transformation and causing the smaller residual stress at the center.

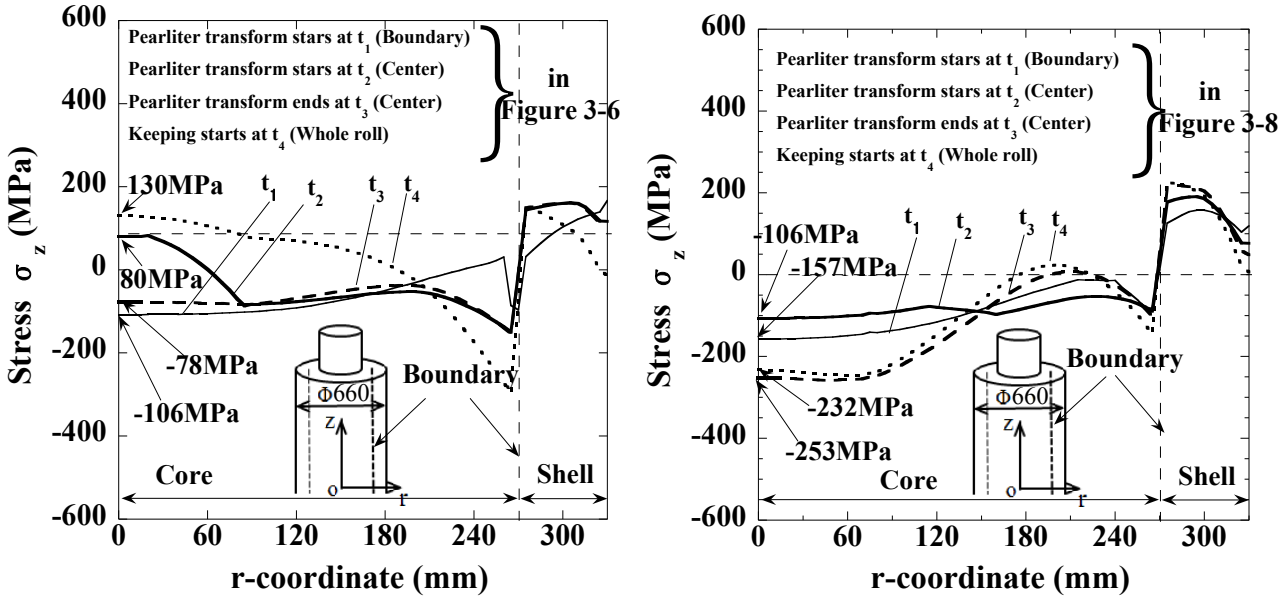

(a) Uniform heating and quenching (b) Non-uniform heating and quenching

Figure 3-11 Stress distribution σ_z during Ⓑ and Ⓒ before keeping process
(Time $t_1 \sim t_4$ is indicated in Figure 3-6 and Figure 3-8)

Figure 3-12 shows the stress distribution σ_z at the central cross section where z=0 after bainite transformation when the surface temperature is 400℃, 300℃ and 200℃. In the case of uniform heating quenching, the core stress distribution shifts to the tension side with decreasing the temperature without changing the distribution shape. In a similar way, the shell stress distribution shifts to the compressive side with decreasing the temperature without changing the distribution shape. The stress gap at the shell-core boundary becomes smaller with decreasing the temperature. In the case of non-uniform quenching, the stress distributions shift without changing the distribution shape in a similar way. Moreover, the center stress change is (336) - (138) = 198MPa and surface stress change is (-435) - (-13) = -422MPa in surface temperature ranges from 400℃ to 200℃ for uniform heating quenching. Similarly, the center stress change is (-94) - (-281) = 197MPa and surface stress change is (-353) - (76) = -429MPa for non-uniform heating quenching. The amounts of center compressive stress changes are very close. It may be

concluded that the final shape of stress distribution is mainly depending on the cooling process before keeping temperature T_{Keep1}.

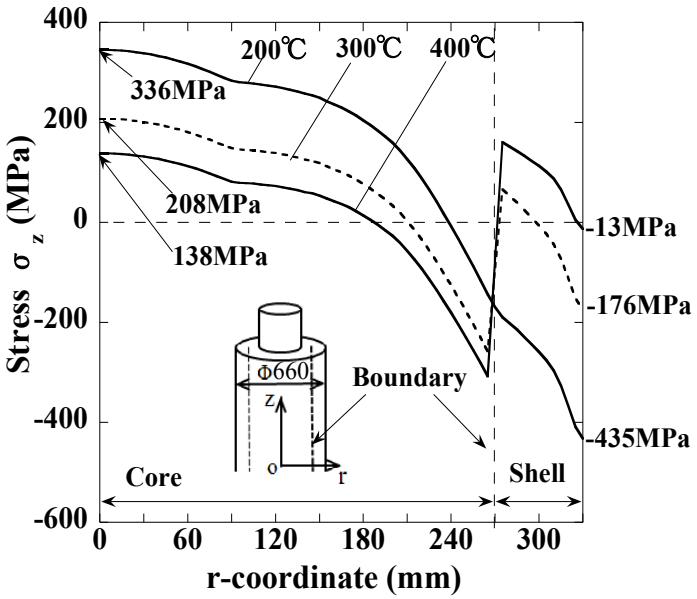

(a) Uniform heating and quenching

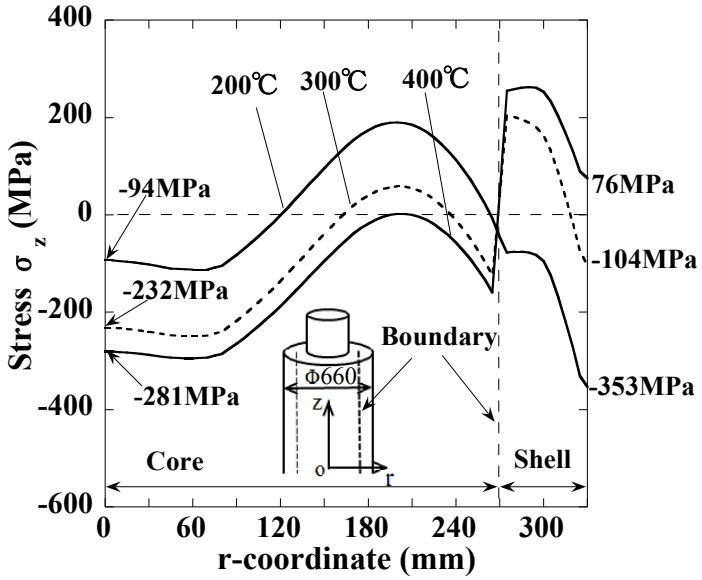

(b) Non-uniform heating and quenching

Figure 3-12 Stress distribution σ_z after keeping process when the surface temperature is 200°C, 300°C and 400°C

3.7 Roll center fracture named thermal barrel breakage may be prevented by non-uniform heating quenching

During the hot rolling process, the roll surface temperature becomes 800℃ due to the contact of hot rolled material, then the roll is rapidly cooled down by water cooling. This repeated temperature changes may cause thermal fatigue cracks at the roll surface. On the other hand, thermal barrel breakage may occur at the beginning of the rolling. This thermal barrel breakage is related to the maximum temperature difference between the roll center and sub-surface. This temperature difference initiates thermal stresses which are superimposed on the existing residual stresses in the roll. In Ref[8], A temperature difference 70°C causes additional thermal stresses about 110Mpa.

It is known that the roll temperature distribution has a sharp thermal gradient near to the roll surface because of the existence of thermal skin layer [3, 17]. The depth of the thermal skin layer can be estimated about only 1％ of the radius. For this reason, the temperature of sub-surface about 1mm below the surface beyond the thermal skin layer should be considered as the base surface temperature. The temperature distribution between the sub-surface and the center can be approximated by the linear distribution as shown in reference [3]. It was confirmed that a linear temperature distribution provides the larger stress at the roll center compared with the real thermal stress. In other words, a linear temperature distribution between the sub-surface and center can be used to evaluate the thermal stress safely. At the initial hot rolling process the maximum temperature difference has been reported as the sub-surface temperature is 70℃[19] and the roll center temperature is 40℃[20]. To verify the usefulness of non-uniform heating and quenching method, those data will be applied to the thermal stress analysis in this study.

In Figure 3-10 the thermal stress caused by temperature difference is also indicated as the dashed line. The thermal stress is calculated by using the FEM simulation. The FEM model is the same as the bimetallic roll as shown in Figure 3-4. The linear temperature distribution

between the sub-surface and center is applied to the model. The required material properties including Young's modulus E(E_{HSS} and E_{DCI}), thermal expansion coefficient α(α_{HSS}, α_{DCI})and Poisson's ratio ν (ν_{HSS}, ν_{DCI}) are given as the material properties at room temperature. Since the residual stresses at the core has a higher fracture risk than the shell, the thermal stress is considered to be added to the existing residual stress at the core.

As shown in Figure 3-10, in the uniform heating quenching, the maximum stress σ_z becomes 388+43=431MPa at the roll center by combining the residual and thermal stresses. In the non-uniform heating quenching, the combined stress σ_z is (-58)+43= -15MPa at the roll center and the maximum stress σ_z is 216+(-6)=210MPa near the boundary.

To discuss the risk of the roll center fracture, the safety factor is defined as σ_B/σ_z from the tensile strength σ_B and the axial stress σ_z. In the non-uniform heating quenching, we have $|\sigma_B / \sigma_z^{center}|$=27.67 at the roll center and $\sigma_B / \sigma_z^{interface}$=1.98 near the boundary. They are quite larger and therefore safer than the value $\sigma_B / \sigma_z^{center}$=1.04 in the uniform heating quenching.

To ensure the safety, it is empirically known that the safety factor $\sigma_B/\sigma_z \geq 1.2$ is required in the roll design. In the uniform heating quenching, the value $\sigma_B / \sigma_z^{center}$=1.04 is much smaller than the required safety factor $\sigma_B/\sigma_z \geq 1.2$. On the other hand, in the non-uniform heating, the safety factor $\sigma_B / \sigma_z^{interface}$=1.98 at the most dangerous point is larger enough than the required safety factor $\sigma_B/\sigma_z \geq 1.2$. Therefore, it may be concluded that the roll safety can be significantly improved by using non-uniform heating quenching method.

In the above thermal stress analysis, the assumed residual stress was obtained from the analysis just after quenching process. However, it is known that the actual residual stress may decrease by 30% through the tempering process repeated 2-4 times. Assuming by 30% reduction in the uniform heating quenching, the center residual stress σ_z becomes 272MPa due to the tempering. Then, we have $\sigma_B / \sigma_z^{center}$ =1.32 satisfying the safety condition $\sigma_B/\sigma_z \geq 1.2$. Therefore, the roll safety is also assured in uniform heating quenching under the roll cooling

system without troubles. It may be concluded that the roll safety is guaranteed more easily in the non-uniform heating quenching than in the uniform heating quenching.

3.8 Conclusions

In this paper, FEM simulation of non-uniform heating quenching for bimetallic roll was performed to predict the residual stress distribution. The residual stresses were compared between uniform heating quenching and non-uniform heating quenching. Moreover, the creep effect on the residual stress has been discussed. The results of the current study can be summarized as follows.

(1) By using non-uniform heating quenching method, the maximum tensile stress in the core appears near the shell/core boundary, the center stress decreases by 446MPa and the maximum tensile stress decreases by 44%. However, the compressive stress at the surface is almost unchanged. It may be concluded that non-uniform heating quenching is useful for reducing the risk of roll failure known as thermal barrel breakage by decreasing the center tensile stress without decreasing the surface compressive stress.

(2) The center stress increases slightly for non-uniform heating quenching before and after pearlite transformation and therefore the smaller residual stress appears at the center. Then, the core stress distribution shifts to the tension side with decreasing the temperature without changing the distribution shape. Similarly, the shell stress distribution shifts to the compressive side with decreasing the temperature without changing the distribution shape.

(3) The thermal stress calculated by considering temperature difference between the sub-surface and the center is simulated and added to residual stress. It may be concluded that the roll safety is guaranteed more easily in the non-uniform heating quenching than in the uniform heating quenching.

Reference

1. C. F. Onisa and D. C. J. Farrugia, Investigations into roll thermal fatigue in hot rolling, Int. J. Mater. Form., 1(1), pp.363-366, 2008.
2. A. Pérez, R. L. Corral, R. Fuentes and R. Colás, Computer simulation of the thermal behavior of a work roll during hot rolling of steel strip, J. Mater. Process. Technol.,153, pp.894-899, 2004.
3. D. Benasciutti, On thermal stress and fatigue life evaluation in work rolls of hot rolling mill, J. Strain Analysis. 47(5), pp.297-312, 2012.
4. D. F. Chang, Thermal stresses in work rolls during the rolling of metal strip, J. Mater. Proc. Technol. 94, pp.45-51, 1999.
5. Sano, Y., Hattori, T. and Haga, M., Characteristics of High-carbon High Speed Steel Rolls for Hot Strip Mill. ISIJ international, 32(11), pp. 1194-1201, 1992.
6. 佐野義一, 木村和夫, ホットストリップミル仕上後段作業ロールに生じるスポーリングの統計的解, 鐵と鋼:日本鐵鋼協會々誌, 73(9), pp.1154-1161, 1987.
7. K. H. Schroder, A basic understanding of the mechanics of rolling mill rolls, Eisenwerk Sulzau-Werfen, ESW-Handbook, pp.71, 2003.
8. Roll failures manual: Hot mill cast work rolls, The European Foundry Association, Roll Section, 2002, 19.
9. H. G. Fu, A. M. Zhao and J. D. Xing, Development of centrifugal casting high speed steel rolls, J. Univ. Sci. Technol. Beijing. 10(6), pp.61-66, 2003.
10. H. G. Fu, H. J. Zhao, Z. Z. Du, Z. J. Feng, Y. P. Lei, Y. Zhang, M. W. Li, Y. H. Jiang, R. Zhou and H. X. Guo, Heat treatment of centrifugally cast high carbon high vanadium high speed steel mill roll, Ironmaking Steelmaking, 38(5), pp.338-345, 2001.
11. H. G. Fu, X. L Chen, Z. Z. Du, Y. P. Lei Zhenjun, Effect of quenching temperature on structure and properties of centrifugal casting high speed steel roll, *Journal China Foundr.,* 6(1), pp.15-19, 2009.

12. B. C. Liu, S. M. Zuo, Poor warm treatment of centrifugal compound high-chromium steel roll, *China Foundry Machinery & Technology*, 4, pp.18-20, 2015.
13. 沈才平，大型锻钢支承辊差温热处理工艺研究和生产实践．金属热处理，28(8), pp.50-53, 2003.
14. S. Li, C. J. Wu, J. X. SU and Y. J. Zhang, Differential heat treatment process of Cr3 compound cast steel backup rollers, *J. Univ. Sci. Technol. Beijing*, 32(3), pp.331-335, 2010.
15. R. Wu, C. Wu, X. Zhang, Effect of heat treatment on property of core of high speed steel-ductile cast iron compound roll. Foundry Technology, 28(2), pp.190-194, 2007.
16. Y. Li, C. Wu, M. Han, Development of simulating temperature field system for differential heat treatment of composite roll, Shandong Metallurgy, 29(1), pp.59-61, 2009.
17. J. Zhang and Z. P. Cheng, Sinosteel Xingtai Machinery& Mill Roll Co., Ltd. CN102352431 B, 2011.
18. N. Oda, Y. Nozaki, R. Honda and T. Ohata, Hitachi Metals, Ltd. WO2013042528 A1, 2013 (in Japanese).
19. 木原諄二．熱間帯板圧延用作業ロールの概況，鐵と鋼:日本鐵鋼協會々誌，80(7), p.386-389, 1994.
20. S. Cerni, A. S. Weinstein and C. F. Zorowski, Temperatures and thermal stresses in the rolling of the metal strip, Iron and Steel Engineer. 40, pp.165-173, 1963.

Chapter 4

Effect of Creep behavior and Tempering Process on Residual Stress Reduction for Bimetallic Roll

4.1 Introduction

Creep can be defined as a time-dependent deformation at elevated temperature under a constant stress. Stress relaxation can be defined as a decrease in stress under constant strain. Those two are closely associated important phenomena which should be considered in the design of engineering components [1-4]. In the previous studies, although many papers deal with the residual stress distribution when the small steel is quenched, there are few reports comparing residual stress reducetion for the large rolling rolls between after quenching and after tempering [5-9]. And in addition, the residual stress reduction considering creep behavior during quenching and tempering is fewly studied in detail.

In this chapter, the FEM simulation which can predict the residual stress distribution considering the creep and tempering process was established. First, the creep test was done using the material cut from core material of bimetallic roll, and the creep formula of core material was clarified. Next, comparison of the experimental and numerical analysis values of the residual stress relaxation were compared between FEM result and experiment result. At the last, the stress reduction after quenching and tempering process was compared considering the creep.

4.2 Creep analysis

The creep effect looks small in the region Ⓑ Ⓒ because the temperature changes quite largely as well as the stress. Also, in the region Ⓔ the creep effect looks small because of the

lower temperature. Therefore, the creep analysis is applied to the keeping process Ⓓ where the roll is put at relatively high temperature for several hours.

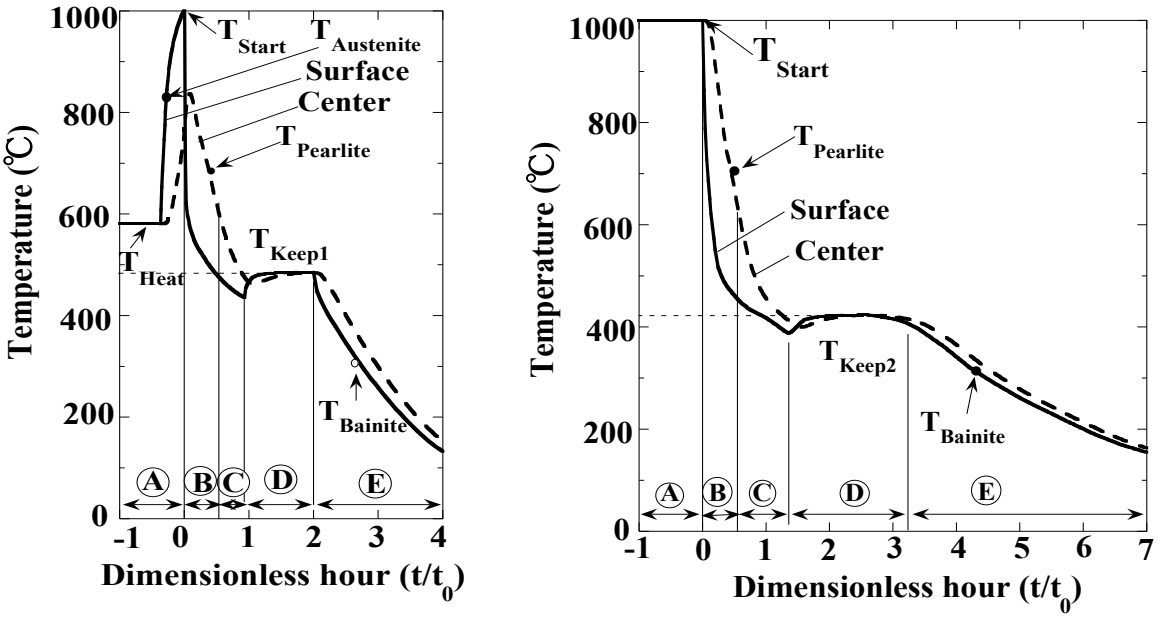

(a) Non-uniform heating quenching (b) Uniform heating quenching

Figure 4-1 Temperature histories of bimetallic during quenching process

In the creep analysis, the transient creep strain also should be considered as well as the steady creep strain. Among several equations available for creep analyses, the time hardening law, sometimes called power law, is used to express the core material which has low strength under high temperature [10]. It should be noted that the creep should be considered in a short hours Ⓓ for the roll quenching compared to the common creep analysis. The core creep can be given as Equation (1).

$$\varepsilon_c = \mathrm{A}\sigma^m t^n \tag{1}$$

where ε_c is the transient strain, σ is stress, t is time, A, m and n are temperature dependent material constants. This time hardening formulation is used to predict the creep

behavior under a variable stress history. In order to determine constants A, m and n, the creep tests are performed.

4.3 Creep and stress relaxation test

4.3.1 Creep test

As shown in Figure 4-2, the creep testing was conducted by using a miniature creep rupture testing machinebased on JISZ2271 [11]. The specimens were prepared from core material as shown in Figure 4-3. Those specimens were respectively heated up to the testing temperatures, T_{keep1} and T_{keep2}, and kept at theses temperatures during the testing process. Then, the creep tests were carried out by applying constant loads 100Mpa, 130MPa and 160MPa. The strain changes were recorded with time. The experiment results of creep strain at the T_{keep1} and T_{keep2} are shown in Figure 4-4. From the strain-time curves obtained, the creep equations can be written as shown in Equations (2) and (3) by using the caculation method in Reference [8].

$$\varepsilon_c = 2.25 \times 10^{-13} \sigma^{3.44} t^{0.672} (T_{keep1}) \quad (2)$$

$$\varepsilon_c = 8.38 \times 10^{-19} \sigma^{5.71} t^{0.514} (T_{keep2}) \quad (3)$$

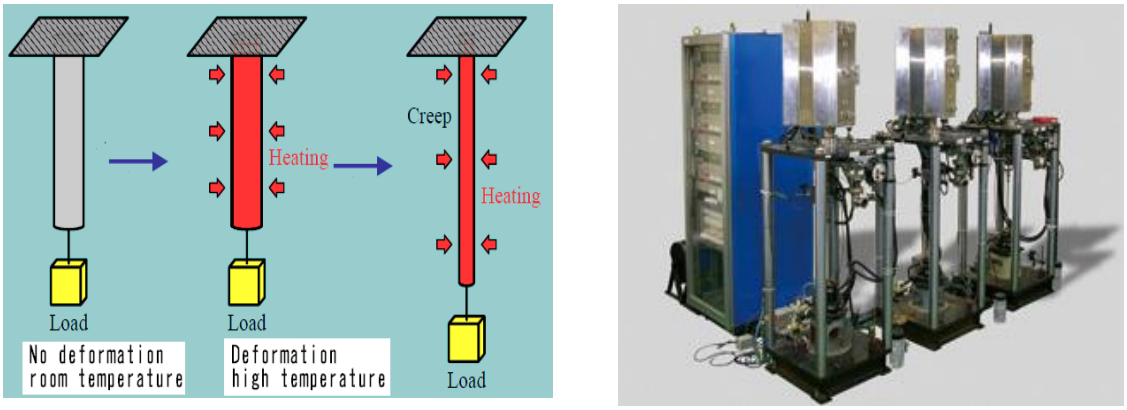

Figure 4-2 Creep test of ductile casting iron

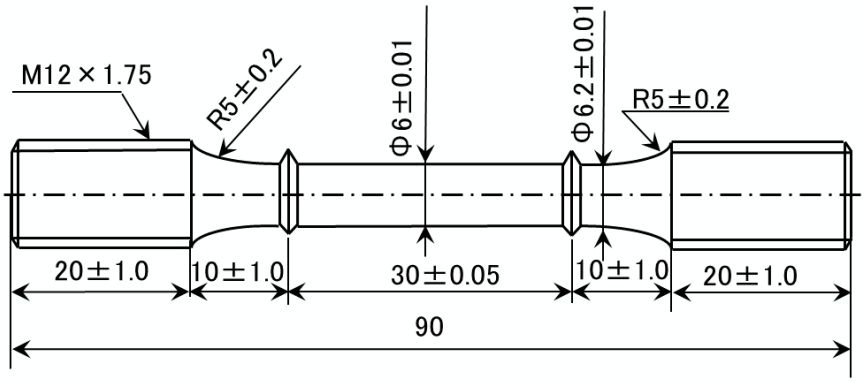

Figure 4-3 Specimen of the creep test (mm)

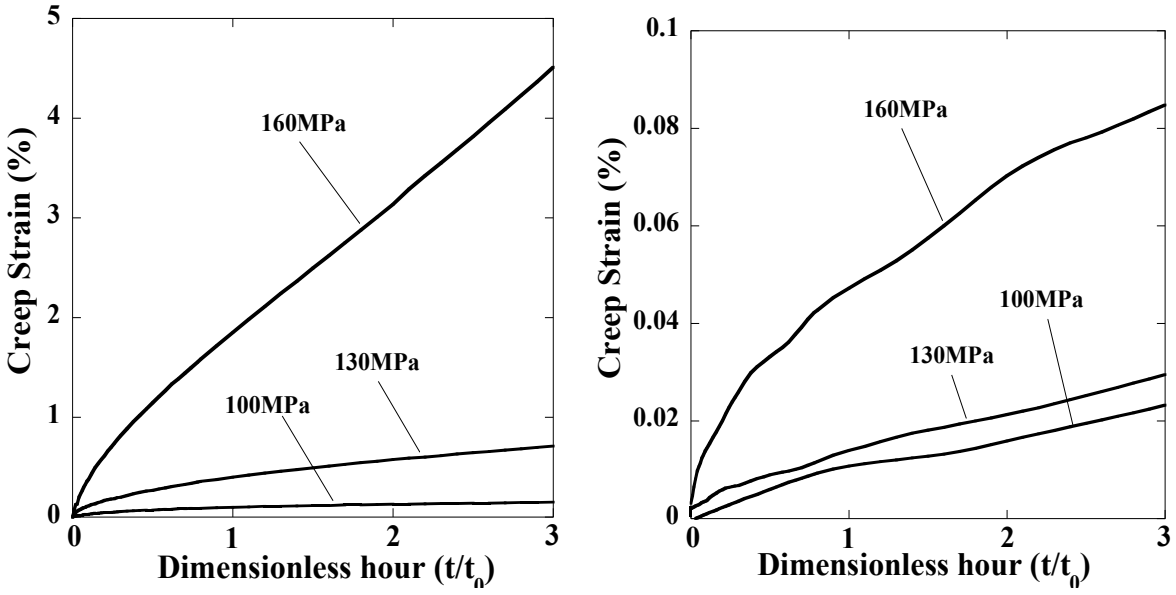

(a) Creep strain depending on time at T_{Keep1} during the non-uniform heating quenching

(b) Creep strain depending on time at T_{Keep2} during the uniform heating quenching

Figure 4-4 Creep strain of ductile casting iron depending on time at T_{Keep1} and T_{Keep2}

4.3.2 Stress relaxation test

As shown in Figure 4-5, the stress relaxation test was conducted for ductile casting iron. The specimens were prepared from the core material as shown in Figure 4-6. Those specimens were respectively heated up to the testing temperature, T_{Keep1} and T_{Keep2}, and kept at theses

temperatures during the testing process. Then, the stress relaxation tests were carried out under the constant strain when the primary stress is 130MPa.

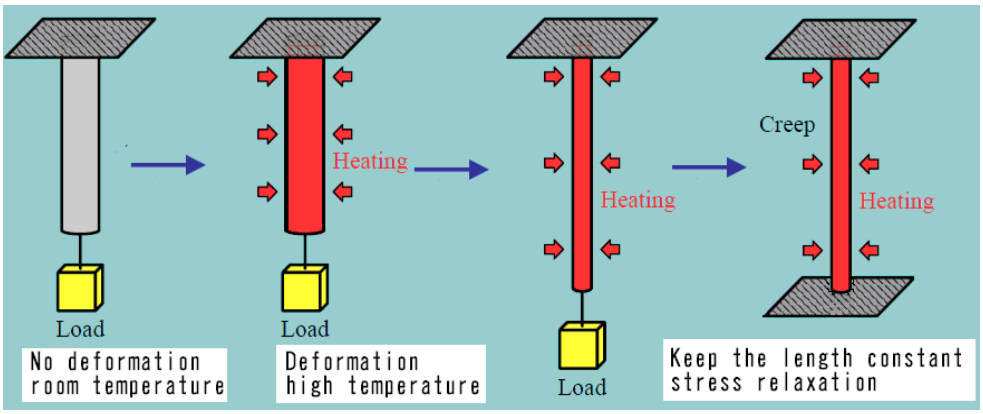

Figure 4-5 Stress relaxation test of ductile casting iron

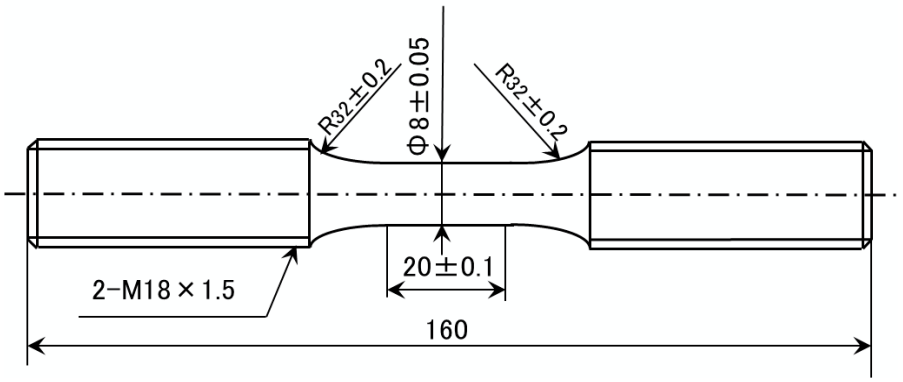

Figure 4-6 Specimen of the stress relaxation test (mm)

4.3.3 Results and discussion for creep and stress relaxation

It is known that creep behavior and stress relaxation are closely associated. The equation of stress relaxation can be written as Equation (4) based on the time hardening law [12].

$$\sigma = \frac{\sigma_0}{[1+AE(m-1)\sigma_0^{m-1}t^n]^{1/(m-1)}} \tag{4}$$

To confirm the validity of Equations (2) and (3), the following stress relaxation testing was conducted. The FEM simulation of stress relaxation is performed to verify Equations (2), (3) in

Figure 4-7 in comparison with the experimental result at T_{Keep1} and T_{Keep2}. The results show that the stress decreases by 69% at Tkeep1 and by 38% at T_{keep2}. It can be found that the stress relaxation ratio is larger at high temperature (T_{Keep1}) than relatively low temperature (T_{Keep2}). The FEM results are in good agreement with the experiment results. It is confirmed that Equations (2), (3) are useful for predicting the creep effect on the residual stress.

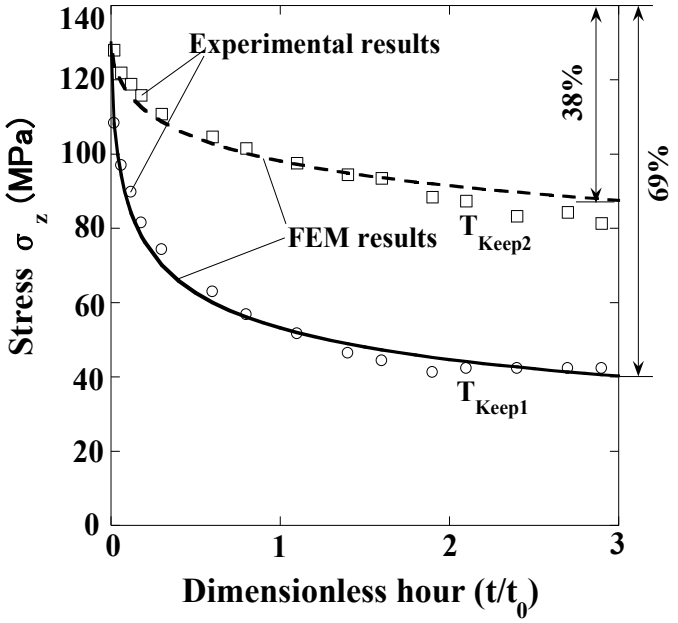

Figure 4-7 Comparison between FEM results and experimental results for stress relaxation

4.4 Effect of creep behavior on residual stress

Figure 4-8 shows the stress histories σ_z during the non-uniform heating quenching and uniform heating quenching processes. From the keeping process, it is seen that the center stresses decrease considering the creep behavior conpared with the results without consideing creep behavior. And in addition, the surface stresses are almost unchanged by considering creep in both quenching processes. After the keeping process, the center stress difference between the considering and without considering creep behavior is unchanged in in both quenching processes.

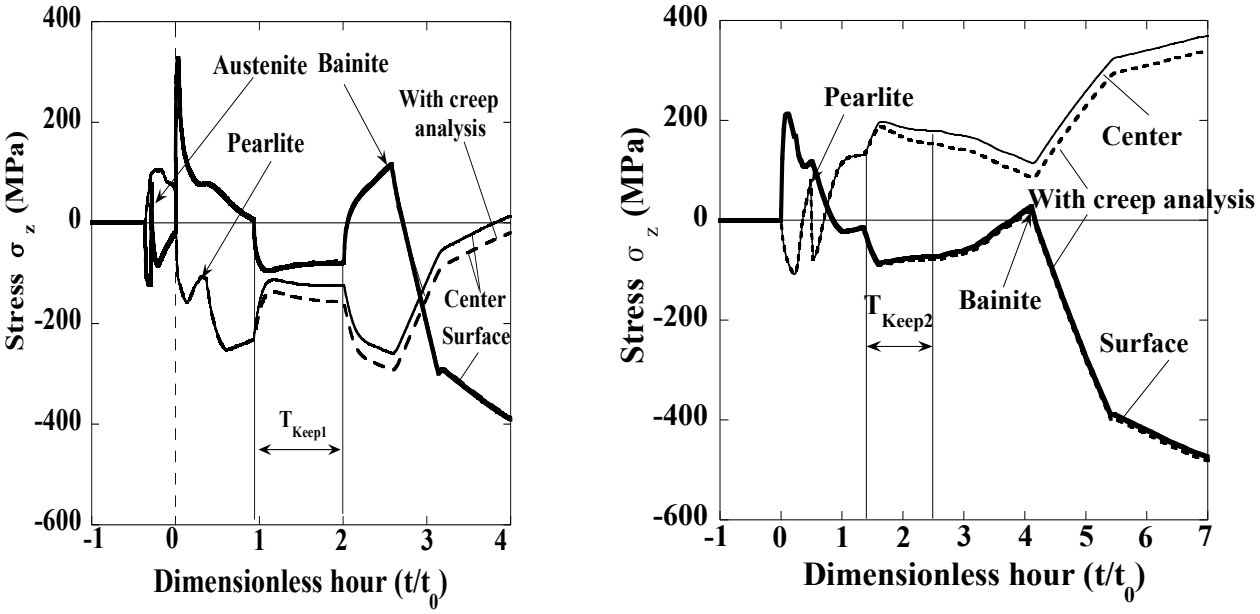

(a) Non-uniform heating quenching process (b) Uniform heating quenching process

Figure 4-8 Stress σ_z histories considering creep analysis

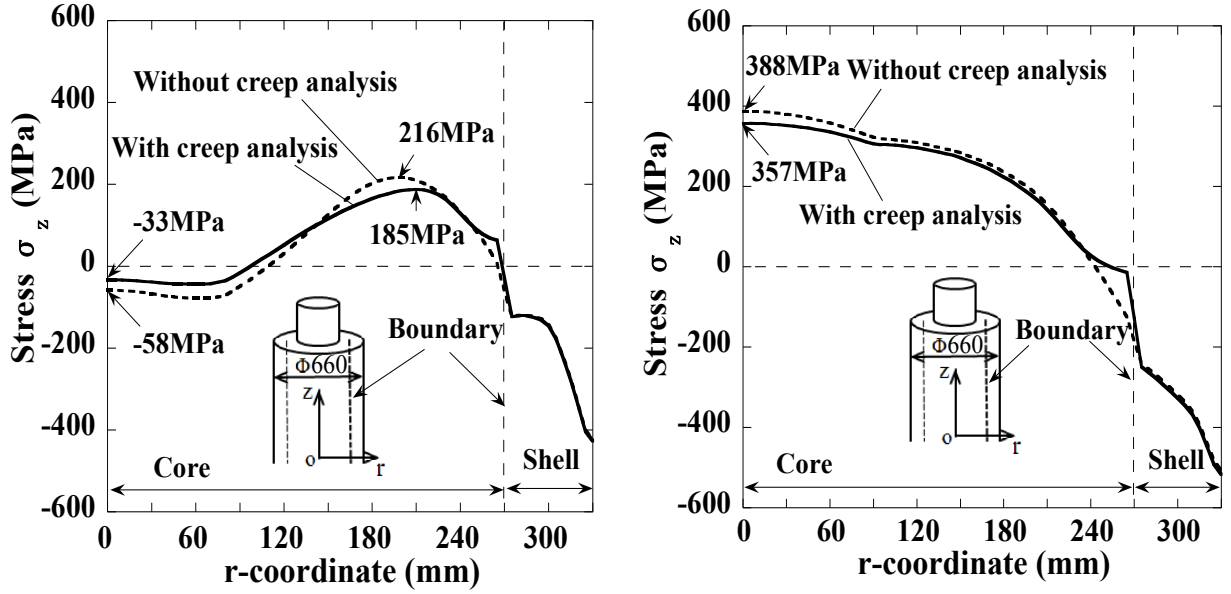

(a) Non-uniform heating quenching process (b) Uniform heating quenching process

Figure 4-9 Effect of creep behavior on the residual stress

Figure 4-9 shows stress distribution σ_z along the central cross section where z=0 with and without considering creep. For non-uniform heating quenching, the maximum stress at the core decreases by 15% from 216MPa to 185MPa and the center stress decreases from -58 MPa to -33 MPa by considering creep. For uniform heating quenching, the center stress decreases by 8% form 388MPa to 357MPa by considering creep. The stresses become uniformly distributed at the core no matter which quenching process (uniform or non-uniform) is considered during heating.

Table 4-1 compares the keeping process between non-uniform heating quenching and uniform heating quenching including the stress relaxation ratio, keeping temperature, Mises stress σ_{eq} and keeping time. The non-uniform heating quenching has larger stress relaxation and larger Mises stress than uniform heating quenching. Among of these factors, the stress relaxation plays a dominant role on the final stress decrease. Because of this reason, as shown in Figure 4-10, the creep effect for non-uniform heating quenching becomes larger than that for uniform heating quenching.

Table 4-1 Comparison of keeping process between non-uniform heating quenching and uniform heating quenching

Heat treatment	Non-uniform	Uniform
Stress relaxation ratio (%)	69	38
Keeping temperature (°C)	$T_{Keep1} > T_{Keep2}$	
σ_{eq} at keeping temperature(MPa)	136	103
Keeping time (h)	5.3	6

4.5 Effect of tempering process on residual stress

4.5.1 Tempering process for bimetallic roll

Figure 4-10 illustrates the tempering processes after uniform heating quenching process and non-uniform heating quenching process. After quenching processes, the roll is slowly heated up

to $T_{Temperting}$, and kept at $T_{Temperting}$ for several hours. Then, the roll is slowly cooled down to room temperature. In this study, the tempering process will be performed 2 times to release the residual stress and obtained the stable microstructure.

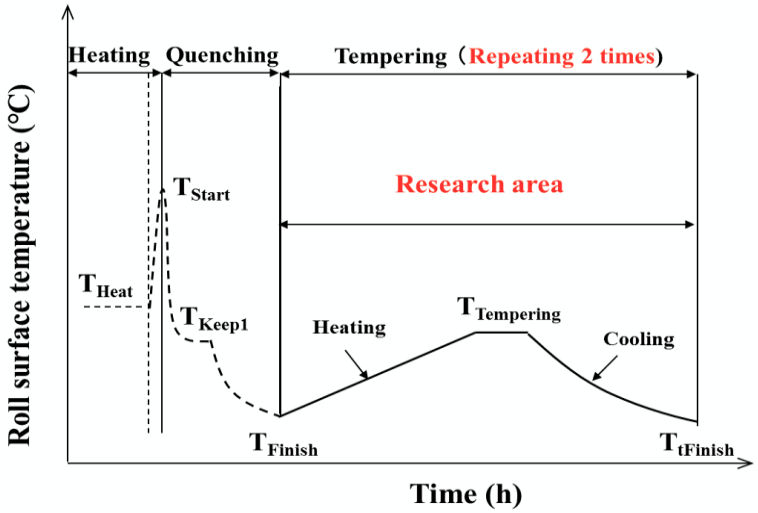

(a) Tempering process after non-uniform heating quenching process

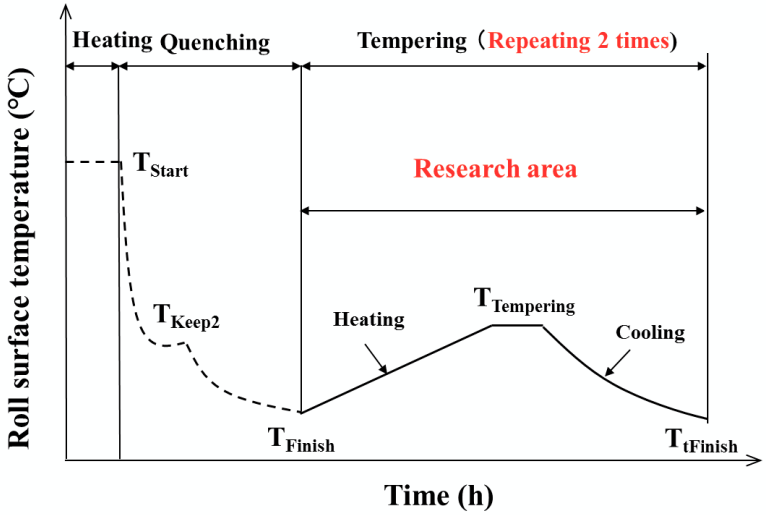

(b) Tempering process after uniform heating quenching process

Figure 4-10 Tempering process after uniform heating quenching and non-uniform heating quenching processes of bimetallic roll

4.5.2 FEM analysis and material properties for bimetallic roll during tempering

The FEM analysis method of tempering process is the same as that of quenching process. As shown in Figure 4-10, the roll surface temperature during tempering process is imposed to the roll surface. For the tempering process, only the material properties of high speed steel were measured. The materimal properties of ductile iron are the same as that during quenching process. The input data of material properties of high speed steel depending on temperature during tempering process are shown in Figure 4-11.

Figure 4-11(d) shows the dilatometer curve of high speed steel during tempering. It can be seen that volume expansion caused by martensite transformation during the cooling process. This curve was obtained by cutting out a specimen from the quenched HSS roll and measuring with a dilatometer. Thus, the obtained martensite transformation is indicated as 100%. However, it is known that the martensitic transformation will be suppressed by compressive residual stress[13]. Therefore, the effect of compressive stress of 300 to 500 MPa existing in the outer layer of the bimetallic roll on martensitic transformation should be taken into consideration. In this study, the extreme case is indicated as 0% that transformation does not occur at all during the cooling.

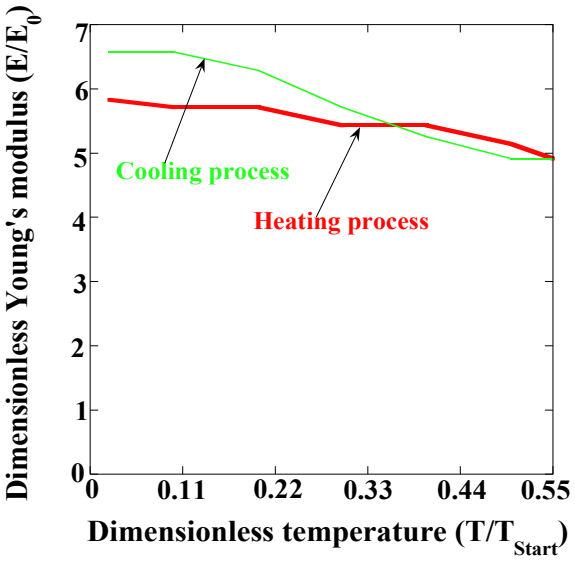

(a) Young's modulus

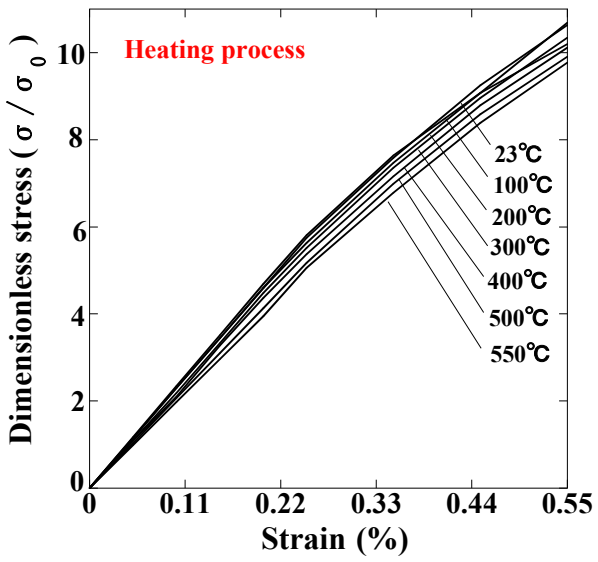

(b) Stress-strain during heating process

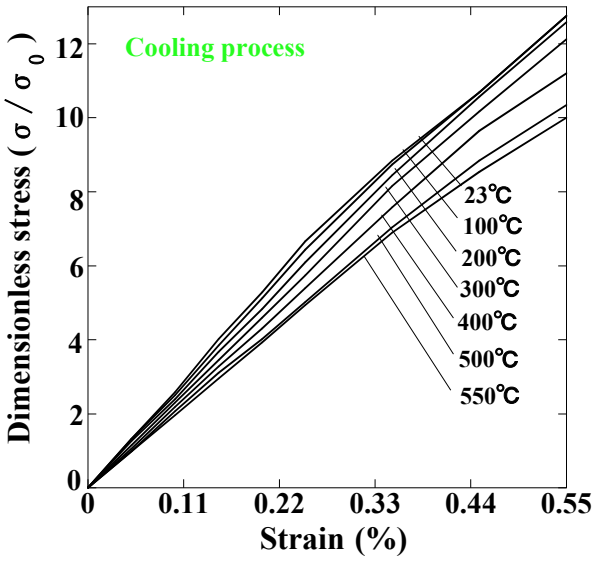

(c) Stress-strain during cooling process

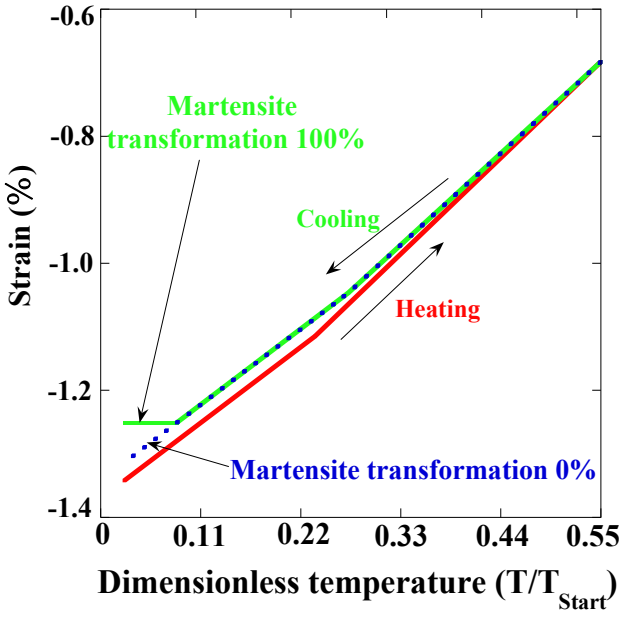

(d) Dilatometer curve

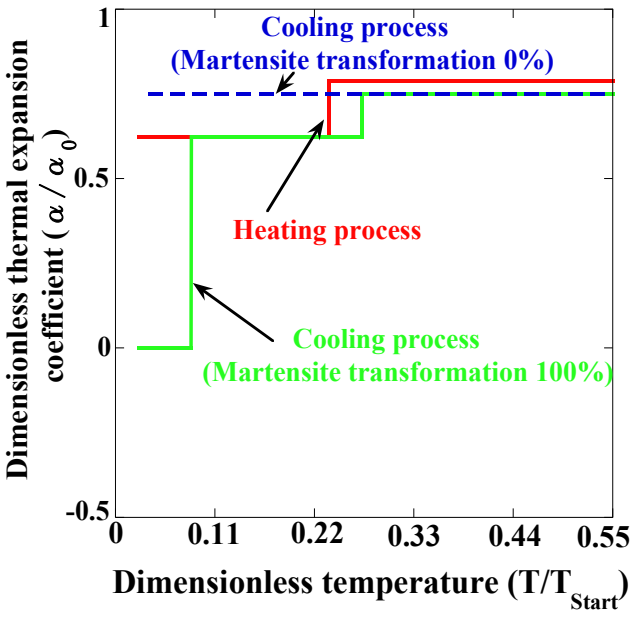

(e) Thermal expansion coefficient

Figure 4-11 Material properties dependent on temperature for high speed steel during the tempering process

4.5.3 Creep analysis during tempering process

Simaliarly to the creep analysis of quenching process, the creep is considered for the core material during the keeping process at $T_{Tempering}$. The experiment results of creep strain at the $T_{Tempering}$ is shown in Figure 4-12. From the strain-time curves obtained, the creep equations can be written as shown in Equations (5).

$$\varepsilon_c = 8.434 \times 10^{-16} \sigma^{5.003} t^{0.4919} (T_{Tempering}) \quad (5)$$

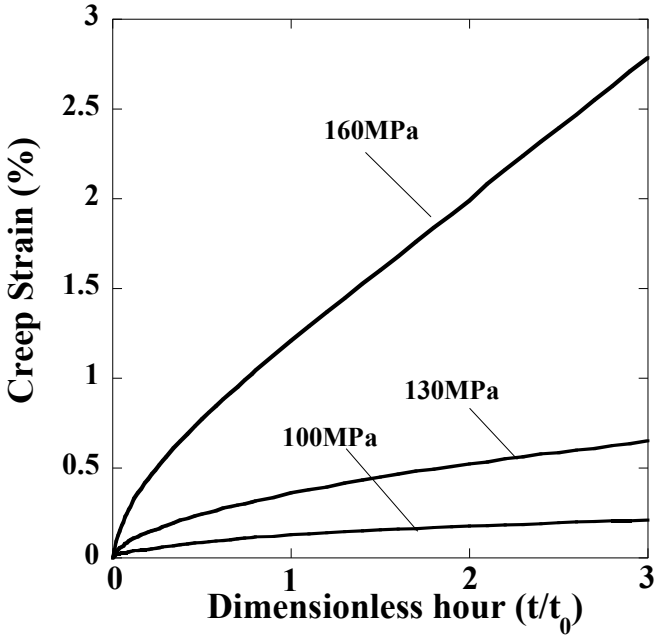

Figure 4-12 Creep strain of ductile casting iron depending on time at $T_{Tempering}$

4.5.4 Effect of tempering process on residual stress

Figure 4-13 shows stress distribution σ_z along the central cross section where z=0 after tempering process for non-uniform heating quenching and uniform heating quenching. It is seen that the tempering process sffectively reduces the maximum tensile residual stress at the roll core and keep large enough compressive residual stresss at the roll surface. In addition, the stresses

become uniformly distributed at the core no matter which tempering process (after uniform or non-uniform quenching) is considered during heating.

For tempering process after non-uniform heating quenching, the maximum stress at the core decreases by 7% from 187MPa to 173Mpa for martensite transformation 100%, and decreases by 25% from 187MPa to 140Mpa for martensite transformation 0%.

For tempering process after uniform heating quenching, the maximum stress at the core decreases by 24% from 357MPa to 273Mpa for martensite transformation 100%, and decreases by 30% from 357MPa to 246Mpa for martensite transformation 0%.

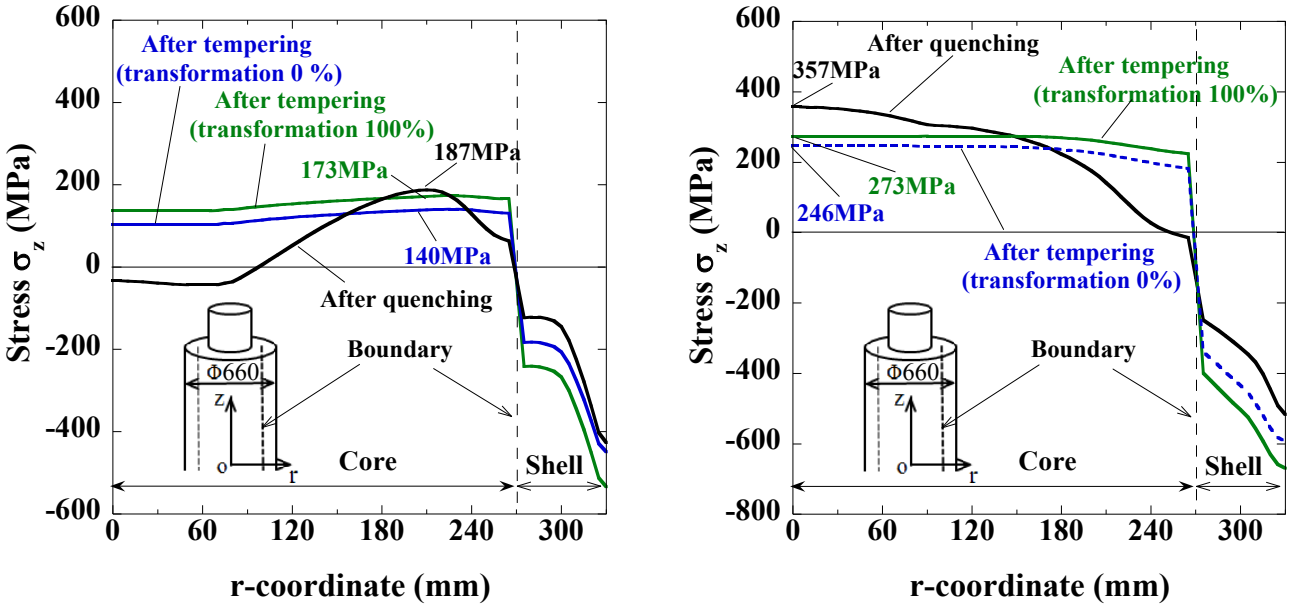

(a) Tempering process after non-uniform heating quenching process

(b) Tempering after uniform heating quenching process

Figure 4-13 Effect of tempering process on the residual stress

4.6 Conclusions

In this chapter, the numerical analysis method which can predict the residual stress reduction considering the creep behavior and tempering process was established. The residual stresses reduction were compared between uniform heating quenching and non-uniform heating quenching. Moreover, the tempering effect on the residual stress reduction has also been discussed. The results of the current study can be summarized as follows.

(1) The time hardening formulation calculated based on creep test data, is used to predict the effect of creep behavior on stress relaxation. The results show that the stress decreases by 69％ at T_{keep1} and by 38％ at T_{keep2}.

(2) For non-uniform heating quenching, by considering creep, the maximum tensile stress at the core decreases by 15％ from 216MPa to 185MPa and the center tensile stress decreases from -58 MPa to -33 Mpa. For uniform heating quenching, by considering creep, the center stress decreases by 8％ form 388MPa to 357Mpa.

(3) For tempering process after non-uniform heating quenching, the maximum stress at the core decreases by 7％ from 187MPa to 173Mpa for martensite transformation 100％, and decreases by 25％ from 187MPa to 140Mpa for martensite transformation 0％.

(4) For tempering process after uniform heating quenching, the maximum stress at the core decreases by 24％ from 357MPa to 273Mpa for martensite transformation 100％, and decreases by 30％ from 357MPa to 246Mpa for martensite transformation 0％.

Reference

1. 鈴木平. リラクゼーションとクリープの相関性について，材料，11(102), pp. 169-175, 1962.
2. J. Betten, Creep mechanics. Springer Science & Business Media, 2008, 49.

3. 多賀谷正義, 足立彰, 高温工具鋼の熱処理と残留応力. 日本金属学会誌, 16(4), pp.218-220, 1952.
4. 田中甚吉, 小幡忠良. 応力除去焼鈍に関する研究 (第 2 報). 溶接学会誌, 36(3), pp.222，1967.
5. 寺崎俊夫，磯谷寿甫，北村貴典，蘭韋明，秋山哲也：固有ひずみ利用による溶接後熱処理条件（PWHT）に関する基礎研究，溶接学会論文集，26(4)，pp. 269-275，2008.
6. 井上達雄, 田中喜久昭, 変態を考慮した焼入れの解析.材料, 22(234), pp. 218-223, 1973.
7. 門河昌宏，長岐滋，井上達雄，鋼の焼入れと低温焼戻しにおける組織変化と応力解析.材料，29(327), pp.1173-1179, 1980.
8. 山本憲司, 岡村一男, 奈良崎道治, 焼入れ残留応力シミュレーション結果に及ぼす前熱処理の影響. 熱処理, 56(3), pp.135-143, 2016.
9. 福谷理明, 寺崎俊夫. 円柱の焼入れにより生じる残留応力について: 第 4 報焼もどしによる応力低減効果の予測方法について. 日本船舶海洋工学会論文集, 17, pp. 83-91 2013.
10. O. Golan, A. Arbel, D. Eliezer, The applicability of Norton's creep power law and its modified version to a single-crystal super-alloy type CMSX-2. Materials Science and Engineering: A, 216(1), pp. 125-130, 1996.
11. JISZ2271, Metallic materials-Uniaxial creep testing in tension-Method of test, Japanese Industrial Standards Committee, **2010**.
12. 郭进全, 段非, 苗晓鹏, 师会超 张伟. 基于时间硬化理论的应力松弛简化归一模型. 机械强度, 34(6), pp. 930-933, 2012.
13. 井上達雄, 変態塑性．材料, 64(4), pp.247-257 , 2015.

Chapter 5

Accuracy of Disk Method to Predict Roll Residual Stress by Measuring the Sliced Disk Stress

5.1 Introduction

In the chapter 2 and 3, different quenching methods were discussed through FEM simulation to produce suitable surface compressive residual stresses and reduce the center tensile residual stress. In real work rolls, however, the existence of suitable residual stress distribution should be confirmed experimentally.

Over the years, different measuring methods have been developed for work rolls in order to confirm the roll residual stress distribution. Those methods are classified into destructive or non-destructive ones [1-7]. Destructive mechanical methods include deep hole-drilling method, ring core method, disk method and Sachs boring method. Non-destructive methods include X-ray diffraction method and Barkhausen magnetic method. However, the X-ray diffraction method and Barkhausen magnetic method are suitable only for measuring the surface regions and unsuitable for the interior regions of large rolls, as well as the hole-drilling method and ring-core method. The deep hole-drilling method and Sachs boring method can be used for measuring the residual stress from the center to surface for very large rolls although the deep hole-drilling method needs special facilities and the Sachs boring method is extremely time consuming. Therefore, the disk method has been developed as a convenient method because of the convenience only by measuring the stress of the disk cut out from the roll [8-11]. However, attention should be paid for the relation between the roll stress and the sliced disk stress.

Since detailed studies are not available, in this paper, the accuracy of disk method will be discussed on the basis of FEM simulation. In the first place, the thermo-elastic analysis and

thermo-elastic-plastic analysis will be considered to verify the relation between the cylinder stress and the sliced disk stress with single material. Next, the thermo-elastic-plastic analysis is performed to investigate the relation between the bimetallic roll residual stresses and the sliced disk residual stresses under different quenching time.

5.2 Disk method

5.2.1 Outline of the disk method

To evaluate the residual stress of the cylinder, the thin disk is sliced from the original cylinder around the middle portion as shown in Figure 5-1. In the first step, a disk with a thickness of about 30mm was cut out from the cylinder. During the disk-slicing process, circumferential and axial strains at the cylinder surface were recorded with the aid of strain gauges. Since the axial stress σ_z^{Disk} on the sliced disk is completely released, the remaining residual stresses in the sliced disk are in plane stress. Then, the sliced disk stresses $\sigma_r^{Disk}$and σ_θ^{Disk} will be obtained by using X-ray diffraction method or some other ways including ring slicing and crack compliance method. Finally, the cylinder stress $\sigma_z^{Cylinder}$ will be estimated by using the sliced disk stresses σ_r^{Disk} and σ_θ^{Disk}.

5.2.2 Fundamental equations useful for calculating thermo-elastic stresses in circular cylinders and disks

To calculate thermo-elastic stresses of the cylinder and disk, the following equations are available [12]. When a disk is subject to the temperature distribution T(r), the thermal stresses σ_r^{Disk} and σ_θ^{Disk} are given by Eq. (1) (2). On the other hand, the cylinder stresses $\sigma_z^{Cylinder}$ $\sigma_r^{Cylinder}$ and $\sigma_\theta^{Cylinder}$ are given by Eq. (3) (4) (5).

$$\sigma_r^{Disk} = \alpha E \left(\frac{1}{b^2} \int_0^b T(\mathrm{r}) r dr - \frac{1}{r^2} \int_0^r T(\mathrm{r}) r dr \right) \quad (1)$$

$$\sigma_{\theta}^{Disk} = \alpha E\left(-T(\mathrm{r}) + \frac{1}{b^2}\int_0^b T(\mathrm{r})rdr + \frac{1}{r^2}\int_0^r T(\mathrm{r})rdr\right) \quad (2)$$

$$\sigma_{r}^{Cylinder} = \frac{\alpha E}{1-\upsilon}\left(\frac{1}{b^2}\int_0^b T(\mathrm{r})rdr - \frac{1}{r^2}\int_0^r T(\mathrm{r})rdr\right) = \frac{1}{1-\upsilon}\sigma_{r}^{Disk} \quad (3)$$

$$\sigma_{\theta}^{Cylinder} = \frac{\alpha E}{1-\upsilon}\left(\frac{1}{b^2}\int_0^b T(\mathrm{r})rdr + \frac{1}{r^2}\int_0^r T(\mathrm{r})rdr - T(\mathrm{r})\right) = \frac{1}{1-\upsilon}\sigma_{\theta}^{Disk} \quad (4)$$

$$\sigma_{z}^{Cylinder} = \frac{\alpha E}{1-\upsilon}\left(\frac{2\upsilon}{b^2}\int_0^b T(\mathrm{r})rdr - T(\mathrm{r})\right) = \sigma_{\theta}^{Cylinder} + \sigma_{r}^{Cylinder} \quad (5)$$

From the above equations, the following relation between the disk stress and the cylinder stress under the same temperature distribution can be found as Eq. (6):

$$\sigma_{z}^{Cylinder} = \frac{1}{1-\upsilon}\left(\sigma_{r}^{Disk} + \sigma_{\theta}^{Disk}\right) \quad (6)$$

Where, b is the cylinder or disk radius, T(r) is the temperature distribution, E is the Young's modulus, α is the thermal expansion coefficient and ν is the Poisson's ratio.

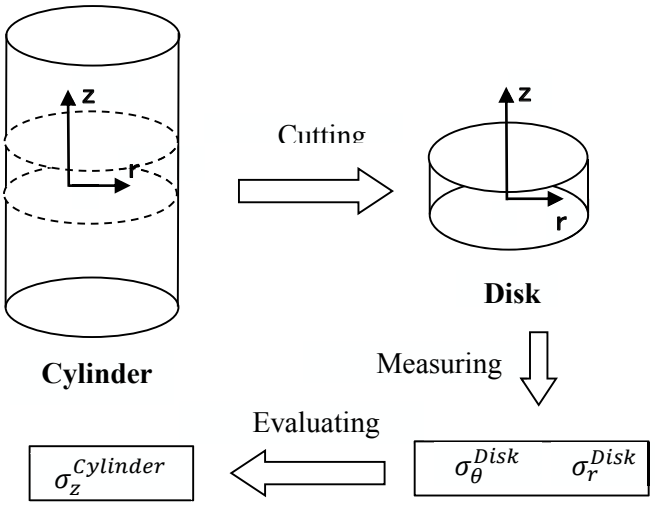

Figure 5-1 Schematic diagram of disk method

5.3 FEM model

Assume bimetallic rolls with diameter of 600mm, body length of 1800mm and shell thickness of 75mm, which consist of the high speed steel (HSS) as the shell material and the ductile casting iron (DCI) as the core material.

Figure 5-2 shows the FEM model and boundary conditions for the single material roll and bimetallic roll. Here, MSC.Marc 2012 software is used to carry out FEM analysis. A 4-node linear axisymmetric quad element with the mesh size of 5×5mm is adopted for the transient-static simulation. The displacement boundary conditions and thermal isolation conditions are applied to z=0 in Figure 5-2 due to the symmetry. In this study, the temperature distribution T(r) imposed to the cylinder for the thermo-elastic stress analysis and temperature is imposed to the roll surface for the thermo-elastic-plastic residual stress analysis during quenching.

In this paper, the disk with the thickness of 30mm is cut out from the roll around the central section z=0. The disk cutting process is performed by using the deactivate element setting in the software MSC.Marc 2012. The element initial status of the sliced disk is set to activate and the rest elements are set to deactivate to simulate the disk cutting operation from the cylinder. First, the disk method is considered for the cylinder under the temperature distribution T(r) by using the DCI material properties of Young's modulus, thermal expansion and Poisson's ratio as shown in Figure 2-7 in Chapter 2.

Then, the disk method is considered for the single material roll and the bimetallic roll under the different quenching time. Before cutting the disk, the roll residual stress can be obtained through the quenching process simulation. As shown in Figure 2-7(a)-(g) in Chapter 2, a large amount of material properties were experimentally measured under various temperatures and utilized as the input data of the quenching simulation.

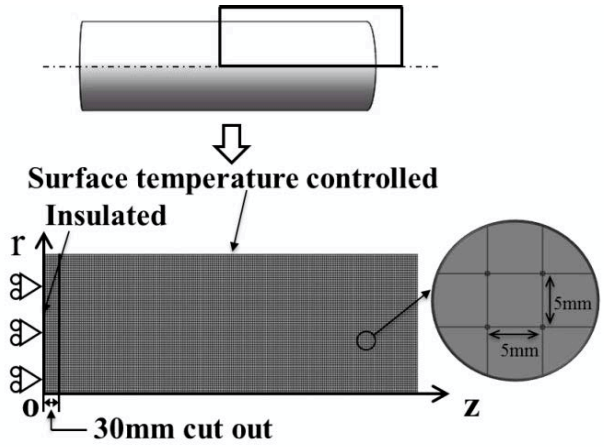

(a) Single material roll

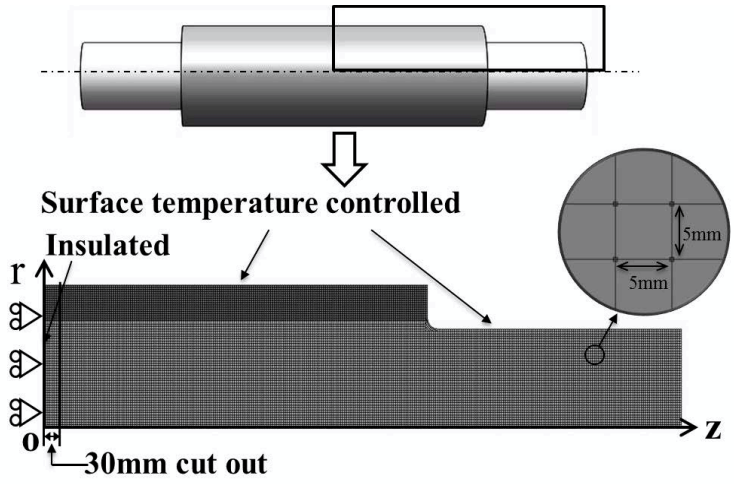

(b) Bimetallic roll

Figure 5-2 FEM model and boundary conditions

5.4 Thermal stress and residual stress during quenching for single material roll

5.4.1 Thermo-elastic stress for cylinder and disk

In the first place, the thermo-elastic analysis is performed for the cylinder and circular disk. Assume the cylinder center temperature Tc= T(0)=200℃, which often appears after the standard quenching. Assume the cylinder surface temperature Ts=T(300)=800, which may produce the surface stress $\sigma_z(300) \cong -600$ MPa often appearing at the surface after the standard quenching[9,10]. First, assume that all material data of DCI are independent of T(r) as shown in Table 2-2 for Young's modulus E, thermal expansion coefficient α and Poisson's ratio ν. Figure 5-3 shows the stress distribution of the cylinder stresses $\sigma_i^{Cylinder}(i = z, \theta, r)$ as the solid lines in comparison with the circular disk stresses $\sigma_i^{Disk}(i = \theta, r)$ as the dashed lines at z=0. The circular disk stress $\left(\sigma_r^{Disk} + \sigma_\theta^{Disk}\right)/(1-\nu)$ calculated from $\sigma_i^{Disk}(i = \theta, r)$ in Eq.(6) is also indicated as the dashed line. It is confirmed that the cylinder stress $\sigma_z^{Cylinder}$ coincides with the circular disk stress $\left(\sigma_r^{Disk} + \sigma_\theta^{Disk}\right)/(1-\nu)$ as shown in Fig.5. In other words, the relation $\sigma_z^{Cylinder} = \left(\sigma_r^{Disk} + \sigma_\theta^{Disk}\right)/(1-\nu)$ in Eq.(6) can be used for the thermo-elastic stress of the cylinder and circular disk. The same analysis is performed for the 3D cylinder and the 3D disk, which is cut out from the cylinder. Then, it is also confirmed the relation $\sigma_z^{Cylinder} = \left(\sigma_r^{Disk} + \sigma_\theta^{Disk}\right)/(1-\nu)$ in Eq.(6) for the cylinder and sliced disk.

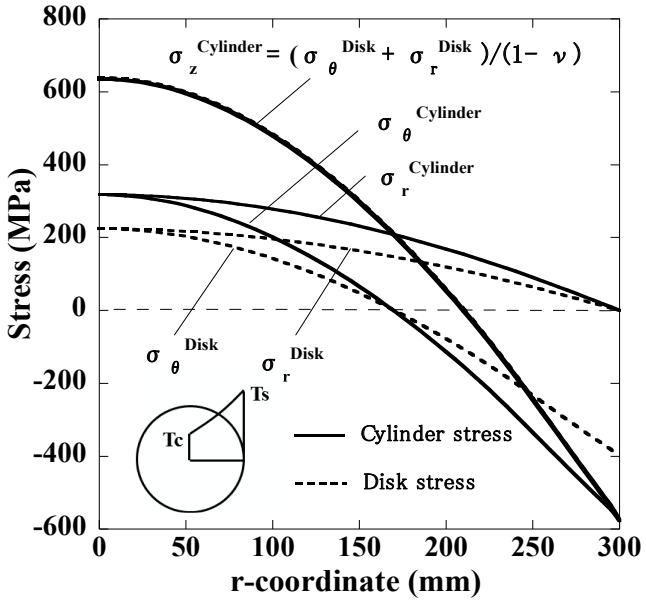

Figure 5-3 Thermo-elastic stresses of the cylinder and circular disk given by Eq.(1)-(5) assuming E=173GPa, α=1.3×10^{-5}/K, ν＝0.3 are independent of temperature T(r) as shown in Table 2-2 (Tc=T(0)=200°C, Ts= T(300)=800°C)

Next, assume that all material data of DCI are depending on temperature distribution T(r) as shown in Figure 2-7(a)-(c) for Young's modulus E, thermal expansion coefficient α and Poisson's ratio ν. Then, the thermo-elastic analysis is performed for the cylinder and the sliced disk when the temperature distribution is the same as above in Figure 5-3. The material is the same as DCI used in real roll. Figure 5-4 shows the stress distribution for the cylinder stresses $\sigma_i^{Cylinder}(i = z, \theta, r)$ as the solid lines in comparison with the sliced disk stresses $\sigma_i^{Disk}(i = \theta, r)$ as the dashed lines at z=0. The sliced disk stress $\left(\sigma_r^{Disk} + \sigma_\theta^{Disk}\right)/(1 - \nu)$ calculated from $\sigma_i^{Disk}(i = \theta, r)$ in Eq.(6) is also indicated as the dashed line. Similarly to the results in Figure 5-3, the cylinder stress $\sigma_z^{Cylinder}$ also coincides with the sliced disk stress $\left(\sigma_r^{Disk} + \sigma_\theta^{Disk}\right)/(1 - \nu)$ as shown in Figure 5-4. Therefore, the relation $\sigma_z^{Cylinder} = \left(\sigma_r^{Disk} + \sigma_\theta^{Disk}\right)/(1 - \nu)$ in Eq.(6) is confirmed for the thermo-elastic stress of the cylinder and sliced disk even when the material properties are depending on the temperature T(r) as shown in Figure 2-7(a)-(c).

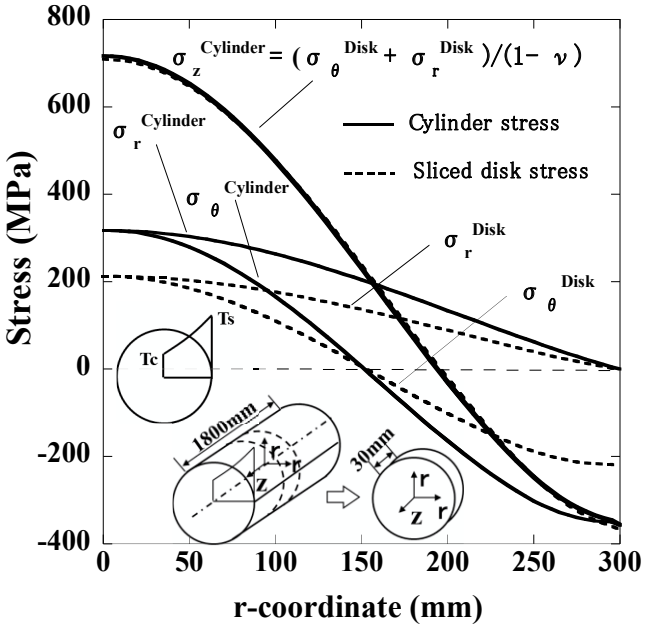

Figure 5-4 Thermo-elastic stresses of the cylinder and sliced disk assuming E = E(T), α = α(T), ν＝ν(T) are depending on temperature T(r) as shown in Fig.4(a), (b), (c) (Tc=T(0)=200℃, Ts= T(300)=800℃)

5.4.2 Residual stress simulation during quenching for single material roll

Next, the thermo-elastic-plastic analysis is performed for the single material roll before and after cutting out the circular disk from the roll considering phase transformation. The residual stress is controlled by the heat treatment condition. In order to investigate the effect of heat treatment on the residual stress, different quenching time is considered. As shown in Figure 5-5, several temperature changes are considered at the roll surface from 1000℃ to 100℃. Here， the different quenching time = 0.5, 1-7h corresponds to Here， the different quenching time = 0.5, 1-7h is assumed considering the real roll quenching time. After the quenching process, the roll is kept at 100℃ until the uniform roll temperature is obtained. Here, the material properties of DCI are used as shown in Figure 2-7.

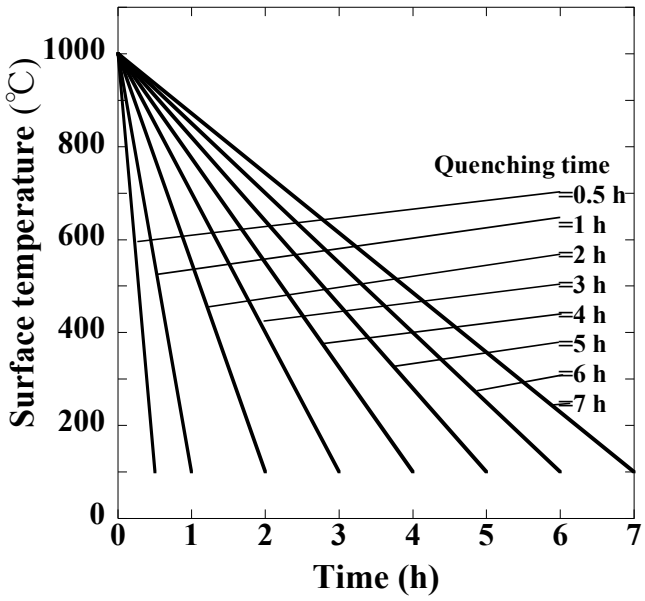

Figure 5-5 Quenching time of the roll surface

Figure 5-6 shows the stress ratio $\sigma_z^{Cylinder}/[(\sigma_r^{Disk}+\sigma_\theta^{Disk})/(1-\nu)]$ of the single material roll under the different quenching time. As shown in Figure 5-6(a), it is seen that the ratio varies in the range of 0.73-1.49 at r=0-100mm. At the roll center, the stress ratio increases with increasing quenching time t=0.5-7h. For the single material roll, the accuracy was discussed by varying the quenching time as shown in Figure 5-6(a). The disk method can be used for predicting the roll residual stress by considering the above amounts of accuracy.

To clarify the effect of sliced disk thickness, FEM analysis is also performed to the disk thickness 90mm and compared to the results of 30mm. When the disk thickness is 90mm shown in Figure 5-5(b), the stress ratio $\sigma_z^{Cylinder}/[(\sigma_r^{Disk}+\sigma_\theta^{Disk})/(1-\nu)]$ varies in the range of 0.78-1.41 at r=0-100mm and becomes smaller by 6% compared with the results of the disk thickness 30mm. It is found that the disk thickness effect is small for the range 30-90mm. The disk thickness results 30mm and 90mm in this study are useful for considering

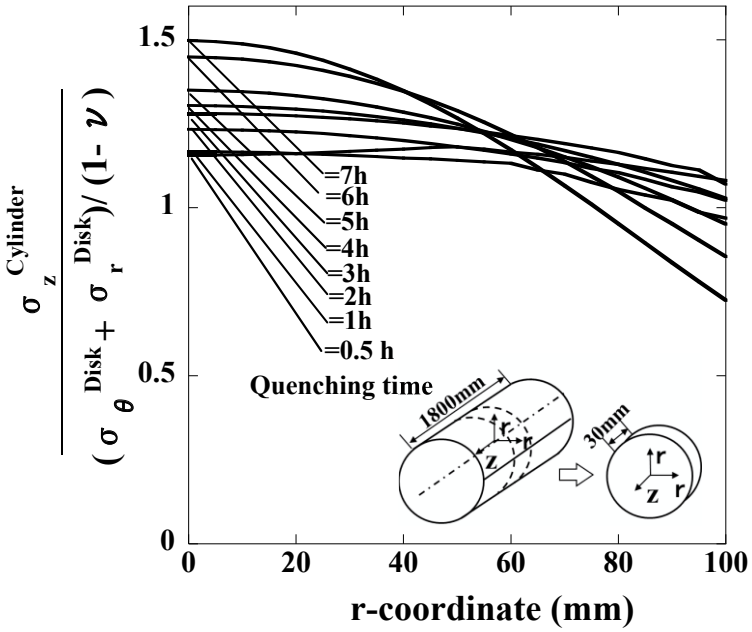

(a) Sliced disk thickness 30mm

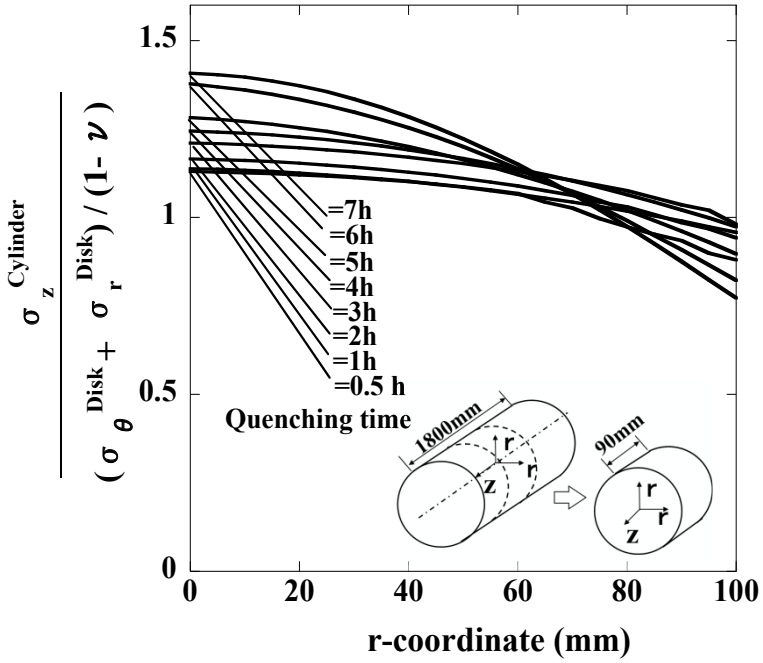

(b) Sliced disk thickness 90mm

Figure 5-6 $\sigma_z^{Cylinder}/[(\sigma_r^{Disk}+\sigma_\theta^{Disk})/(1-\nu)]$ of the single material roll under the different quenching time

5.5 Residual stress simulation for bimetallic rolls

5.5.1 Residual stress simulation during quenching for bimetallic rolls

Figure 5-7 shows the residual stress distribution σ_z^{Roll} of the bimetallic roll under the different quenching time in Fig.8. It is seen that both the center tensile stress and the surface compressive stress increases with decreasing the quenching time. This is because the maximum temperature difference between the surface and center increases with decreasing the quenching time. Figure 5-8 shows the equivalent plastic strain distribution ε_{eq} of the roll under the different quenching time in Fig.8. With decreasing the quenching time, the plastic strain ε_{eq} becomes larger because the temperature difference between surface and center becomes larger. It is also seen that residual stresses in Figure 5-7 are closely related to the plastic strain in Figure 5-8, and both stresses at the center and surface are increasing with increasing the plastic strain.

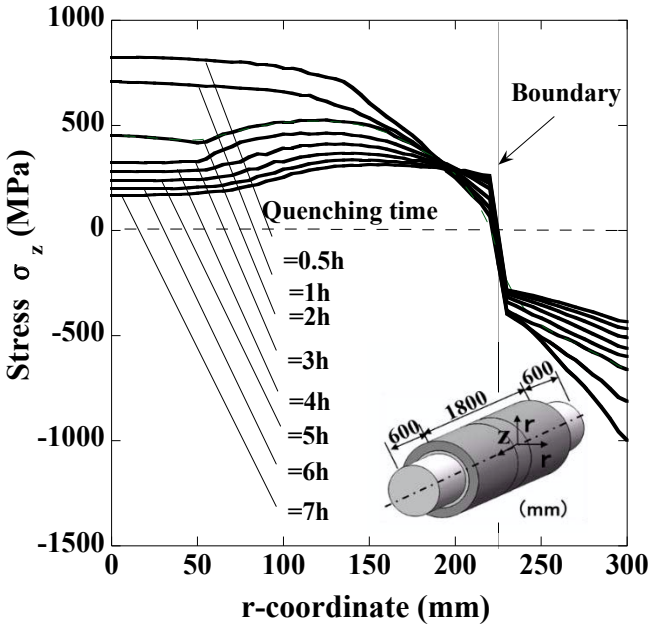

Figure 5-7 Residual stress distributions σ_z^{Roll} of the bimetallic roll under the different quenching time

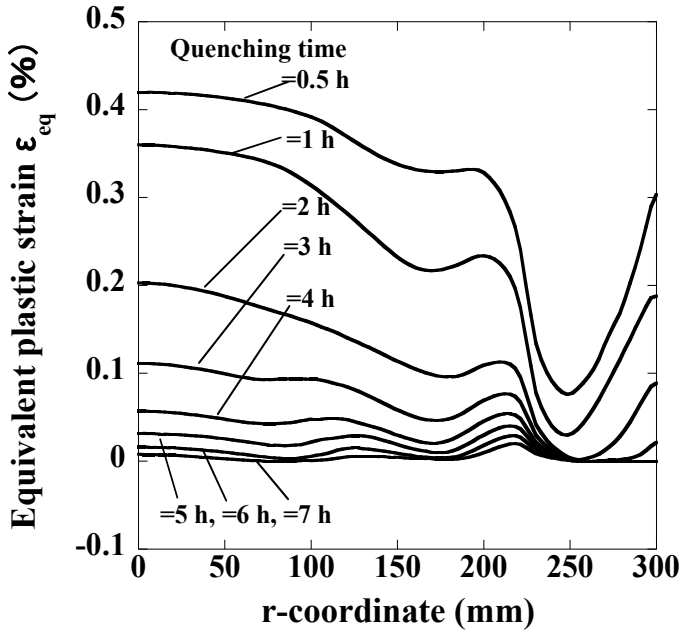

Figure 5-8 Plastic strain ε_{eq} of the bimetallic roll under the different quenching time

5.5.2 Relation between the bimetallic roll stress and the sliced disk stress

As shown in Figure 5-3, 5-4, 5-6, the relation between the roll stress $\sigma_z^{Cylinder}$ and the sliced disk stress $\left(\sigma_r^{Disk}+\sigma_\theta^{Disk}\right)/(1-\nu)$ for single material roll has been discussed. In this section, the relationship between the roll stress σ_z^{Roll} and the sliced disk stress $\left(\sigma_r^{Disk}+\sigma_\theta^{Disk}\right)/(1-\nu)$ for the bimetallic roll will be discussed.

Figure 5-9 shows the residual stress distributions σ_r^{Disk} and σ_θ^{Disk} of the sliced disk from the bimetallic roll. Figure 5-10 shows the stress ratio $\sigma_z^{Roll}/[\left(\sigma_r^{Disk}+\sigma_\theta^{Disk}\right)/(1-\nu)]$ of the bimetallic roll under the different quenching time. As shown in Fig.13, the ratio is larger than 1 for the most cases and varies in the range 0.85-2.12 at r=0-100mm. In other words, the real roll stress σ_z^{Roll} is usually larger than the sliced disk stress $\sigma_z^{Cylinder}=\left(\sigma_r^{Disk}+\sigma_\theta^{Disk}\right)/(1-\nu)$ as shown in Figure 5-10.For the bimetallic roll, the accuracy was discussed by varying the quenching time as shown in Fig.13. The disk method can be used for predicting the roll residual stress by considering the above amounts of accuracy.

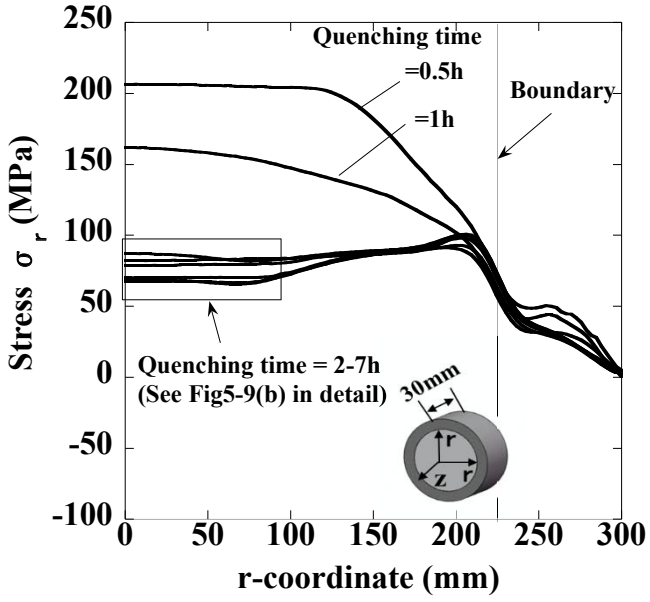

(a) Residual stress distributions σ_r^{Disk}

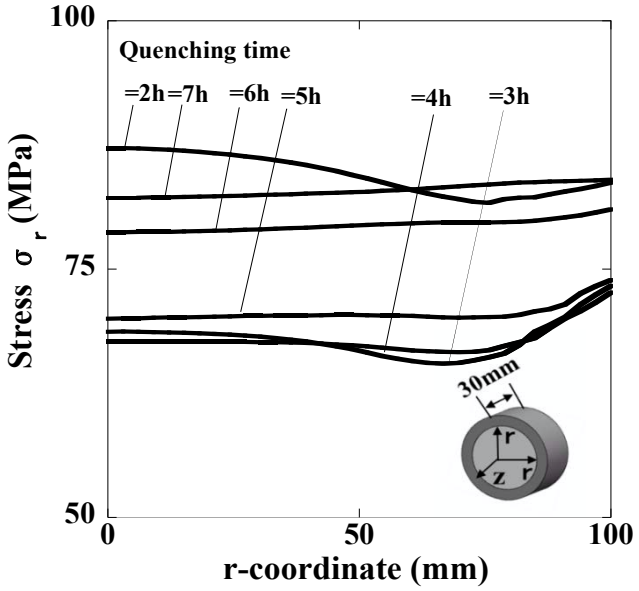

(b) Stress distributions σ_r^{Disk} of quenching time = 2-7h

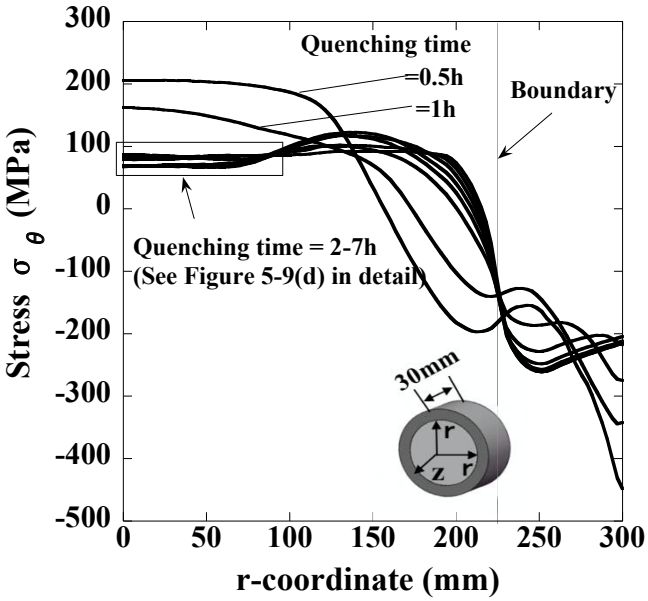

(c) Residual stress distributions σ_θ^{Disk}

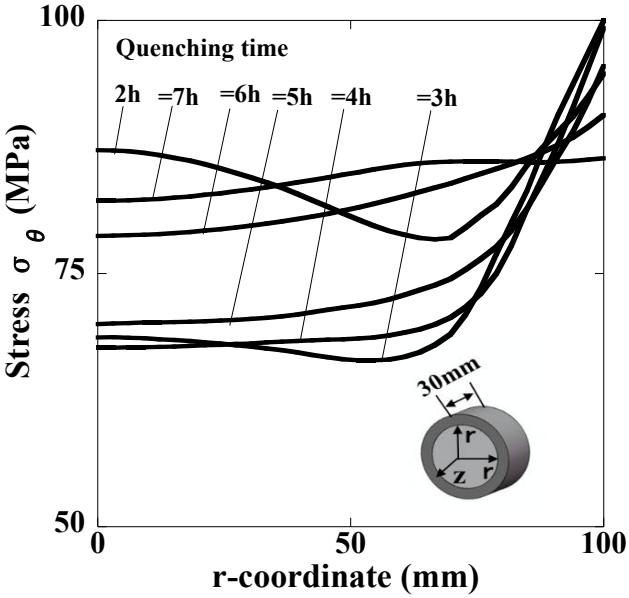

(d) Stress distributions σ_θ^{Disk} of quenching time=2-7h

Figure 5-9 Residual stress distribution of the sliced disk under the different quenching time

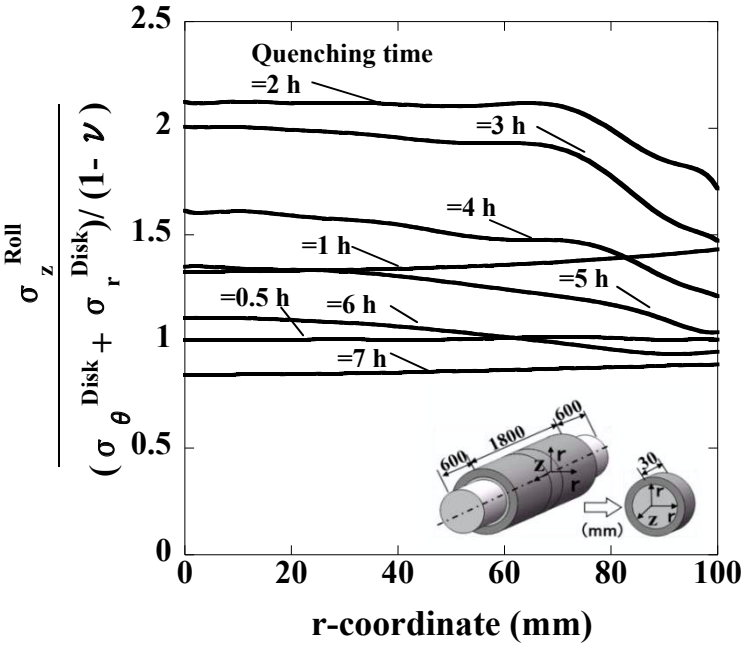

Figure 5-10 $\sigma_z^{Roll}/[(\sigma_r^{Disk}+\sigma_\theta^{Disk})/(1-\nu)]$ of bimetallic roll under the different quenching time

5.6 Conclusions

In real work rolls, it is necessary to confirm suitable residual stress distributions. In this paper, therefore, the accuracy of disk method was investigated on the basis of FEM simulation. The relation was discussed between the bimetallic roll residual stress and the sliced disk residual stress by varying the quenching time. The conclusions can be summarized in the following way.

1. For the single material rolls it is confirmed that the thermo-elastic stress can be predicted exactly from the sliced disk from the relation $\sigma_z^{Cylinder}/[(\sigma_r^{Disk}+\sigma_\theta^{Disk})/(1-\nu)]$ as shown in Figure 5-3 and Figure 5-4.

2. For the single material rolls the thermo-elastic-plastic residual stress can be predicted by the

disk method by considering the error in the range $\sigma_z^{Cylinder}/[(\sigma_r^{Disk}+\sigma_\theta^{Disk})/(1-\nu)]$ = 0.73-1.49 as shown in Figure 5-6. It is confirmed that the error is insensitive to the disk thickness.

3. For the bimetallic roll the residual stress can be predicted by the disk method considering the accuracy in the range $\sigma_z^{Roll}/[(\sigma_r^{Disk}+\sigma_\theta^{Disk})/(1-\nu)]$ = 0.85-2.12 as shown in Figure 5-10.

4. The disk method has been widely used for measuring the roll residual stress. However, the accuracy of this method has not been clarified yet. In this paper, therefore, the accuracy was discussed by varying the quenching time as shown in Figure 5-6 for the single material roll and shown in Figure 5-10 for the bimetallic roll. The disk method can be used for predicting the roll residual stress by considering the above amounts of accuracy.

References

1. E. Kingston and D. J. Smith, Residual stress measurements in rolling mill rolls using deep hole drilling technique, Ironmaking & Steelmaking, 32, pp.379-380, 2005.
2. F. Hosseinzadeh, D. J. Smith and C. E. Truman, Through thickness residual stresses in large rolls and sleeves for metal working industry. Materials Science and Technology, 25(7), pp.862-873, 2009.
3. X. Zhang, X. Song, L. Zhu and M. V. Li, Measurement and Prediction of Residual Stresses in Heat Treated Large Forgings, 5th International Conference on Thermal Process Modeling and Computer Simulation, USA, pp. 9-13, 2014.
4. Q. He and J. J. Xu, Residual stress assessment of the larger forged steel bearing roller, 6th Baosteel Biennial Academic Conference, Shanghai, 2015.
5. E. Kingston and D. J. Smith, Residual stress measurements in rolling mill rolls using deep

hole drilling technique, Ironmaking & Steelmaking, 32, pp.379-380, 2005.

6. J. H. Zheng. Analysis of residual stress and residual austenite detection in roller, Henan Metallurgy, 15, pp.53-56, 2007.
7. J. Pacyna, A. Kokosza and A. S Wojtas, Residual Stress Measurement in Steel Mill Rolls Using Magnetic Barkhausen Noise Analysis, NDT.net, 4(8), 1994
8. Y. Higashida, T. Kikuma, T. Kawanami and K. Kimura, Tetsu-to-Hagane. 72, pp.308, 1986.
9. M. Hinnemann, P. J. Mauk, V. Goryany, C. Zybill, and R. Braun, Measurement of residual stress in work roll and backup rolls for strip and plate mills and its effect on the finial load situation, Key Engineering Materials, 622, pp.949-955, 2014.
10. Y. Jimbo, A study of measuring method of rolls' residual stress. Journal of Advanced Science, 3(3), pp.157-160, 1991.
11. W. Cheng and I. Finnie, Residual stress measurement and the slitting method. Springer US, New York, USA, pp.117-119, 2007.
12. S. P. Timoshenko and J. N. Goodier, Theory of Elasticity, McGraw-Hill Book Company, Inc., New York, USA, pp.408, 1951.

Chapter 6

Conclusions of Present Study

Bimetallic rolls are widely used in hot rolling mills because of excellent hardness, wear resistance and high temperature properties. During hot rolling process, thermal tensile-compressive stresses are caused by a cyclic sequence of heating – cooling over the roll surface due to hot strip contact and water cooling, resulting in thermal crack at the roll surface. Therefore, suitable compressive stresses are necessary for preventing the thermal crack extension. However, the tensile residual stress always appears at the roll center to balance the surface compressive residual stress. Under the combined action of thermal tensile stress and residual tensile stress at the roll center, another form of roll fracture known as thermal barrel breakage is originating near to the roll center and breaking out to the barrel surface. Therefore, keeping optimum surface compressive residual stress and minimizing the center tensile residual stress are desirable to reduce the risk of roll fracture and improve bimetallic roll using life. Since the residual stress can be controlled by the heat treatment, thus this thesis concentrated on the residual stress analysis of bimetallic roll during heat treatment. The conclusions can be summarized as follows.

(1) Chapter 1 gives the introduction of the high speed steel (HSS) bimetallic rolls used for hot strip rolling. The HSS bimetallic rolls were firstly developed in Japan and aroused great interest in hot rolling industrial over the word. In this chapter, the characteristics of the HSS rolls were introduced compared with the conventional single material rolls. An in addition, the development, applications and the different manufacture methods of the HSS rolls were briefly introduced. Then the issues of the research on residual stress in the rolling rolls were reviewed, and it's

found that residual stress was mainly measured experimentally and there are only few papers concentrated on the analysis of residual stress for the large rolling rolls during the heat treatment. Then the research motivation and purpose of this thesis was introduced.

(2) Chapter 2 analyzes the residual stress of bimetallic roll during uniform heating quenching process. The residual stress generation mechanism and stress distribution during the uniform heating quenching process was investigated. Then, in order to obtain of the research purpose of keeping optimum surface compressive residual stress and minimizing the center tensile residual stress, the effects of the shell-core ratio, roll diameter, phase transformation and material heat treatment process on the residual stress are discussed. The conclusions can be summarized as follows.

1) Predicting the residual stress of the bimetallic roll during quenching is realized by FEM simulation efficiently with lower cost and higher accuracy compared with experimental measurement. After quenching, the compressive stress appears at the shell while the tensile stress appears at the core.
2) The effect of shell-core ratio on the residual stress is very small. The center stress increases only by 2% and the surface stress is almost unchanged with increasing As/Ac from 0.4 to 0.6.
3) The roll diameter has a significant effect on the residual stress. The center stress increases by 13% and the surface stress increases by 19% with increasing the diameter from D=600mm to D=800mm. However, the center stress decreases with increasing from D=900 to D=1000mm.
4) Phase transformation has a significant effect on the residual stress. Pearlite transformation contributes to decreasing the stress, while bainite transformation leads to increasing of stress.

5) Material properties depend on the heat treatment as well as the temperature. Therefore, by using the cooling process data, the center residual stress decreases by 15% and the surface residual stress decreases by 27% compared with the results by using the heating process data.

(3) Chapter 3 analyzes the residual stress of bimetallic roll during non-uniform heating quenching process. In this chapter, the residual stress simulation was preformed including rapid heating and quenching process. The residual stresses were compared between uniform heating quenching process and non-uniform heating quenching process. The reason of the center tensile residual stress reduction in non-uniform heating quenching was investigated. Then, the usefulness of non-uniform heating quenching decreasing the roll center tensile residual stress is discussed considering the thermal stress during hot rolling process. The conclusions can be summarized as follows.

1) By using non-uniform heating quenching method, the maximum tensile stress in the core appears near the shell/core boundary, the center stress decreases by 446MPa and the maximum tensile stress decreases by 44%. However, the compressive stress at the surface is almost unchanged. It may be concluded that non-uniform heating quenching is useful for reducing the risk of roll failure known as thermal barrel breakage by decreasing the center tensile stress without decreasing the surface compressive stress.

2) The center stress increases slightly for non-uniform heating quenching before and after pearlite transformation and therefore the smaller residual stress appears at the center. Then, the core stress distribution shifts to the tension side with decreasing the temperature without changing the distribution shape. Similarly, the shell stress distribution shifts to the compressive side with decreasing the temperature without changing the distribution shape.

3) The thermal stress calculated by considering temperature difference between the sub-surface and the center is simulated and added to residual stress. It may be concluded that the roll safety is guaranteed more easily in the non-uniform heating quenching than in the uniform heating quenching.

(4) Chapter 4 briefly describes and explains the effect of creep analysis and tempering on residual stress reduction of bimetallic roll during uniform heating quenching and non-uniform heating quenching processes. Firstly, the creep equations were calculated based on the creep test using the time hardening law. Then the accuracy of creep equations is verified by the comparison of stress relaxation between FEM result and experimental result. The comparison of residual stress reduction between uniform heating quenching process and non-uniform heating quenching process was also discussed. At the last, the effect of the tempering process on residual stress reduction was also investigated. The conclusions can be summarized as follows.

1) The time hardening formulation calculated based on creep test data, is used to predict the effect of creep behavior on stress relaxation. The results show that the stress decreases by 69% at T_{keep1} and by 38% at T_{keep2}.

2) For non-uniform heating quenching, by considering creep, the maximum tensile stress at the core decreases by 15% from 216MPa to 185MPa and the center tensile stress decreases from -58 MPa to -33 Mpa. For uniform heating quenching, by considering creep, the center stress decreases by 8% form 388MPa to 357Mpa.

3) For tempering process after non-uniform heating quenching, the maximum stress at the core decreases by 7% from 187MPa to 173Mpa for martensite transformation 100%, and decreases by 25% from 187MPa to 140Mpa for martensite transformation 0%.

4) For tempering process after uniform heating quenching, the maximum stress at the core decreases by 24% from 357MPa to 273Mpa for martensite transformation 100%, and decreases by 30% from 357MPa to 246Mpa for martensite transformation 0%.

(5) Chapter 5 analyzes the accuracy of disk method to predict roll residual stress. In this chapter, therefore, the accuracy of disk method was investigated on the basis of thermo-elastic-plastic FEM analysis. Firstly, the stress simulations of single material rolls were performed using thermos-elastic analysis and thermos-elastic-plastic analysis considering the different quenching time, and in addition, the effect of disk thickness on the residual stress was also discussed. Then, the stress simulations of real bimetallic rolls were performed using thermos-elastic-plastic analysis under the different quenching time. The conclusions can be summarized as follows.

1) For the single material rolls it is confirmed that the thermo-elastic stress can be predicted exactly from the sliced disk from the relation $\sigma_z^{Cylinder}/[(\sigma_r^{Disk}+\sigma_\theta^{Disk})/(1-\nu)]$ as shown in Figure 5-3 and Figure 5-4.

2) For the single material rolls the thermo-elastic-plastic residual stress can be predicted by the disk method by considering the error in the range $\sigma_z^{\mathrm{Cylinder}}/[(\sigma_r^{\mathrm{Disk}}+\sigma_\theta^{\mathrm{Disk}})/(1-\nu)]$ = 0.73-1.49 as shown in Figure 5-6. It is confirmed that the error is insensitive to the disk thickness.

3) For the bimetallic roll the residual stress can be predicted by the disk method considering the accuracy in the range $\sigma_z^{Roll}/[(\sigma_r^{Disk}+\sigma_\theta^{Disk})/(1-\nu)]$ = 0.85-2.12 as shown in Figure 5-10.

4) The disk method has been widely used for measuring the roll residual stress. However,

the accuracy of this method has not been clarified yet. In this paper, therefore, the accuracy was discussed by varying the quenching time as shown in Figure 5-6 for the single material roll and shown in Figure 5-10 for the bimetallic roll. The disk method can be used for predicting the roll residual stress by considering the above amounts of accuracy.

Acknowledgements

Firstly, I would like to express the sincere appreciation to my supervisors Prof. Nao-Aki NODA for his guidance, encouragement, and support and for helping me complete my work. Without his consistent and illuminating instruction, this thesis could not have reached its present form. I also want to thank Dr. Yoshikazu SANO for his kind help and support through the last three years and for his advice for this study.

The contributions and insightful observations of my committee members, Prof. Kenji MATSUDA , Prof. Tetsuya AKIYAMA, Prof. Yasuhiro AKAHOSHI and Prof. Kazuhiro ODA are also most appreciated and acknowledged. Also, I would like to thank Dr. Yasushi TAKASE for his help during my research work.

I also would like to thank Prof. Bin LIANG, Prof. Hongyu XU and Mr. Liuqiang YAN for providing an opportunity to pursue my doctoral study in Kyushu Institute of Technology.

Special thanks to all of Kyushu Institute of Technology's professors and administrative staff with whom I have had the opportunity to take courses. I would also like to thank all Fracture Mechanics and Elasticity lab-mates, and all those who have helped me carry out my work.

Last, I want to express my sincere gratitude to my beloved wife and family who have given me great continuous support, time and encouragement more than I need throughout my years of study.